PB89-122238

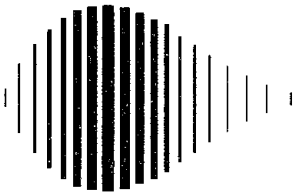

NATIONAL CENTER FOR EARTHQUAKE
ENGINEERING RESEARCH
State University of New York at Buffalo

BASE ISOLATION OF A MULTI-STORY BUILDING UNDER A HARMONIC GROUND MOTION - A COMPARISON OF PERFORMANCES OF VARIOUS SYSTEMS

by

F-G. Fan, and G. Ahmadi
Department of Mechanical and Industrial Engineering
Clarkson University
Potsdam, New York 13676

I. G. Tadjbakhsh
Department of Civil Engineering
Rensselaer Polytechnic Institute
Troy, New York 12180-3590

Technical Report NCEER-88-0010

May 18, 1988

This research was conducted at Clarkson University and Rensselaer Polytechnic Institute and was partially supported by the National Science Foundation under Grant No. ECE 86-07591.

NOTICE

This report was prepared by Clarkson University and Rensselaer Polytechnic Institute as a result of research sponsored by the National Center for Earthquake Engineering Research (NCEER). Neither NCEER, associates of NCEER, its sponsors, Clarkson University, Rensselaer Polytechnic Institute, nor any person acting on their behalf:

a. makes any warranty, express or implied, with respect to the use of any information, apparatus, method, or process disclosed in this report or that such use may not infringe upon privately owned rights; or

b. assumes any liabilities of whatsoever kind with respect to the use of, or for damages resulting from the use of, any information, apparatus, method or process disclosed in this report.

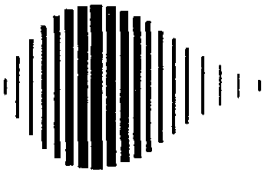

BASE ISOLATION OF A MULTI-STORY BUILDING UNDER A HARMONIC GROUND MOTION - A COMPARISON OF PERFORMANCES OF VARIOUS SYSTEMS

by

Fa-Gung Fan[1], Goodarz Ahmadi[2] and Iradj G. Tadjbakhsh[3]

May 18, 1988

Technical Report NCEER-88-0010

NCEER Contract Numbers 86-3021 and 87-2007

NSF Master Contract Number ECE 86-07591

1 Graduate Student, Dept. of Mechanical and Industrial Engineering, Clarkson University
2 Professor, Dept. of Mechanical and Industrial Engineering, Clarkson University
3 Professor, Dept. of Civil Engineering, Rensselaer Polytechnic Institute

NATIONAL CENTER FOR EARTHQUAKE ENGINEERING RESEARCH
State University of New York at Buffalo
Red Jacket Quadrangle, Buffalo, NY 14261

PREFACE

The National Center for Earthquake Engineering Research (NCEER) is devoted to the expansion of knowledge about earthquakes, the improvement of earthquake-resistant design, and the implementation of seismic hazard mitigation procedures to minimize loss of lives and property. Initially, the emphasis is on structures and lifelines of the types that would be found in zones of moderate seismicity, such as the eastern and central United States.

NCEER's research is being carried out in an integrated and coordinated manner following a structured program. The current research program comprises four main areas:

- Existing and New Structures
- Secondary and Protective Systems
- Lifeline Systems
- Disaster Research and Planning

This technical report pertains to Program 2, Secondary and Protective Systems, and more specifically to base isolation, a passive protective system Protective Systems are devices or systems which, when incorporated into a structure, help to improve the structure's ability to withstand seismic or other environmental loads. These systems can be passive, such as base isolators or viscoelastic dampers; or active, such as active tendons or active mass dampers; or combined passive-active systems.

Base isolation and base-isolated structures constitute one of the important areas of research in protective systems. Current research activities, as shown schematically in the figure below, include the following:

1. Compilation and evaluation of available data on base isolation.
2. Development of comprehensive analytical models for isolated structures and experimental verification.
3. Development of performance criteria for base-isolated structures and standardized testing procedures.
4. Development of simplified, code-type methods for the analysis and design of base-isolated structures.

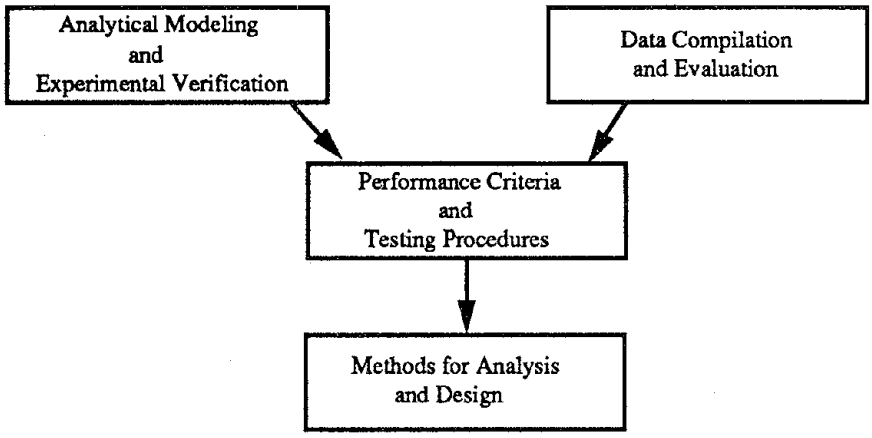

This report describes a comparative performance study of several leading base isolation systems. Based on a carefully chosen set of performance criteria, the performances of this class of base isolation systems are evaluated and their relative merits are discussed.

ABSTRACT

Performances of several leading base isolation devices (Pure-Friction/Sliding-Joint, Rubber Bearing, French System, New Zealand System, and Resilient-Friction) and a newly proposed system (Sliding Resilient-Friction) for a multi-story building subject to a horizontal harmonic ground motion are studied. The governing equations of motion of various systems and the criteria for stick-slip transitions are described and a computational algorithm for obtaining their numerical solutions is developed. The responses of the structure with different base isolation systems under various conditions are analyzed. The peak absolute acceleration, the maximum structural deflection, and the peak base displacement responses are obtained. A series of sensitivity analysis is also carried out. The effectiveness of various base isolators are studied and advantages and disadvantages of different systems are discussed. The results show that the base isolation devices effectively reduce the column stresses and the acceleration transmitted to the superstructure. Furthermore, the frictional base isolation systems are less sensitive to severe frequency content of ground excitation. When the intensity of ground excitation is doubled, the peak responses of the frictional system increase by only about 10% to 25%. It is also observed that small variations in friction coefficient lead to slight changes in the peak responses of frictional isolators. Furthermore, the velocity-dependence of friction coefficient, variations of mass ratio, and damping ratio of the isolator have negligible effects on peak responses of the base isolated structure.

ACKNOWLEDGEMENTS

Thanks are given to Dr. N. Mostaghel of the University of Utah for many helpful discussions. The financial support of the National Center for Earthquake Engineering Research at the State University of New York at Buffalo under Grant Numbers 86-3021F and 87-2007A is gratefully acknowledged.

TABLE OF CONTENTS

LIST OF ILLUSTRATIONS

LIST OF ILLUSTRATIONS (Cont'd)

LIST OF TABLES

SECTION 1

INTRODUCTION

Using base isolators for aseismic design of structures has attracted considerable attention in recent years. The main concept here is to isolate the structures from ground instead of the conventional techniques of strengthening the structural members. This new design methodology appears to have considerable potential in preventing earthquake damages to structures and their internal equipments.

Isolating structures from ground to protect them from damaging earthquakes is not a totally new idea. As early as 1909, a British physician had applied for a patent on separating a building from ground by a layer of talc or sand (Kelly [1,2]). However, the civil engineer designers have preferred, so far, to strengthen the structures instead of isolating them. During recent decades, the economy and safety of the traditional strengthening design versus base isolation concept have been re-evaluated. Strengthening a structure to withstand strong earthquakes inevitably leads to higher mass and hence higher seismic forces. The construction cost of such a massive building is also ever increasing. Furthermore, even though the structures are designed to survive a strong earthquake, there may be untolerable damages to the sensitive internal equipments. These are particularly evident in the cases of nuclear power plants and buildings containing computer facilities or other expensive electronic equipments. A number of base isolation systems have been developed, and used for protection of buildings, nuclear power plants, bridges, and other structures in the last two decades. Extensive reviews of the earlier and recent developments of base isolation devices were provided by Kelly [1,2]. Here, only brief descriptions of several base isolation systems which are considered in this study are given.

Base isolators in which the only isolation mechanism is sliding friction are classified as Pure-Friction (P-F) or Sliding-Joint base isolation systems. In this class of isolators, the horizontal friction force offers resistance to motion and dissipates energy. These isolation devices have no restoring force and residual slip displacement between the structure and the foundation will remain after each earthquake. A schematic diagram for the behavior of the P-F base isolator is shown in Figure 1-1a. A number of theoretical studies on performances of various P-F and Sliding-Joint base isolation systems have appeared in the literatures. Chen and Clough [3],

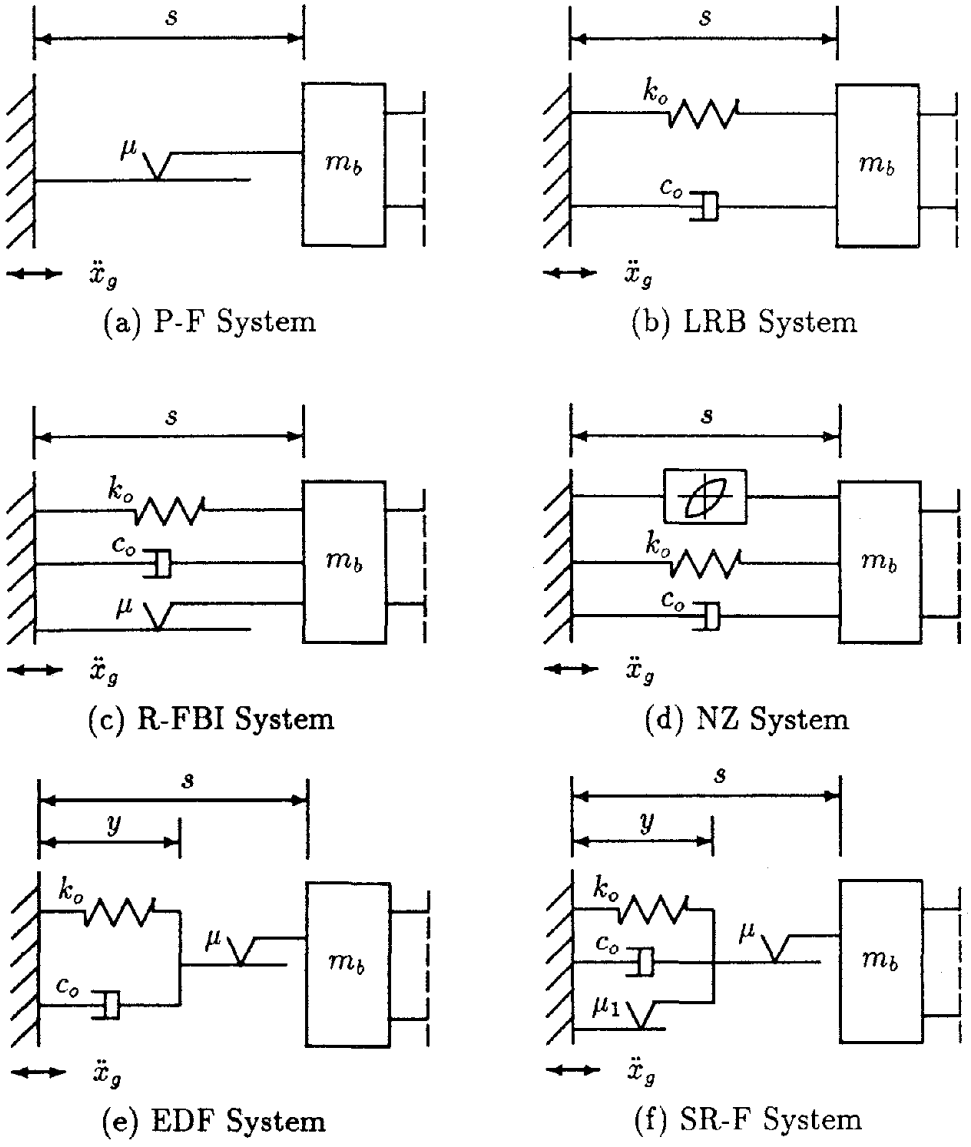

Figure 1-1 Schematic Diagrams of Isolation Systems

Mostaghel and Tanbakuchi [4], Kelly and Beucke [5], Ahmadi and Mostaghel [6], Younis and Tadjbakhsh [7], Ahmadi [8], Constantinou and Tadjbakhsh [9] and Su et al. [10] studied the behavior of the P-F isolators under various deterministic or stochastic excitations. Li [11,12] described the construction of a building in Beijing, China which is isolated with a layer of sand.

The most common base isolation system which has been studied extensively at the University of California by Kelly and co-workers [1,2,13] is the Laminated Rubber Bearing (LRB) base isolation system. A LRB is made of alternating layers of rubber and steel with the rubber being vulcanized to the steel plates. Therefore, the bearing is rather flexible in the horizontal direction but quite stiff in the vertical direction. With its horizontal flexibility, the LRB provides protection against earthquakes by shifting the fundamental frequency of vibration to a much lower value and away from the energy containing range of the earthquake ground motion. The horizontal stiffness of the bearing is also designed in such a way that it can resist the wind forces with little or no deformation. This base isolation system has been used in a number of buildings in Europe, Japan and New Zealand. The recently constructed four-story Foothill Communities Law and Justice Building in San Bernardino County, California was built on a LRB base isolation system. Figure 1-1b shows a schematic diagram for a Laminated Rubber Bearing System.

A recent base isolation device was developed by Mostaghel [14-16] which is referred to as the Resilient-Friction Base Isolation (R-FBI) system. This isolator is composed of several layers of teflon coated friction plates with a central core of rubber. The rubber provides the resilient force for the system while energy is dissipated by the friction forces. An extensive study of the responses of a five-story building isolated by the R-FBI system was provided by Mostaghel and Khodaverdian [17]. The mechanical behavior of the R-FBI system is illustrated in the schematic diagram shown in Figure 1-1c.

A laminated rubber bearing system in which a central lead core is used to reduce the base relative displacement and to provide an additional mean of energy dissipation has been used widely in New Zealand. This system is referred to as the New Zealand (NZ) base isolation system. The performance of the NZ isolator (Lead core laminated rubber bearing) under a variety of conditions were reported in [2,13,18]. The rubber provides the flexibility for the lateral displacement of the isolator while

the yielding property of the lead core serves as a mechanism for dissipating energy and hence reducing the lateral displacement of the isolator. The mechanical behavior of this system is equivalent to a hysteretic damper [13,19-21]. The schematic diagram of the NZ base isolation system is shown in Figure 1-1d.

A system which was designed mainly for base isolation of nuclear power plants in regions of high seismicity was developed under the auspices of Electricite de France (EDF) [22]. This system is standardized for base isolation of power plants which are constructed by the French Company Framatome. It has been used in the design of nuclear power plants in France, South Africa, and Iran. An EDF base isolator unit consists of a laminated (steel-reinforced) neoprene pad topped by a lead-bronze plate which is in frictional contact with a steel plate anchored to the base raft of the structure. Whenever there is no sliding in the friction plate, the EDF system behaves as a LRB. In this case, the flexibility of the neoprene pad provides isolation for the structure. The presence of the friction plate serves as an additional safety feature for the system. Whenever the ground acceleration becomes very large, sliding occurs which dissipates energy and limits the acceleration transmitted to the superstructure. The behavior of the EDF base isolator is shown schematically in Figure 1-1e.

Recently, a new design for base isolation which combines the desirable features of the R-FBI and the EDF systems was proposed in [23]. The mechanical behavior of the new device which is referred to as the Sliding Resilient-Friction (SR-F) base isolator is shown schematically in Figure 1-1f. Having two frictional elements is the main feature of this system. Whenever there is no sliding in the upper friction plate, the SR-F base isolator behaves as a R-FBI unit. For high intensity earthquake ground accelerations, sliding in the upper friction plate occurs which provides an additional mechanism for energy dissipation and increases the effectiveness of the isolation system.

In spite of the large number of studies on performances of different base isolation systems indicated earlier, the advantages and disadvantages of various systems are not well understood. Recently, Su et al. [23,24] provided comparative studies of different base isolation devices for rigid and shear beam structures. Presently, base isolation systems are mainly considered for bridges, nuclear power plants, and low to medium rise multi-story buildings. However, a comprehensive study which compares

the performances of different base isolation devices for a multi-story structure under a specific ground excitation is not available as yet.

In this work, performances of several leading base isolation systems described earlier for a multi-story, lumped-mass building subject to a horizontal harmonic ground motion are studied. The equations of motion for various base isolation systems are described. Utilizing the fourth order Runge-Kutta scheme, a computational algorithm for numerical evaluation of the response of the base isolated structure is developed. The governing equations for frictional isolation devices are highly nonlinear. The criteria used for transition between different phases of motion are crucial to the accuracy of the response analysis. These criteria are carefully studied and their accuracy are verified by a number of numerical experiments.

The peak absolute acceleration of each floor signifies the force that it experiences and is the main source of damage to the structure, the internal equipment and secondary systems. The peak base relative displacement is the most important parameter for the design of life line connections to the ground. (This is particularly evident in designing the isolation systems for nuclear reactors, since the connecting pipe lines can be damaged by the motion of the building relative to its foundation.) The deflection of the structure is directly proportional to the column stresses and base shear. In this study, the peak absolute acceleration, the maximum structural deflection and the maximum base displacement responses for various base isolation systems are evaluated and the results are compared with each other and with those of the fixed-base structure. A series of sensitivity studies for variations in damping and mass ratio of the structure, friction coefficient and natural period of the isolator, and intensity and frequency content of the ground excitation are also carried out.

Based on the presented results, it is concluded that the transmitted acceleration and the column stresses of the structure can be effectively reduced by using properly designed base isolation systems. The results of the sensitivity analyses show that when the period of the ground excitation is close to the natural period of the isolation systems, the LRB, the NZ, and the R-FBI systems may amplify the ground acceleration. Furthermore, the friction-type isolation systems are less sensitive to the variations in the amplitude and frequency content of the ground excitation in comparison to the LRB, and the NZ base isolators. The study also shows that the peak accelerations transmitted by the friction-type isolators are not significantly affected

by small variations in friction coefficient; furthermore, the velocity-dependence of friction coefficient has no noticeable effects on the peak responses. The results also show that variations in mass ratio and the damping of the structure or the isolator do not significantly affect the peak responses.

SECTION 2

GOVERNING EQUATIONS

In this section, the equations governing the motions of various base isolation systems and the criteria used for motion transitions for the frictional base isolators are presented and discussed. While the formulation is presented for general multi-story, lumped-mass, shear buildings, a three-story frame as shown in Figure 2-1 is used as the working structural model in the subsequent analyses. To understand the effects of the frequency content of the ground acceleration, sinusoidal excitations are considered throughout this work. While Coulumb friction model is used in most cases, the sensitivity of the results to the velocity-dependence of friction coefficient is also studied.

By applying Newton's Second Law to the base isolated structure shown in Figures 1-1 and 2-1, the equations of motion are derived and the results for various base isolation systems are described in the following sections.

2.1 P-F System

Figure 1-1a shows the schematic diagram for a Pure-Friction base isolation system. The governing equations for a multi-story, lumped-mass structure with a P-F system during the sliding phase are given as,

$$\ddot{s} + \mu g \, \widehat{sgn}(\dot{s}) + \sum_{i=1}^{n} \alpha_i \ddot{x}_i = -\ddot{x}_g \ , \tag{2.1}$$

$$[m]\{\ddot{x}\} + [c]\{\dot{x}\} + [k]\{x\} = -(\ddot{s} + \ddot{x}_g)[m]\{1\} \tag{2.2}$$

where s is the relative displacement between the base of the structure and the ground, x_i is the relative displacements of each floor with respect to the base, $\ddot{x}_g$ is the horizontal ground acceleration, μ is the friction coefficient, g is the acceleration of gravity, and [m], [c], [k] represent mass matrix, damping matrix, and stiffness matrix, respectively. In these equations, $\{1\}$ is a vector all of whose elements are unity, $\widehat{sgn}(\dot{s})$ is a function which is equal to $+1$ when $\dot{s}$ is positive, and -1 when $\dot{s}$ is negative. The value of $\widehat{sgn}(0)$ is undefined but it is bounded between -1 and $+1$. The mass-ratio parameter α_i is defined as

$$\alpha_i = \frac{m_i}{M} \ , \qquad \alpha_b = \frac{m_b}{M} \ , \qquad M = m_b + \sum_{i=1}^{n} m_i \ , \tag{2.3}$$

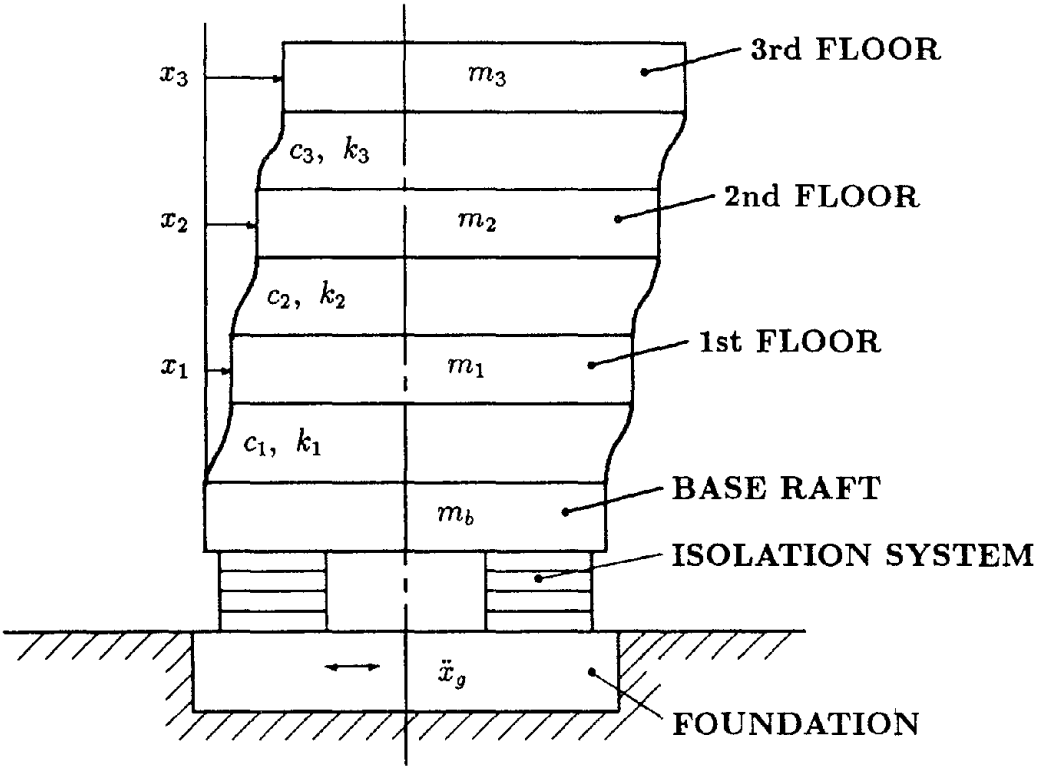

Figure 2-1 Structural Model of a Three-Story Building with a Base Isolation System

where m_i is the mass of the ith floor, m_b is the mass of the base and M is total mass of the structure.

In the sliding phase, Eqs.(2.1) and (2.2) govern the motion of the structure and its isolator. For the nonsliding phase,

$$\ddot{s} = \dot{s} = 0, \tag{2.4}$$

and the deformation of the structure is governed by Eq.(2.2).

The criteria for transition from the nonsliding phase to the sliding phase and vice versa, and for reversing the sliding direction without sticking are as follows. The nonsliding phase continues as long as

$$|\ddot{x}_g + \textstyle\sum_{i=1}^{n} \alpha_i \ddot{x}_i| < \mu g \ . \tag{2.5}$$

As soon as the condition,

$$|\ddot{x}_g + \textstyle\sum_{i=1}^{n} \alpha_i \ddot{x}_i| = \mu g \ , \tag{2.6}$$

is met the sliding phase starts and Eq.(2.1) governs the slip displacement. At this moment of transition, the direction of sliding is determined from the following equation:

$$\widehat{sgn}(0) = - \frac{\ddot{x}_g + \sum_{i=1}^{n} \alpha_i \ddot{x}_i}{\mu g} \ . \tag{2.7}$$

That is, for $\widehat{sgn}(0) = +1$ (or -1), the direction of sliding of the base mass is in positive (or negative) direction. The sliding of the structure in one direction may be terminated by a transition to a stick condition, or by a reversal of the sliding direction. During the sliding phase, whenever $\dot{s}$ becomes zero, the criterion,

$$|\ddot{s}| \geq 2\mu g \, \frac{M}{m_b} \ , \tag{2.8}$$

is checked for determining the subsequent behavior. Validity of the inequality given by (2.8) is the necessary and sufficient condition for the reversal of the sliding direction (Appendix A). That is, if the inequality holds, Eqs.(2.1) and (2.2) continue to govern the subsequent sliding phase motion with $\widehat{sgn}(\dot{s})$ taking the sign of $\ddot{s}$ at the moment of transition. If the criterion given by (2.8) is not satisfied, the structure will stick to its foundation and Eqs.(2.2) and (2.4) apply. Under exceptional conditions, $\dot{s}$ and $\ddot{s}$ might become simultaneously zero. Such a case corresponds to a smooth transition to the stick condition. Usually, a friction coefficient between 0.05

and 0.2 are used for the P-F (Sliding-Joint) base isolation systems [3-10]. In this study, $\mu = 0.1$ is used in most of the numerical experiments.

2.2 LRB System

Figure 1-1b shows the schematic diagram for the Laminated Rubber Bearing base isolation system. When a multi-story building is isolated by the LRB system, the equation governing the displacement of the isolator is given as,

$$\ddot{s} + 2\zeta_o\omega_o\dot{s} + \omega_o^2 s + \sum_{i=1}^{n} \alpha_i \ddot{x}_i = -\ddot{x}_g \ , \tag{2.9}$$

where the natural circular frequency of the bearing ω_o, and its effective damping ratio ζ_o are defined as

$$2\zeta_o\omega_o = \frac{c_o}{M} \ , \qquad \omega_o^2 = \frac{k_o}{M} \ . \tag{2.10}$$

Here c_o and k_o are the damping and the horizontal stiffness of the bearing, respectively. The deflection of the isolated structure is governed by Eq.(2.2) which is coupled to Eq.(2.9) through the inertial forces. Note also that the GERB system [25], which is composed of helical springs and viscodampers behaves similar to the LRB system in the horizontal direction and its motion may be described by Eq.(2.9). A natural period T_o of about 2 sec ($\omega_o = \pi$ rad/sec) is commonly suggested for the LRB base isolation systems. The effective damping ratio of the isolator ζ_o varies considerably with the strain of the rubber. It may be as high as 0.3 for low strain and reduced to about 0.05 for high strain [26,27]. Here, an average value of 0.08 for ζ_o is considered in most cases.

2.3 R-FBI System

The schematic diagram describing the mechanical behavior of the Resilient-Friction Base Isolation system is given in Figure 1-1c. A multi-story shear structure which is isolated by the R-FBI system is considered. During the sliding phase, the displacement of the isolator is governed by,

$$\ddot{s} + 2\zeta_o\omega_o\dot{s} + \omega_o^2 s + \mu g \ \widehat{sgn}(\dot{s}) + \sum_{i=1}^{n} \alpha_i \ddot{x}_i = -\ddot{x}_g \ . \tag{2.11}$$

The deformation of structure is still described by Eq.(2.2). For the nonsliding phase, the responses are evaluated from Eqs.(2.2) and (2.4).

Whenever the friction plates are sticking to each other, the nonsliding phase continues as long as

$$|\ddot{x}_g + \omega_o^2 s + \sum_{i=1}^{n} \alpha_i \ddot{x}_i| < \mu g \ . \tag{2.12}$$

As soon as the condition,

$$|\ddot{x}_g + \omega_o^2 s + \sum_{i=1}^{n} \alpha_i \ddot{x}_i| = \mu g \ , \tag{2.13}$$

is satisfied, slip occurs and Eq.(2.11) coupled with Eq.(2.2) govern the motion. The direction of sliding is given by

$$\widehat{sgn}(0) = - \frac{\ddot{x}_g + \omega_o^2 s + \sum_{i=1}^{n} \alpha_i \ddot{x}_i}{\mu g} \ , \tag{2.14}$$

at this moment of transition.

Like the P-F base isolator, during the sliding phase whenever $\dot{s} = 0$, a transition to the stick condition may occur. The criterion that determines the subsequent behavior of the R-FBI system is similar to that of the P-F base isolator. If the inequality given by (2.8) holds, the sliding continues with $\widehat{sgn}(\dot{s})$ taking the sign of $\ddot{s}$ at the transition moment; otherwise, the stick condition prevails. The values of $T_o = 4\ sec$ ($\omega_o = \pi/2\ \ rad/sec$) are suggested for the R-FBI base isolation system in [14-16] . In this study, unless stated otherwise, $T_o = 4\ sec$, $\mu = 0.05$ and $\zeta_o = 0.08$ are used.

The Alexisismon base isolation system developed by Ikonomou [28] makes use of the parallel actions of sliding joints and rubber bearings. Although the designs of the Alexisismon and R-FBI systems are different, their governing equations are quite similar. In fact, Eqs.(2.11) - (2.14) are directly applicable to the Alexisismon system as long as the deformation in its rubber bearing part remains small.

2.4 NZ System

Figure 1-1d shows the schematic diagram of the New Zealand system. In [20,23] it was suggested that the restoring force generated by the hysteretic behavior of the lead core of the NZ isolator may be approximated by Wen's hysteretic model [29]. When a multi-story building is isolated by the NZ (or a hysteretic damper) base isolation system, the deflection of the structure is governed by Eq.(2.2), and the equation governing the base displacement is given as,

$$\ddot{s} + 2\zeta_o \omega_o \dot{s} + \omega_o^2 s + \frac{N}{M} Q + \sum_{i=1}^{n} \alpha_i \ddot{x}_i = -\ddot{x}_g \ , \tag{2.15}$$

where N is the number of base isolators used, and M is the total mass of structure as defined in Eq.(2.3). Here, Q is the hysteretic restoring force generated by the lead core which is given as

$$Q(s,\dot{s}) = \alpha\frac{F_y}{Y}s + (1-\alpha)F_y Z \ , \tag{2.16}$$

where Z is the dimensionless hysteretic displacement that satisfies the following nonlinear first order differential equation :

$$Y\dot{Z} = -\gamma|\dot{s}|Z|Z|^{\eta-1} - \beta\dot{s}|Z|^{\eta} + \theta\dot{s} \ . \tag{2.17}$$

In Eqs.(2.16) and (2.17), F_y and Y represent the force and the yield displacement of the equivalent hysteretic dampers, β, γ, and θ are dimensionless parameters, η is an integer which controls the smoothness of transition from elastic to plastic response, α is the post to preyielding stiffness ratio.

For the predicted responses from this model to fit the experimental results for certain lead-core laminated rubber bearings, the values of $F_y = 46\ KN$, $Y = 7.7\ mm$, $\alpha = 0.157$, $\beta = -0.54$, $\gamma = 1.4$, $\theta = 1.0$, and $\eta = 1$ were suggested in [20]. These values together with the natural period T_o of 2 sec ($\omega_o = \pi\ \ rad/sec$), a damping ratio ζ_o of 0.08 and the mass per isolator ratio, M/N, of 200 $tons$ are used in this study.

2.5 EDF System

Figure 1-1e shows the schematic diagram for the EDF base isolation system. In practical applications, the laminated neoprene pad is designed to have a natural period of about 0.8 to 1.2 sec, and the friction coefficient of the friction plate is about 0.2. The mass of the reinforced elastomeric bearings and the friction plate of the EDF system are negligible when compared with the mass of the base raft and the structure. Therefore, the mass of the bearing is neglected in the present analysis and in the schematic diagram shown in Figure 1-1e.

The governing equations of motion for a multi-story building isolated by an EDF system are described in the sequel. During the sliding phase, the equations of motion of the EDF isolator are given as,

$$2\zeta_o\omega_o\dot{y} + \omega_o^2 y = \mu g\ \widehat{sgn}(\dot{s}-\dot{y}) \ , \tag{2.18}$$

$$\ddot{s} + \mu g \ \widehat{sgn}(\dot{s} - \dot{y}) + \sum_{i=1}^{n} \alpha_i \ddot{x}_i = -\ddot{x}_g \ , \tag{2.19}$$

where y is the deflection of the rubber and s is the total relative displacement (sum of y and the slip displacement in the friction plate) between the base raft of the structure and the ground. In the nonsliding phase, the EDF system behaves as a LRB system. The equations of motion of the isolator then become

$$\ddot{s} = \ddot{y} \ , \quad \dot{s} = \dot{y} \ , \tag{2.20}$$

$$\ddot{y} + 2\zeta_o \omega_o \dot{y} + \omega_o^2 y + \sum_{i=1}^{n} \alpha_i \ddot{x}_i = -\ddot{x}_g \ , \tag{2.21}$$

The deflections of the structure for both phases of motion are governed by Eq.(2.2).

The criterion for the nonsliding phase to continue to persist is :

$$|\ddot{s} + \ddot{x}_g + \textstyle\sum_{i=1}^{n} \alpha_i \ddot{x}_i| < \mu g \ . \tag{2.22}$$

As soon as the condition,

$$|\ddot{s} + \ddot{x}_g + \textstyle\sum_{i=1}^{n} \alpha_i \ddot{x}_i| = \mu g \ , \tag{2.23}$$

is satisfied, sliding commences and Eqs.(2.18) and (2.19) coupled with Eq.(2.2) govern the subsequent motion in the sliding phase. The direction of sliding is given by

$$\widehat{sgn}(0) = -\frac{\ddot{x}_g + \ddot{s} + \sum_{i=1}^{n} \alpha_i \ddot{x}_i}{\mu \ g} \tag{2.24}$$

at the moment of transition.

A nonsliding phase is bound to occur at the end of each sliding phase. This is because when the base raft changes its direction of motion, the massless bearing has to stick to it due to the absence of inertial resistance. This behavior of the EDF base isolator which is the consequence of having the elastic and the friction elements in series is in contrast to that of the R-FBI system. As noted earlier, the R-FBI system makes use of parallel actions of the elastic element and the friction plates.

In the present study, unless stated otherwise the values of $T_o = 1 \ sec$ ($\omega_o = 2\pi \ \ rad/sec$), $\zeta_o = 0.08$, and $\mu = 0.2$ are used.

2.6 SR-F System

Figure 1-1f shows the mechanical behavior of the Sliding Resilient-Friction base isolation system. This system is characterized by two friction plates. One acts in parallel with the isolator spring and is referred to as body friction plate. The other acts as sliding interface with the structure. In this section, the equations of motion for a multi-story shear structure isolated by the SR-F system are described. When sliding occurs in both the upper friction plate and the body of the isolator, the equations of motion of the SR-F base isolator are given as

$$2\zeta_o\omega_o\dot{y} + \omega_o^2 y + \mu_1 g\ \widehat{sgn}(\dot{y}) = \mu g\ \widehat{sgn}(\dot{s} - \dot{y})\ , \tag{2.25}$$

$$\ddot{s} + \mu g\ \widehat{sgn}(\dot{s} - \dot{y}) + \sum_{i=1}^{n} \alpha_i \ddot{x}_i = -\ddot{x}_g\ , \tag{2.26}$$

where y is the deflection of the isolator, s is the total displacement which indicates the relative displacement between the base raft of the structure and the ground, μ and μ_1 represent the friction coefficients of the upper and the body friction plates, respectively.

In the case that the upper friction is sticking while the body friction plates are sliding, the SR-F isolator behaves as a R-FBI unit. The equations of motion of the isolator then are given as,

$$\ddot{s} = \ddot{y}\ , \quad \dot{s} = \dot{y}\ , \tag{2.27}$$

$$\ddot{y} + 2\zeta_o\omega_o\dot{y} + \omega_o^2 y + \mu_1 g\ \widehat{sgn}(\dot{y}) + \sum_{i=1}^{n} \alpha_i \ddot{x}_i = -\ddot{x}_g\ . \tag{2.28}$$

Whenever there is no sliding in the body friction plate, while the upper interface friction plate is sliding, the system behaves as a simple Sliding-Joint isolator and the displacement of the isolator is governed by

$$\ddot{y} = \dot{y} = 0\ , \tag{2.29}$$

$$\ddot{s} + \mu g\ \widehat{sgn}(\dot{s}) + \sum_{i=1}^{n} \alpha_i \ddot{x}_i = -\ddot{x}_g\ . \tag{2.30}$$

When all friction plates are sticking, the equations of motion of the isolator is given as

$$\ddot{s} = \dot{s} = 0\ , \quad \ddot{y} = \dot{y} = 0\ , \tag{2.31}$$

which correspond to a fixed-base structure. In all these different phases of motion, the deformation of structure is governed by Eq.(2.2).

The nonsliding phase in the body friction plates continues as long as

$$|\ddot{s} + \ddot{x}_g + \omega_o^2 y + \textstyle\sum_{i=1}^{n} \alpha_i \ddot{x}_i| < \mu_1 g \ . \tag{2.32}$$

As soon as the lefthand side of (2.32) becomes equal to $\mu_1 g$, the body friction plates begin to slide, and the direction of sliding is determined by

$$\widehat{sgn}(0) = - \frac{\ddot{s} + \ddot{x}_g + \omega_o^2 y + \sum_{i=1}^{n} \alpha_i \ddot{x}_i}{\mu_1 g} \ . \tag{2.33}$$

For $\widehat{sgn}(0)$ equal to $+1$ or -1 the body friction plates will slide in positive or negative direction, respectively. Likewise, the nonsliding phase in the upper friction plate continues as long as the criterion

$$|\ddot{s} + \ddot{x}_g + \textstyle\sum_{i=1}^{n} \alpha_i \ddot{x}_i| < \mu g \ , \tag{2.34}$$

holds. Sliding starts when the lefthand side of (2.34) becomes equal to μg, and

$$\widehat{sgn}(0) = - \frac{\ddot{s} + \ddot{x}_g + \sum_{i=1}^{n} \alpha_i \ddot{x}_i}{\mu g} \ , \tag{2.35}$$

gives the sliding direction of the upper friction plate.

For a proper operation of the SR-F base isolators, the friction coefficient of the upper friction plate, μ, has to be larger than that of the body friction plates, μ_1. Under this condition, a motion in which the upper plate is sliding while the body plate are sticking to each other is rather unlikely to occur. Such a state of motion is only possible under exceptional cases when μ and μ_1 are close to each other and rather large amount of residual displacement exists in the body of the isolator.

During the fully sliding phase, whenever $(\dot{s} - \dot{y})$ becomes zero the motion of the isolator is replaced by a state of motion for which the body friction plates are sliding while the upper friction plate is sticking. Likewise, whenever $\dot{y}$ becomes zero in the fully sliding phase, the motion of the isolator is replaced by a state of motion for which the body friction plates are sticking while the upper friction plate is sliding. When $\dot{y}$ becomes zero during the sliding of the body friction plates, the inequality

$$|\ddot{y}| \geq 2\mu_1 g \frac{M}{m_b} \tag{2.36}$$

is checked to determine the subsequent behavior. If the inequality given by (2.36) holds, body friction plates reverse their sliding directions without stick. In this case,

Eqs.(2.27) and (2.28) continue to govern the subsequent motion of the SR-F isolator with $\widehat{sgn}(\dot{y})$ taking the sign of $\ddot{y}$ at this transition moment. If inequality (2.36) does not hold, a transition to fixed-base motion occurs.

In the subsequent analysis, unless stated otherwise the values of $\mu_1 = 0.05$, $\mu = 0.2$, $\zeta_o = 0.08$, and a natural period of $T_o = 4\ sec$ ($\omega_o = \pi/2\ \ rad/sec$) are used.

SECTION 3

TECHNIQUES OF SOLUTION

In this section, the structural model is described, and the procedure of numerical evaluation is discussed. A three-story building as shown in Figure 2-1 is used as the structural model. The corresponding mass, damping, and stiffness matrices are given in Appendix B. It is assumed that the masses of different floors and the base raft are identical and the stiffness and damping of columns of various stories are also equal. The natural frequencies of the structure are evaluated and the modal equations and modal matrix are listed in Appendix B. Accordingly,

$$\omega_2 = 2.802\ \omega_1\ , \quad \omega_3 = 4.049\ \omega_1\ , \tag{3.1}$$

and

$$\zeta_2 = 2.802\ \zeta_1\ , \quad \zeta_3 = 4.049\ \zeta_1\ , \tag{3.2}$$

where ω is the natural circular frequency, ζ is the modal damping ratio and subscripts $1, 2$, and 3 identify the mode of vibration. The fundamental natural period $T_1 = 2\pi\omega_1$ is varied between 0.1 to 1 *sec* to cover the range of stiff to flexible structures. Numerical results are also presented for the extreme case of $1\ sec < T_1 \leq 4\ sec$ in order to better understand the interaction between highly flexible structures and various base isolation systems. Except for the section on sensitivity analysis of the effects of variation of ζ_1, a damping ratio of 0.02 for the fundamental mode is used throughout this study.

The values of natural periods T_o, damping ratios ζ_o, and friction coefficients μ (or μ_1) of the isolators studied are summarized in Table 3-1. These values are used throughout this work except for the sections on sensitivity studies. In these cases, the value of one particular parameter is varied while for the others which are kept fixed the values listed in Table 3-1 are used.

Based on the fourth order Runge-Kutta scheme, a double precision FORTRAN routine for numerical evaluation of the equations of motion is developed. A time step of $\Delta t = 0.00025\ sec$ is used in the continuous phases of motion away from the transitions. The accuracy of the results is verified by comparing the results with those obtained by finer time steps on several occasions. For frictional systems, the

Table 3-1 Values of Parameters Used for Various Base Isolators

Base Isolation System	Natural Period T_o (sec)	Damping Ratio ζ_o	Friction Coefficient μ (μ_1/μ)
Pure-Friction (P-F)	–	–	0.1
Larminated Rubber Bearing (LRB)	2	0.08	–
Resilient-Friction (R-FBI)	4	0.08	0.05
Electricite de France (EDF)	1	0.08	0.2
New Zealand (NZ)	2	0.08	–
Sliding Resilient Friction (SR-F)	4	0.08	0.05/0.2

precise evaluation of the time of phase transitions are crucial to the accuracy of response analysis. Therefore, a successive time-step-cutting procedure is used to approach each of these transitions with an accuracy of 10^{-10} m/sec^2 in evaluating the stick-slip criteria and an accuracy of 10^{-10} m/sec in evaluating the zeros of $\dot{s}$ (or $\dot{s} - \dot{y}$ and $\dot{y}$ for the EDF and the SR-F systems). In this fashion, the time of transition is accurately determined, and based on the appropriate criteria, the equations governing the subsequent phase are specified. It should be noted here that the compact form of the equations of motion presented earlier are not quite suitable for a direct Runge-Kutta integration scheme. This is because the second derivative terms (i.e., the accelerations $\ddot{s}$ and $\ddot{x}_i$) appear also on the righthand side of these equations and they can not be written conveniently in the state variable form. Therefore, the equations of motion are rearranged in such a way that the accelerations terms appeared explicitly on the lefthand side of the equations before the Runge-Kutta scheme is applied. As an example, the rearranged form of the equations for the R-FBI system used in the numerical evaluation are listed in Appendix C.

A sinusoidal ground excitation given as

$$\ddot{x}_g = a \ sin(\frac{2\pi t}{T_g}), \tag{3.3}$$

is used throughout this work. Unless stated otherwise, a ground period of $T_g = 0.8$ sec and an amplitude of $a = 0.5g$ are employed. The time duration of excitation is taken to be 8 sec which covers ten complete cycles and the response approaches a nearly quasi-steady state limit. Several numerical experiments are also carried out for larger time durations but no noticeable change in the peak responses are observed. Therefore, it is concluded that a ten cycle duration is sufficient for the determination of the peak responses.

The responses of the three-story structure with various base isolators are evaluated. The peak absolute accelerations for various floors, $(\ddot{x}_g + \ddot{s} + \ddot{x}_i)|_{max}$, the peak deflection, $x_3|_{max}$, the peak relative base displacement, $s|_{max}$, for different period ratios, T_1/T_g, are evaluated. A series of sensitivity studies on the effects of variations of parameters of the isolators and the structure are carried out. The effects of the velocity-dependent friction coefficient are also studied. Unless stated otherwise a structure with a fundamental natural period of 0.3 sec is considered, and the peak responses are evaluated and discussed. To simulate the effects of the high intensity earthquakes, a sinusoidal ground excitation with $T_g = 0.8$ sec and $a = g$ is used and

the peak responses are plotted versus period ratio, T_1/T_g. In the sensitivity study on the effects of the frequency contents of the ground excitation, a structure with a fundamental natural period of 0.3 *sec* is considered and the period of the sinusoidal excitation, T_g, is varied. A time duration of 10 T_g is usually used for evaluating the peak responses; however, for $T_g < 0.3$ *sec*, a time duration of 3 *sec* is used. The variations of peak responses with T_g are discussed.

SECTION 4

RESPONSE ANALYSIS

In this section, responses of the base isolated three-story structure described earlier subject to a sinusoidal horizontal ground excitation are analyzed. Several different base isolation systems are considered and their performances under a variety of conditions are studied. The acceleration response time histories and their frequency decompositions for the base isolated structure and the fixed-base one are examined. The peak absolute accelerations, the peak displacement, and the peak deflection responses for structures with various base isolation systems under a variety of condition are evaluated and discussed. Several series of sensitivity analyses for variations in damping coefficient of structure, mass ratio, friction coefficient, damping ratio, and natural period of various isolators, and amplitude and period of ground excitation are carried out. The effects of velocity-dependent friction coefficient are also studied.

4.1 Sample Responses

For the purpose of understanding the characteristic behaviors of various base isolation systems, several sample acceleration response time histories of the base isolated structure and their Fourier decompositions are studied. For the isolators, the recommended parameters as listed in Table 3-1 are used. The ground excitation is assumed to be a sinusoidal function with an amplitude of $0.5g$ and a period of 0.8 *sec*. The time histories are evaluated for a structure with a fundamental period $T_1 = 0.3$ *sec* (which corresponds to a period ratio of 0.375). The results are shown in Figures 4-1 through 4-3 and discussed in the sequel.

Figure 4-1 compares the absolute acceleration time histories of the top floor for the fixed-base (F-B) and the base isolated structure. The ground acceleration $\ddot{x}_g$ is also plotted for reference. For the intensity of the ground excitation considered, no sliding in the upper plate of the SR-F base isolation system occurs; thus, the responses of the SR-F system becomes identical to those of the R-FBI system. This figure shows that, the fixed-base structure significantly amplifies the ground acceleration, while the base isolation systems generally reduce the peak accelerations transmitted to the structure. It is also observed that the acceleration responses

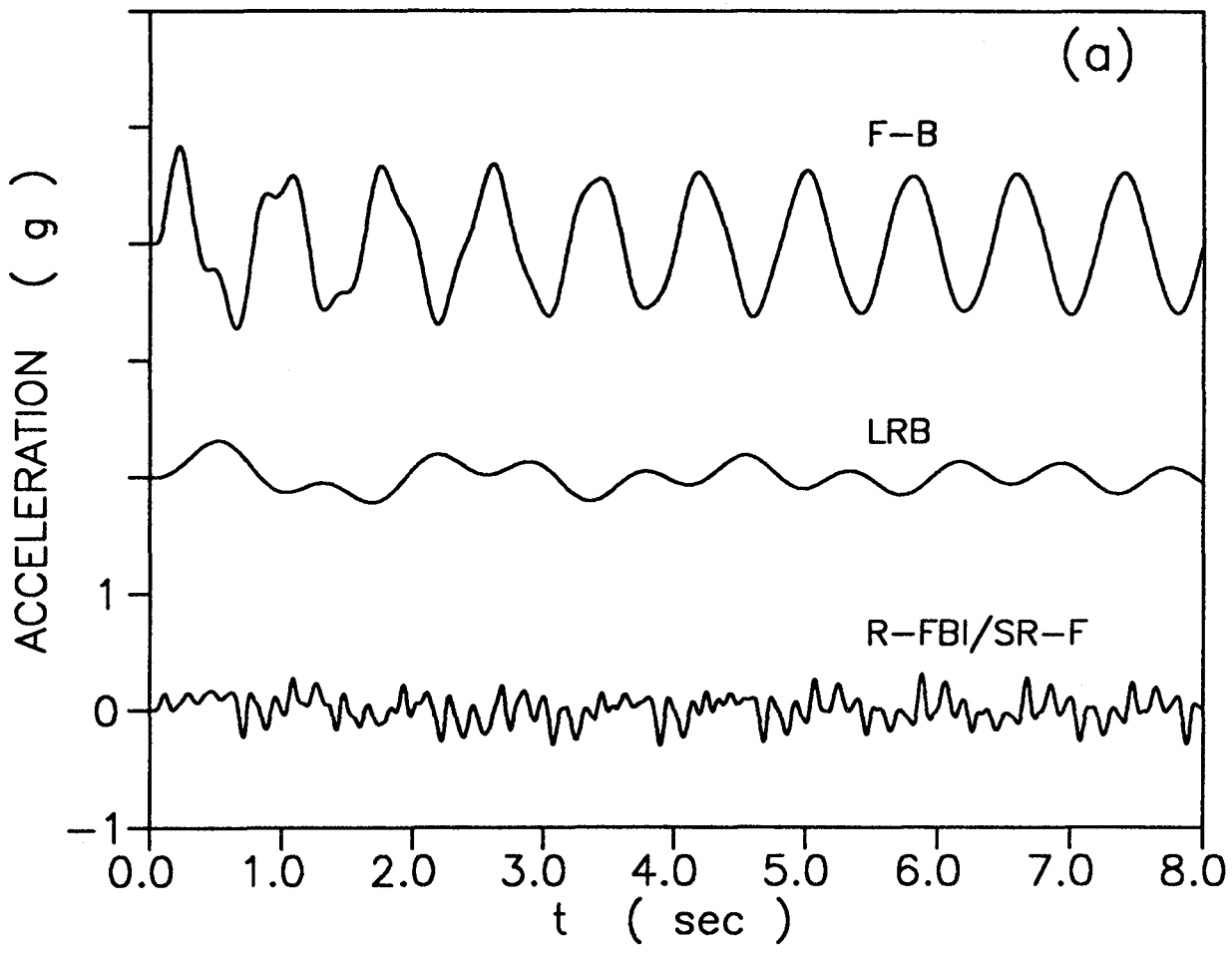

Figure 4–1 Sample Absolute Acceleration Responses at the Top of Structure

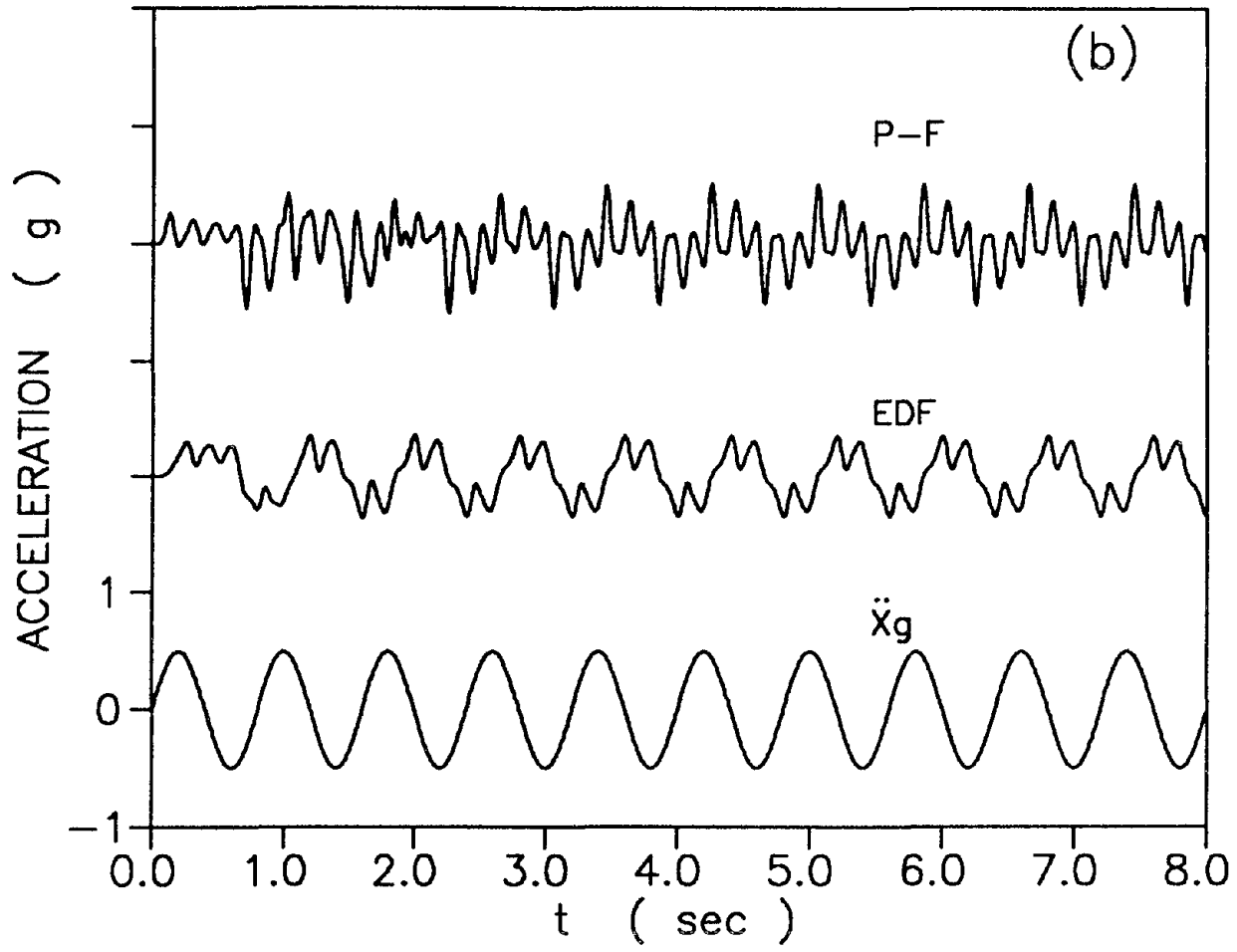
(b)
P–F
EDF
$\ddot{X}_g$
ACCELERATION (g)
1
0
–1
0.0
1.0
2.0
3.0
4.0
5.0
6.0
7.0
8.0
t (sec)

Figure 4–1

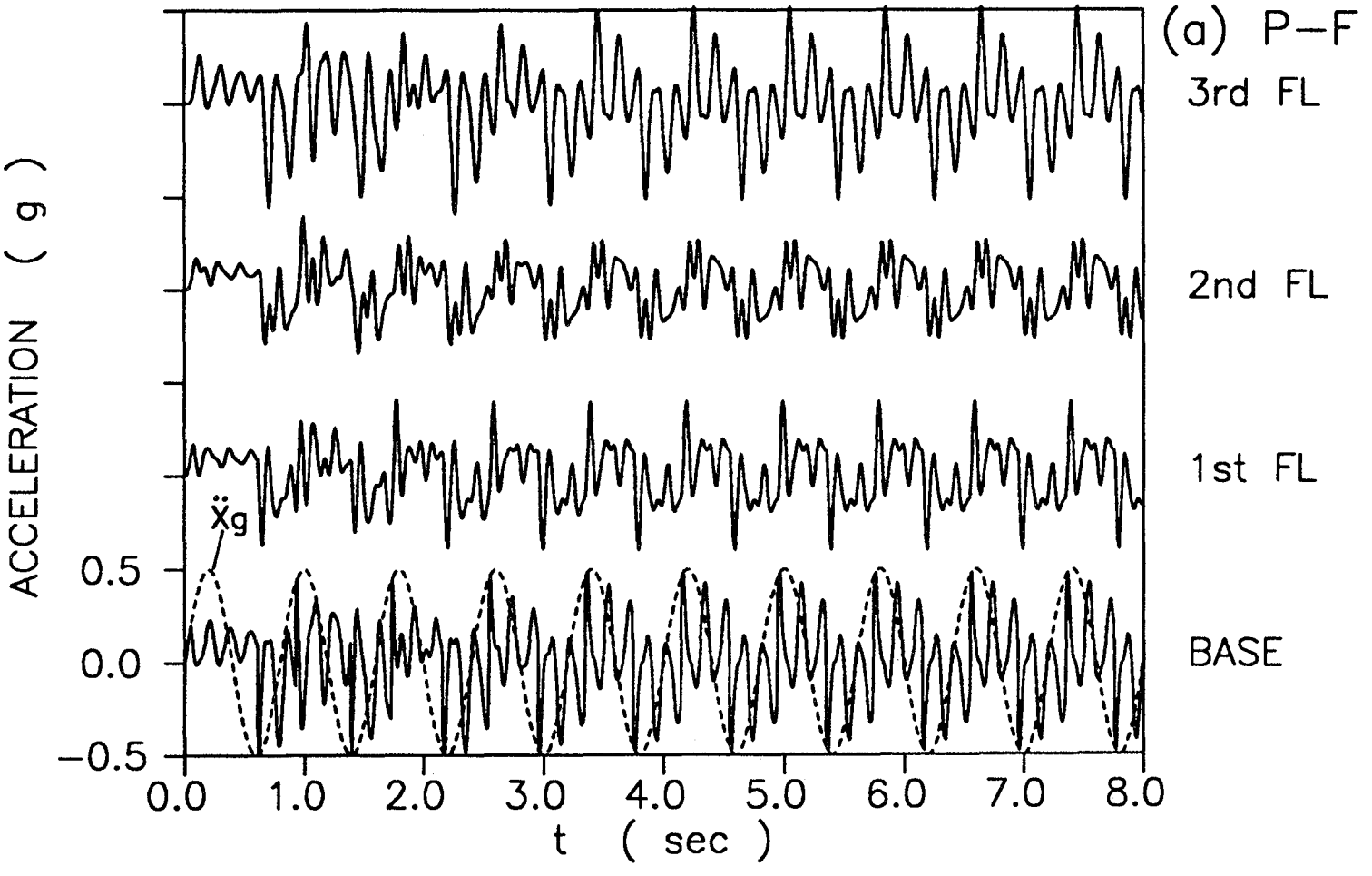

Figure 4–2 Sample Absolute Acceleration Responses at Various Floors for Different Base Isolation Systems

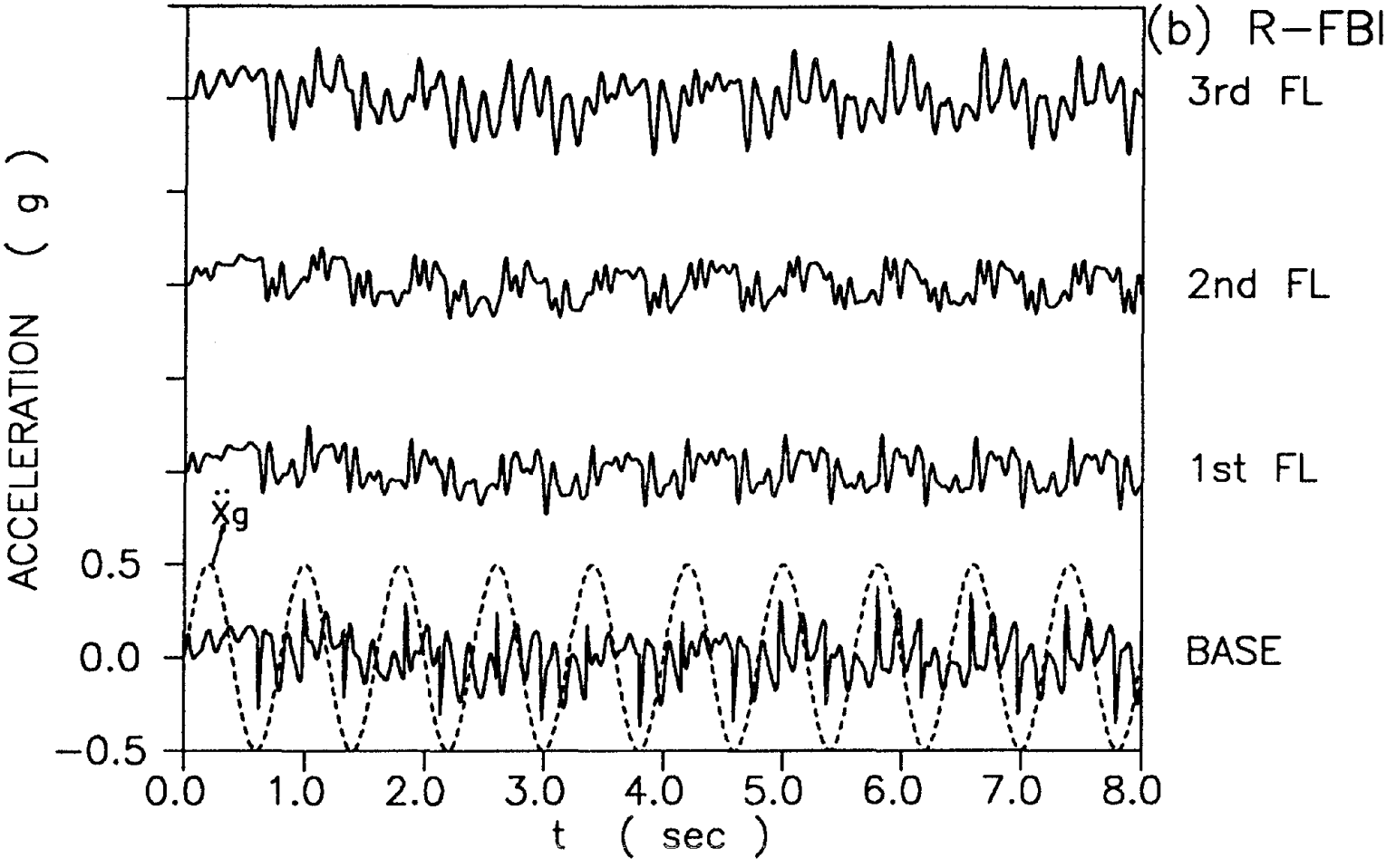
(b) R-FBI
3rd FL
2nd FL
1st FL
BASE
ACCELERATION (g)
0.5
0.0
-0.5
0.0
1.0
2.0
3.0
4.0
5.0
6.0
7.0
8.0
t (sec)

Figure 4-2

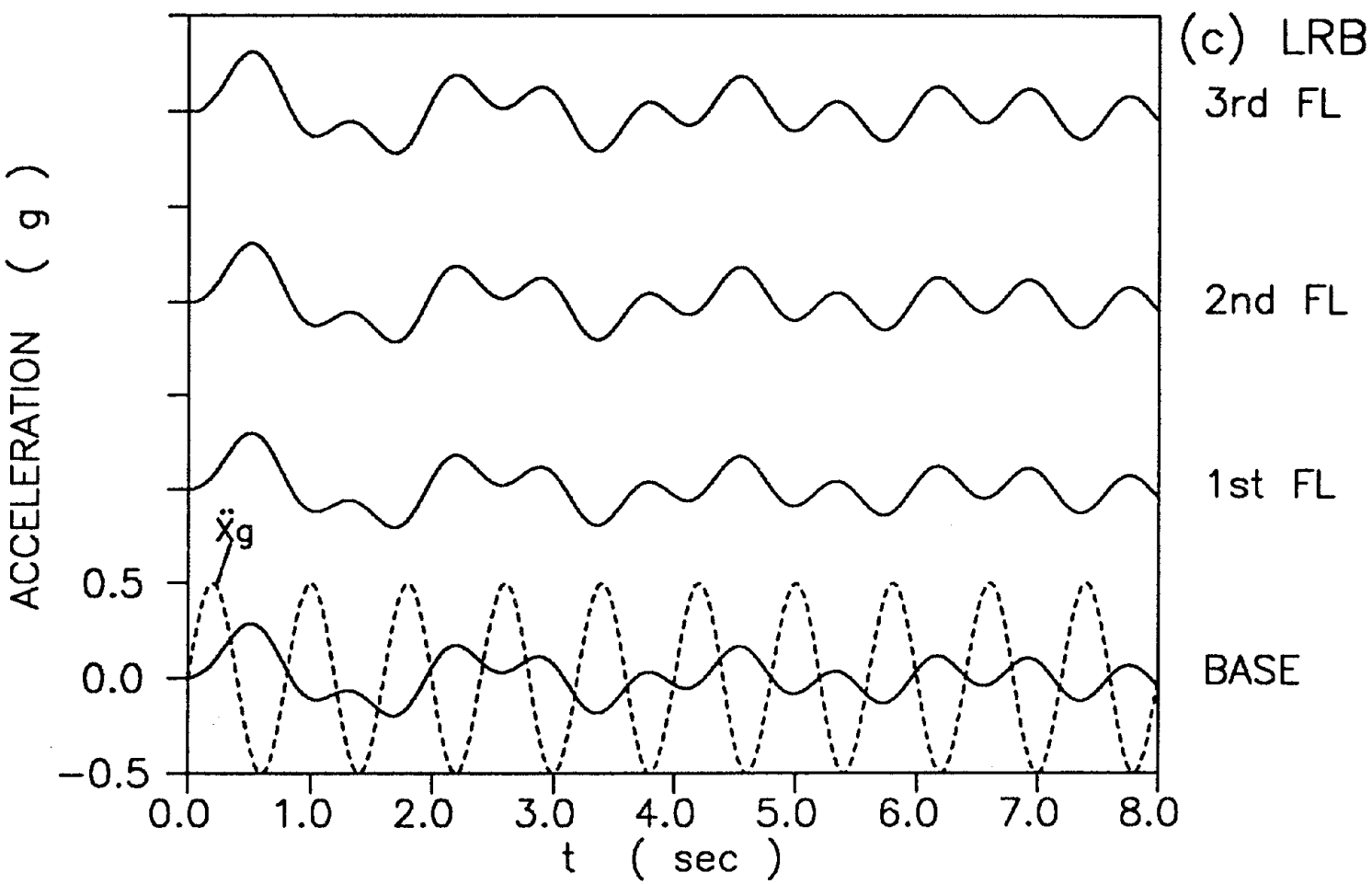
(c) LRB
3rd FL
2nd FL
1st FL
BASE
ACCELERATION (g)
$\ddot{X}_g$
0.5
0.0
−0.5
0.0
1.0
2.0
3.0
4.0
5.0
6.0
7.0
8.0
t (sec)

Figure 4–2

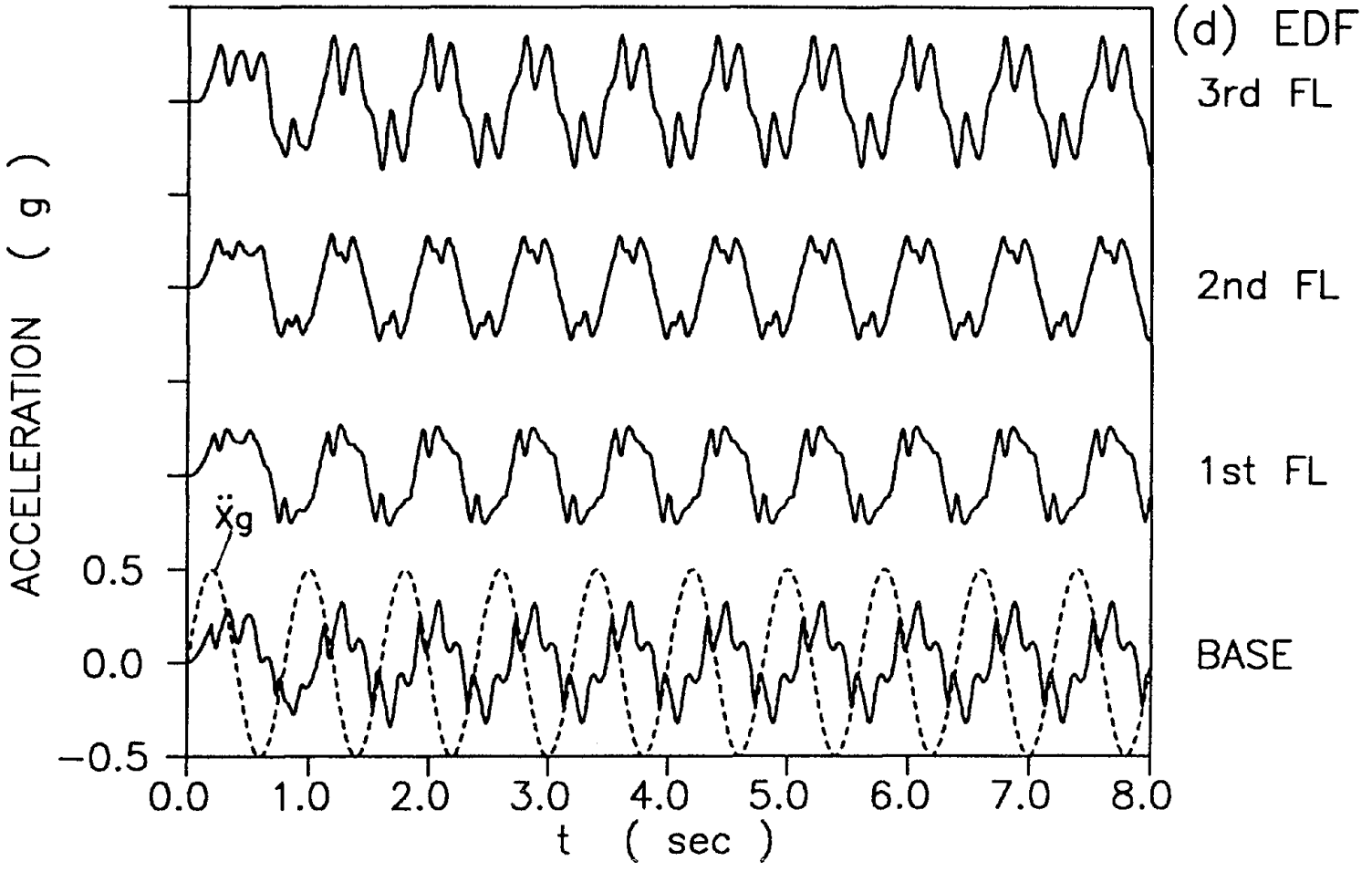
(d) EDF
3rd FL
2nd FL
1st FL
BASE
ACCELERATION (g)
$\ddot{X}_g$
0.5
0.0
−0.5
0.0
1.0
2.0
3.0
4.0
5.0
6.0
7.0
8.0
t (sec)

Figure 4–2

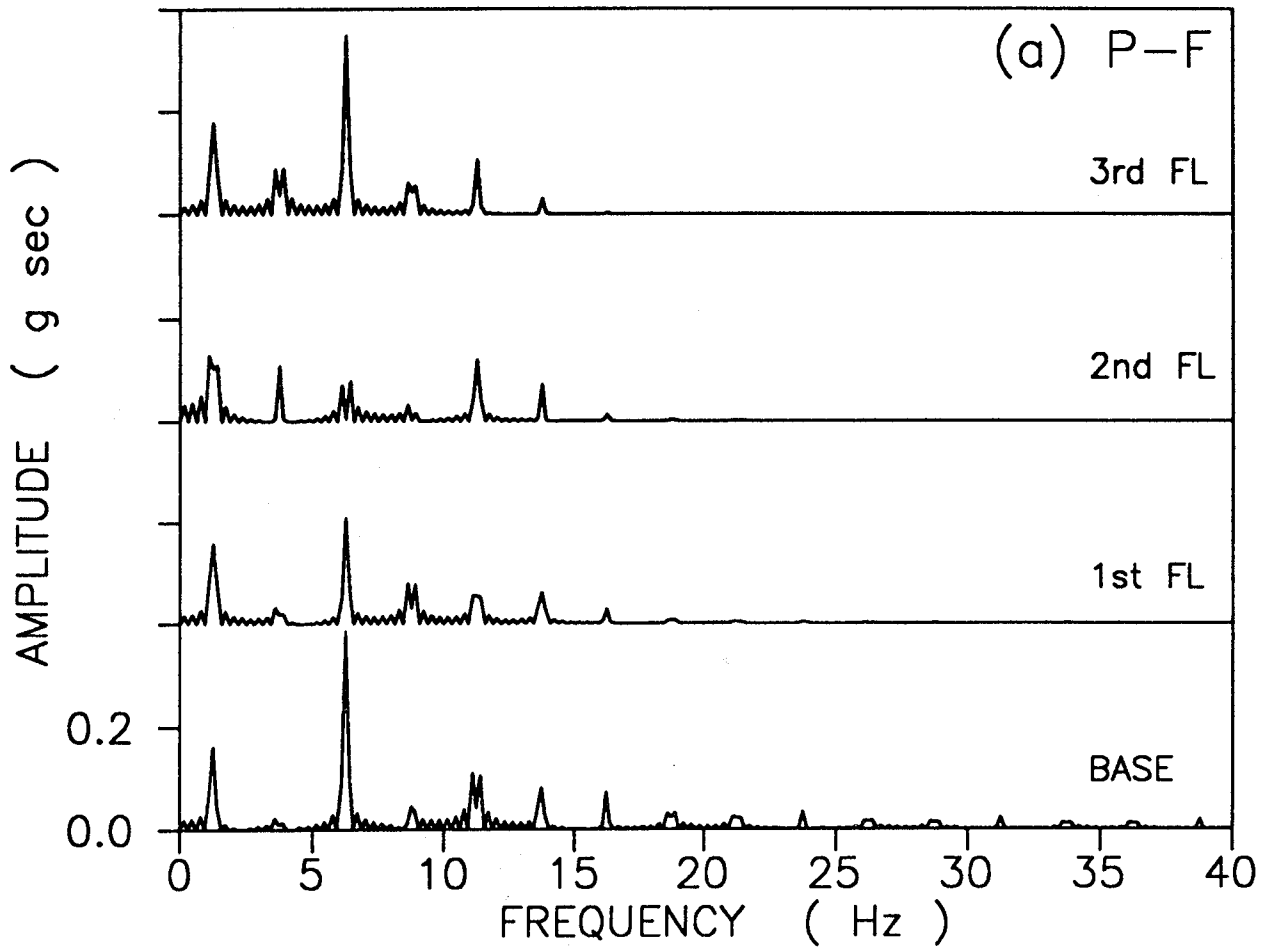

Figure 4-3 Fourier Spectra of Acceleration Response at Various Floors

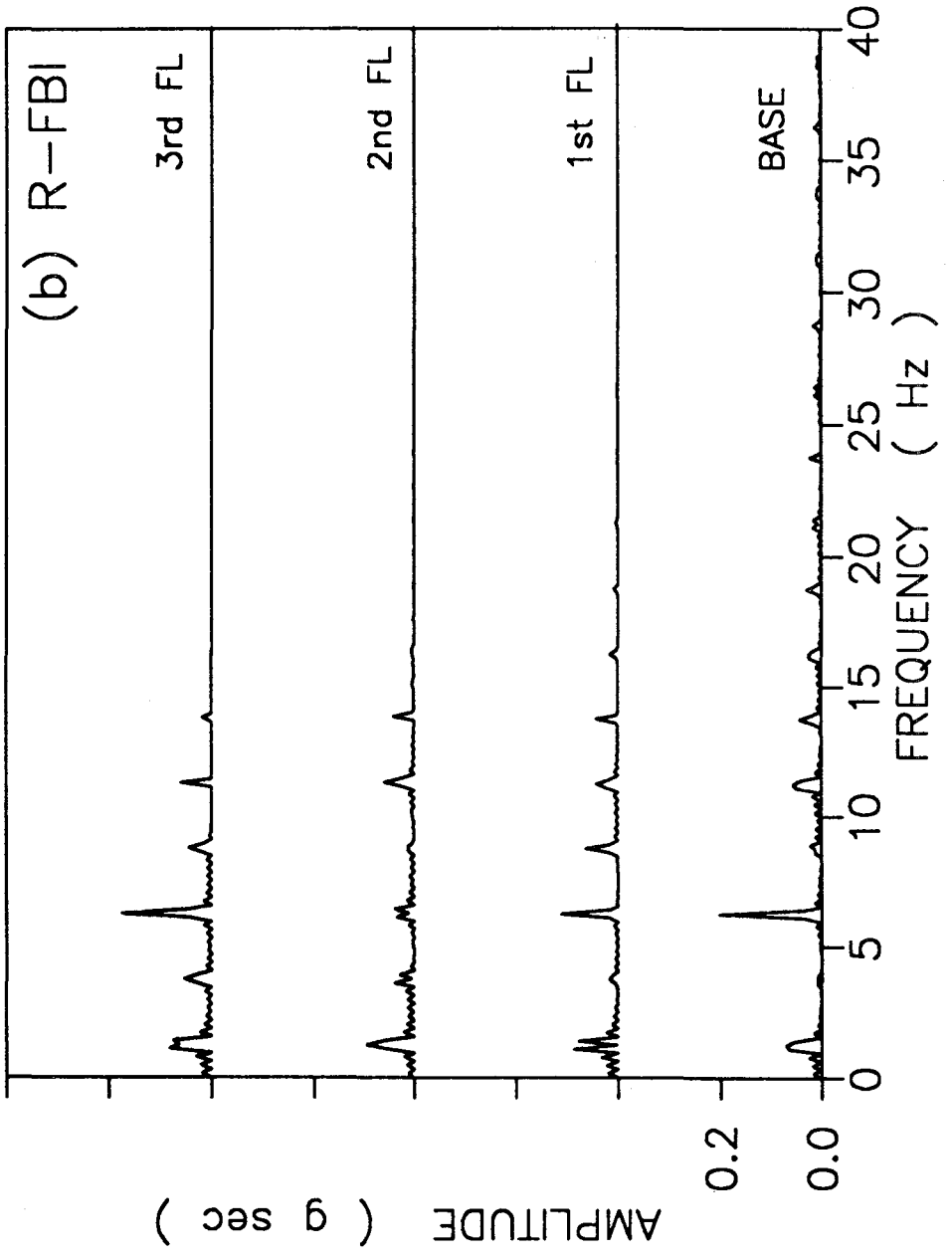
(b) R-FBI
3rd FL
2nd FL
1st FL
BASE
AMPLITUDE (g sec)
0.0
0.2
0
5
10
15
20
25
30
35
40
FREQUENCY (Hz)

Figure 4-3

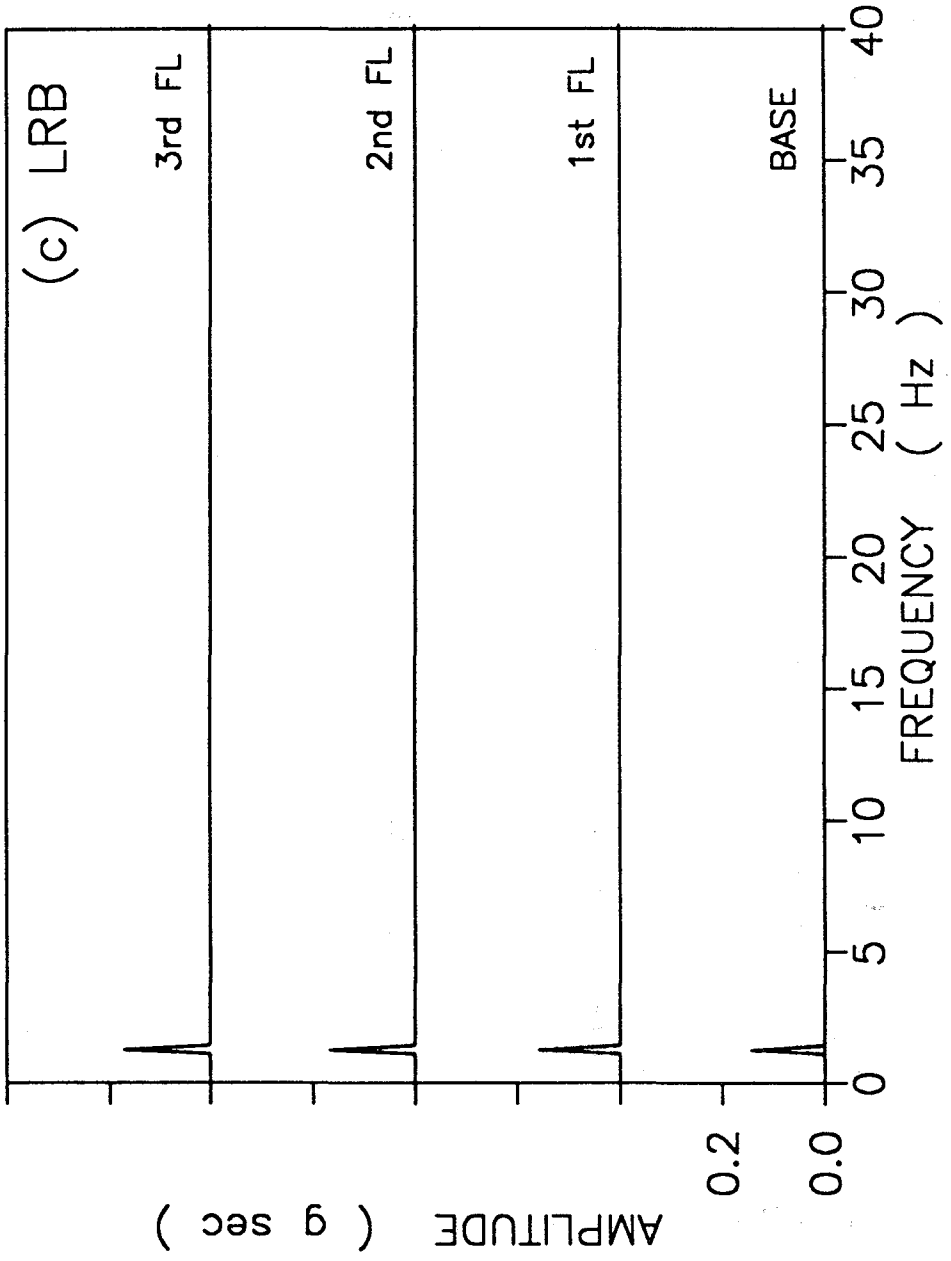
(c) LRB
3rd FL
2nd FL
1st FL
BASE
AMPLITUDE (g sec)
0.0
0.2
0
5
10
15
20
25
30
35
40
FREQUENCY (Hz)

Figure 4–3

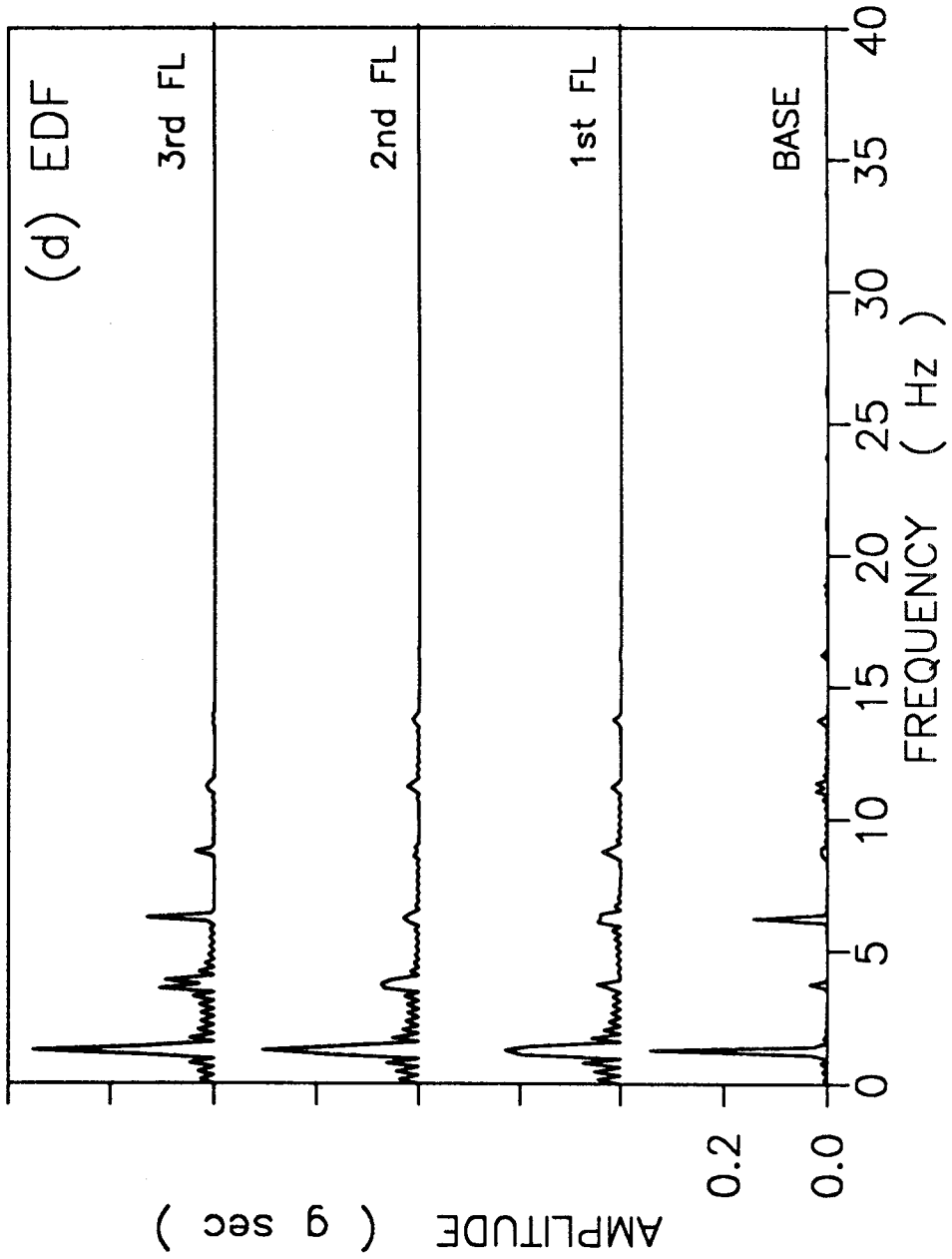
(d) EDF
3rd FL
2nd FL
1st FL
BASE
AMPLITUDE (g sec)
0.0
0.2
0
5
10
15
20
25
30
35
40
FREQUENCY (Hz)

Figure 4–3

of the fixed-base structure, and a structure with the LRB system, show relatively smooth time variations. While, the acceleration time histories of a structure with the P-F isolator or the R-FBI/SR-F systems show many sharp peaks. These sharp peaks are generated by the slip-stick and the reversal transitions for which the discontinuous changes of friction force exert shock loadings on the base of the structure. The continuous but nonlinear stick-slip transitions of the P-F and the R-FBI/SR-F systems also generate high frequency wiggles in the absolute acceleration time histories. From Figure 4-1b, it is observed that the acceleration response for the EDF base isolator shows a somewhat smoother response in comparison to those of the P-F and the R-FBI/SR-F systems. This is because the slip-stick transitions of the EDF system do not generate discontinuities in acceleration, and therefore, no shock force acts on the structure. Nevertheless, the continuous but nonlinear stick-slip transitions still generate high frequency wiggles in its acceleration response time histories.

Figure 4-2 shows sample absolute acceleration time histories of various floors for different base isolation systems. Many features of the responses of the structure with various isolation systems may be studied from these figures. The acceleration time histories of various floors for the P-F base isolator are shown in Figure 4-2a. It is observed that acceleration response of the base contains a large number of sharp pulses. Peaks of some of these acceleration pulses become identical to the ground acceleration level for short time durations. These pulses are due to the slip-stick and stick-slip transitions. As expected, during the stick period the acceleration of the base becomes identical to $\ddot{x}_g$. Figure 4-2a also shows that as the acceleration is transmitted to the higher floors certain modifications occur. The pulses become somewhat broader and their peaks become smoother. Except for reduction of the peaks of the pulses, the acceleration is amplified. From Figure 4-2a, one finds that the peak absolute acceleration of the third floor is highest while that of the second floor is the lowest. This is because the acceleration responses of the base and the first floor contain sharp peaks which are somewhat smoothed out in the acceleration record of the second floor. The amplifying effects of the structure makes the peak acceleration of the third floor larger than the others.

Figure 4-2b shows the floor acceleration time histories for the R-FBI system. Like that of the P-F base isolator, the base acceleration time history contains sharp

pulses. However, the acceleration transmitted to the base and, in particular, the amplitude of the acceleration pulses are much lower than those of the P-F base isolator. Furthermore, unlike the P-F system, the peaks of the acceleration pulses for the base do not reach the value of $\ddot{x}_g$. This means that the criterion given by (2.8) holds for all motion transitions occurred in this case, and the structure reverses the direction of sliding without sticking to the foundation. From Figure 4-2b, it is also noticed that the acceleration levels remain the same or amplify slightly as transmitted through the floors. Furthermore, the sharp pulses of the base acceleration time history become much smoother at the higher floors. As a result, the peak acceleration at the top floor is somewhat less than that of the base for the record shown in Figure 4-2b. From these results, it may be concluded that the structure in this case behaves approximately as a rigid body. As mentioned earlier, for this level of excitation, no sliding in the upper plate of the SR-F base isolator occurs and hence its behavior is identical to that of the R-FBI system.

Figure 4-2c shows the acceleration time histories of various floors for the LRB base isolator. It is observed that the absolute accelerations of various floors and the base are almost identical. This implies that the structure responds in its rigid body mode. This behavior is as expected, since the horizontal stiffness of the isolator is much lower than that of the structure. From Figure 4-2c, it is also observed that the acceleration responses are quite smooth and devoid of high frequency pulses observed for the frictional systems. The acceleration time histories for the NZ system are quite similar to those of the LRB system and hence are not shown here.

Figure 4-2d shows the acceleration responses of various floors for the EDF system. It appears that the base acceleration contains the high frequency wiggles generated by the motion transitions. However, the sharp pulses observed for the P-F and the R-FBI systems are absent. This figure also shows that the shape of the acceleration wave is modified as it is transmitted through different floors, while its peak remains almost the same or increases slightly.

To quantify the frequency content of the acceleration responses presented in Figure 4-2, the Fourier transform technique may be used. In the followings, the Fourier decompositions of the acceleration responses are presented and discussed. For $t > 16$ *sec*, for which the responses reach quasi-steady periodic states, segments of four periods of acceleration sample responses are considered and the IMSL Fast

Fourier Transform routine FCOST [30] is used in these analyses. Figure 4-3 shows the Fourier spectra of the acceleration responses at different floors for various base isolation systems. The intervals of frequency presented in these figures are about 0.156 Hz.

The Fourier spectra of the acceleration responses at various floors for the P-F base isolation system are presented in Figure 4-3a. This figure shows that the acceleration spectra contain sharp peaks at certain distinct frequencies. A careful examination of the figure shows that the energy containing frequencies are located at $(2n-1)\ f_g,\ n = 1, 2, 3, ...$, where $f_g = 1/T_g$ is the frequency of ground excitation which is 1.25 Hz for the present case. The lowest frequency is that of ground excitation, and the friction force generates higher energy containing frequencies which are odd multiples of this frequency. Figure 4-3a also shows that the Fourier amplitudes at frequencies higher than 20 Hz vanish rapidly as the acceleration is transmitted from the base to the upper floors. This results is consistent with the observation made earlier from Figure 4-2a that the peaks of acceleration time history becomes broader and smoother as it is transmitted to the upper floors. It is also noticed that, as the acceleration is transmitted through various floors, the amplitudes of the peaks are modified significantly; however, the energy containing frequencies do not change. Furthermore, frequencies of 1.25 Hz and 6.25 Hz are dominant for these acceleration responses.

Figure 4-3b shows the Fourier spectra at various floors for the R-FBI system. The general features are similar to those observed for the P-F system. The acceleration response of the base floor contains a broad spectrum which is sharply peaked at distinct frequencies of $(2n-1)\ f_g$. The energy contained in the high frequency range decays rapidly as the acceleration is transmitted to the upper floors. It is also observed that amplitudes of the acceleration spectra for the R-FBI system are much lower than those for the P-F isolator.

Figure 4-3c shows the Fourier spectra of acceleration response at various floors for the LRB base isolation system. Unlike the frictional systems, there is only one peak occurring at frequency of 1.25 Hz. This clearly shows that , the LRB system does not alter the frequency of ground excitation.

Figure 4-3d displays the Fourier spectra of various floors for the EDF system. It is observed that these acceleration spectra combine the features of the frictional

and the LRB base isolators. While the peaks at frequency of 1.25 Hz are dominant, additional energy containing high frequencies appear in the Fourier spectra of the EDF system. These high frequencies are identical to those of the P-F and the R-FBI systems.

Based on the results presented in Figures 4-1 through 4-3, it is noticed that the peak acceleration transmitted to the base of the structure is generally lower than that of the ground excitation. The isolated structure generally responds approximately in its rigid body mode and, unlike the fixed base structure, do not amplify the ground acceleration to a significant extent. Furthermore, the Fourier analyses show that the frictional systems scatter energy into high frequency regions in the transmitted acceleration responses.

4.2 Comparative Study

Using a ground acceleration with an amplitude of $0.5g$ and $T_g = 0.8$ sec, the performances of various base isolation systems are evaluated and the resulting response spectra are described in this section of the study. The parameters of the base isolation systems studied are selected within the range of recommended values and are listed in Table 3-1.

The variations of the peak absolute acceleration at the top of the structure, $(\ddot{x}_g + \ddot{s} + \ddot{x}_3)|_{max}$, the peak relative base displacement, $s|_{max}$, the peak deflection, $x_3|_{max}$, versus period ratio, T_1/T_g, for various base isolation systems are shown in Figures 4-4 through 4-6. The corresponding responses of the fixed-base structure are also plotted in these figures for comparison. As noted earlier, for the ground excitation considered, no sliding on the upper friction plate of the SR-F system occurs; hence, the peak responses of the SR-F and the R-FBI systems coincide.

Comparing the acceleration response spectra of the fixed-base structure with those of the isolated structures as shown in Figure 4-4, it is observed that all base isolation systems considered here reduce the peak accelerations significantly. In particular, this figure shows the acceleration resonance peak of the fixed-base structure is reduced by a factor more than ten. This is perhaps the most attractive feature of using base isolation systems. For period ratios less than one, the peak accelerations for the LRB, the NZ, and the R-FBI/SR-F systems are about $0.3g$ to $0.4g$ and the structure behaves approximately as a rigid body. The P-F system (with

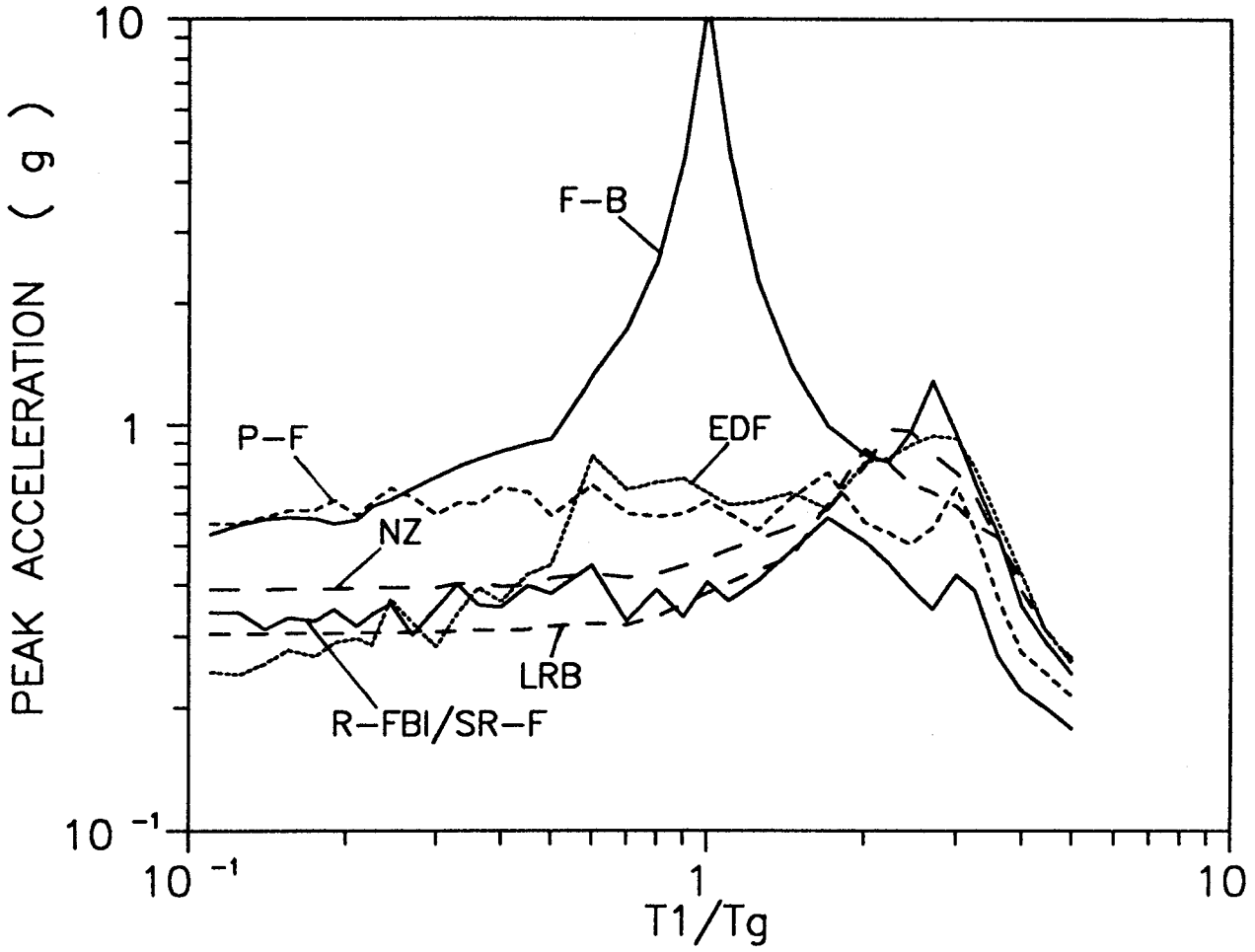

Figure 4-4 Variations of Peak Absolute Acceleration at the Top of Structure with Period Ratio

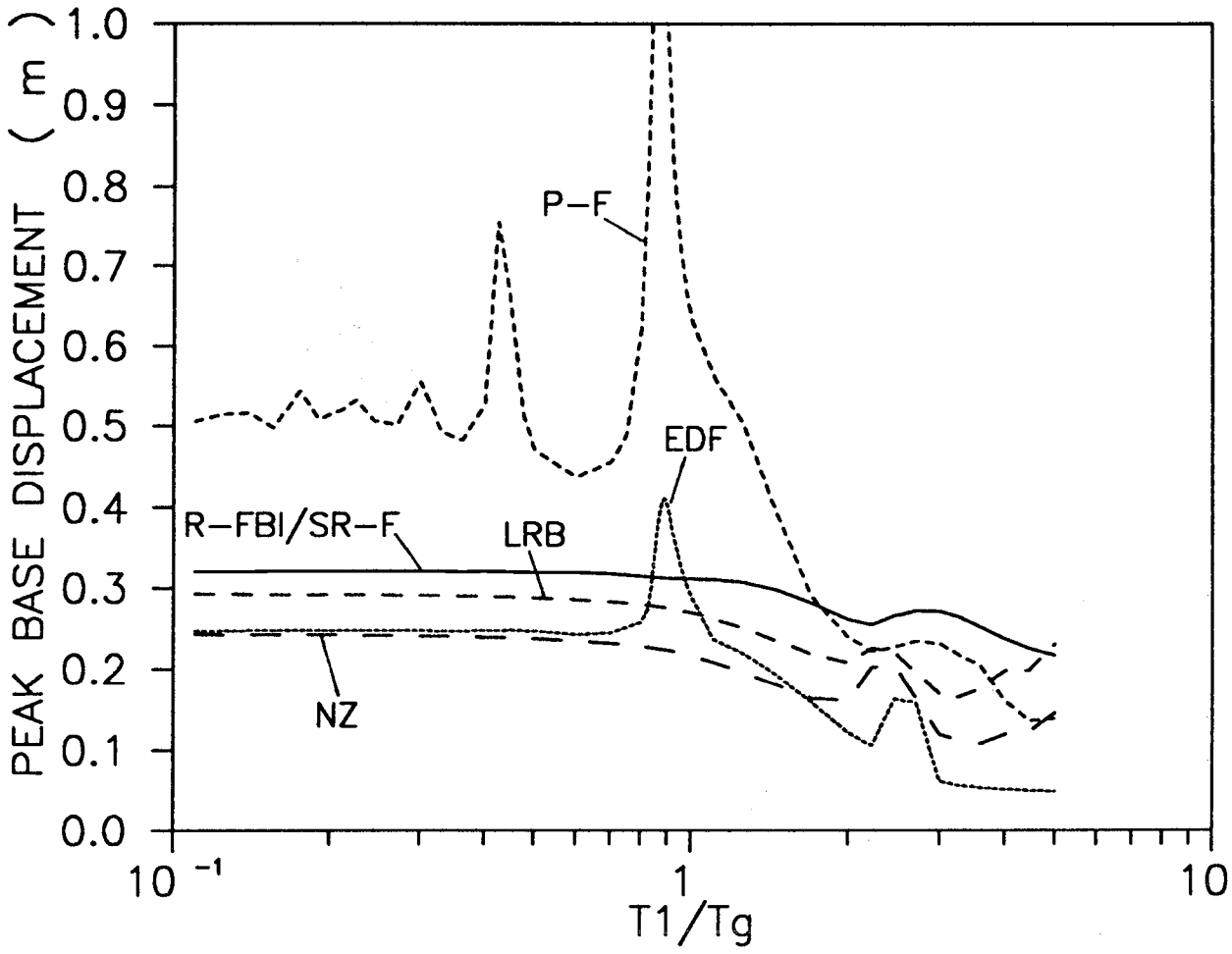

Figure 4-5 Variations of Peak Base Displacement with Period Ratio

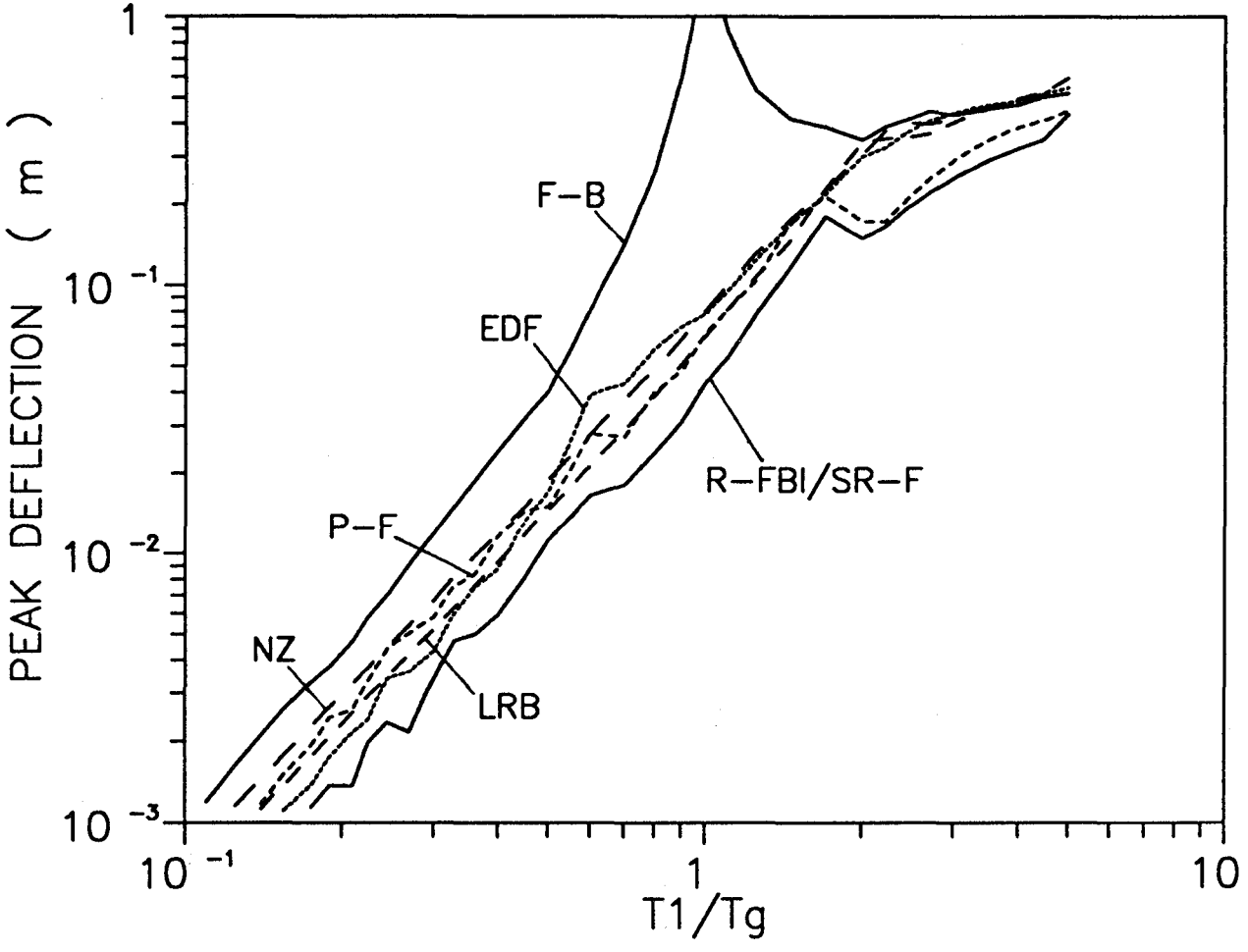

Figure 4-6 Variations of Peak Deflection with Period Ratio

$\mu = 0.1$) transmits an acceleration of about $0.6g$ which is generally higher than those of other isolators in the entire range of $T_1/T_g < 2$. For period ratios less than 0.5, the maximum acceleration for the EDF system is about $0.25g$ to $0.4g$ which is comparable with those of the LRB, the NZ, and the R-FBI/SR-F systems. However, in the range $0.6 < T_1/T_g < 2$, the acceleration spectrum of the EDF system jumps to about $0.7g$ which is even higher than that of the P-F system. It is also observed that the spectrum of the fixed-base structure shows a secondary peak at about $T_1/T_g = 2.8$. This is due to the resonance between the second mode of the structure (with $T_2 \simeq T_1/2.8$) and the ground excitation ($T_g = 0.8\ sec$). For period ratios about 1.5 to 3.5, the peak absolute acceleration responses of the LRB, the NZ, and the EDF systems increase partly due to the resonance of the second mode and partly due to the structure-isolator interactions.

From Figure 4-5, it is observed that the maximum relative base displacements of the NZ, the LRB, and the R-FBI/SR-F systems are roughly constant in the entire range of $T_1/T_g < 1$ with magnitudes about 0.25 m to 0.32 m. That is, in this respect, the isolated structure behaves essentially as a rigid body in this range. The P-F isolator shows a larger level of base displacement of the order of 0.5 m and shows a sharp peak of more than 1 m for a period ratio of about 0.9. There seems to be a sort of resonance of the fundamental mode of the structure with ground excitation for the base displacement, while no peaks exist in the corresponding acceleration or deflection response spectra curves. A similar peak is also observed for the EDF base isolator with a maximum of about 0.4 m. The peak base displacement for the EDF isolator is quite low and is about 0.25 m away from this resonance peak.

As mentioned before, the maximum deflection is directly proportional to the column stresses of the structure. An excessive column stress is one main source of damage to the structure during a strong earthquake. Figure 4-6 shows the maximum deflection, $x_3|_{max}$, versus period ratio T_1/T_g. As expected, the maximum deflection increases as the flexibility of the structure increases. The maximum deflection of the fixed-base structure shows a very large peak (more than a few meters) at the resonance condition. The deflection response spectra curves for the isolated structure are generally much lower than that of the fixed base one and do not show sharp peaks at $T_1/T_g = 1$. At the resonance condition, $x_3|_{max}$ for the R-FBI/SR-F systems is only about 4 cm. The other isolators lead to a peak deflection of about 6 to 8 cm.

That is, the column stresses for the structure isolated by the R-FBI/SR-F systems is less than half of those isolated by the other base isolators. It is perhaps of interest to emphasize that the peak absolute acceleration levels shown in Figure 4-4 for the R-FBI/SR-F and the LRB systems are comparable; therefore, the peak forces exerted at different floors are about the same for these systems. Nevertheless, the column stresses for the R-FBI/SR-F base isolation systems are about half of those for the LRB. The reason for this apparent discrepancy is that the acceleration response time histories for the R-FBI/SR-F systems contains short duration sharp peaks. These acceleration pulses, however, have negligible energy and do not generate high stresses in the structure.

The peak absolute acceleration responses of various floors are plotted versus T_1/T_g in Figure 4-7. Figure 4-7a shows the acceleration response spectra for the fixed-base structure. The constant peak base acceleration of $0.5g$ is also shown in this figure for reference. It is noticed that the peak acceleration responses of the upper floors are generally higher than those of the lower floors. This clearly shows the amplifying effects of the structure. From Figure 4-7a, it is also observed that the response spectra curves have a rather high resonance peak at $T_1/T_g = 1$; in particular, the magnitude of the resonance peak for the third floor is more than $10g$. This figure also shows that for flexible structures, the peak acceleration responses of the lower floors could become comparable or larger than those of the upper floors. As mentioned before, the appearance of secondary peaks at period ratio of about 2.8 in Figure 4-7a are due to the resonance of the second mode of the structure with the ground excitation.

Figures 4-7b through f compare the acceleration response spectra at different floors for the base isolated structure. These figures show that the sharp resonance peak of the fixed-base structure totally disappears which is the most striking feature of using a base isolation system. Furthermore, the peak accelerations at various floors of the isolated structure remain almost the same and do not vary appreciably with T_1/T_g.

Figure 4-7b shows the peak acceleration responses at various floors for the P-F base isolator. As mentioned earlier, the presence of the motion transition shock loadings accompanied with damping and amplifying effects of the structure form the dominant features of the acceleration response time histories for the P-F isolator. For

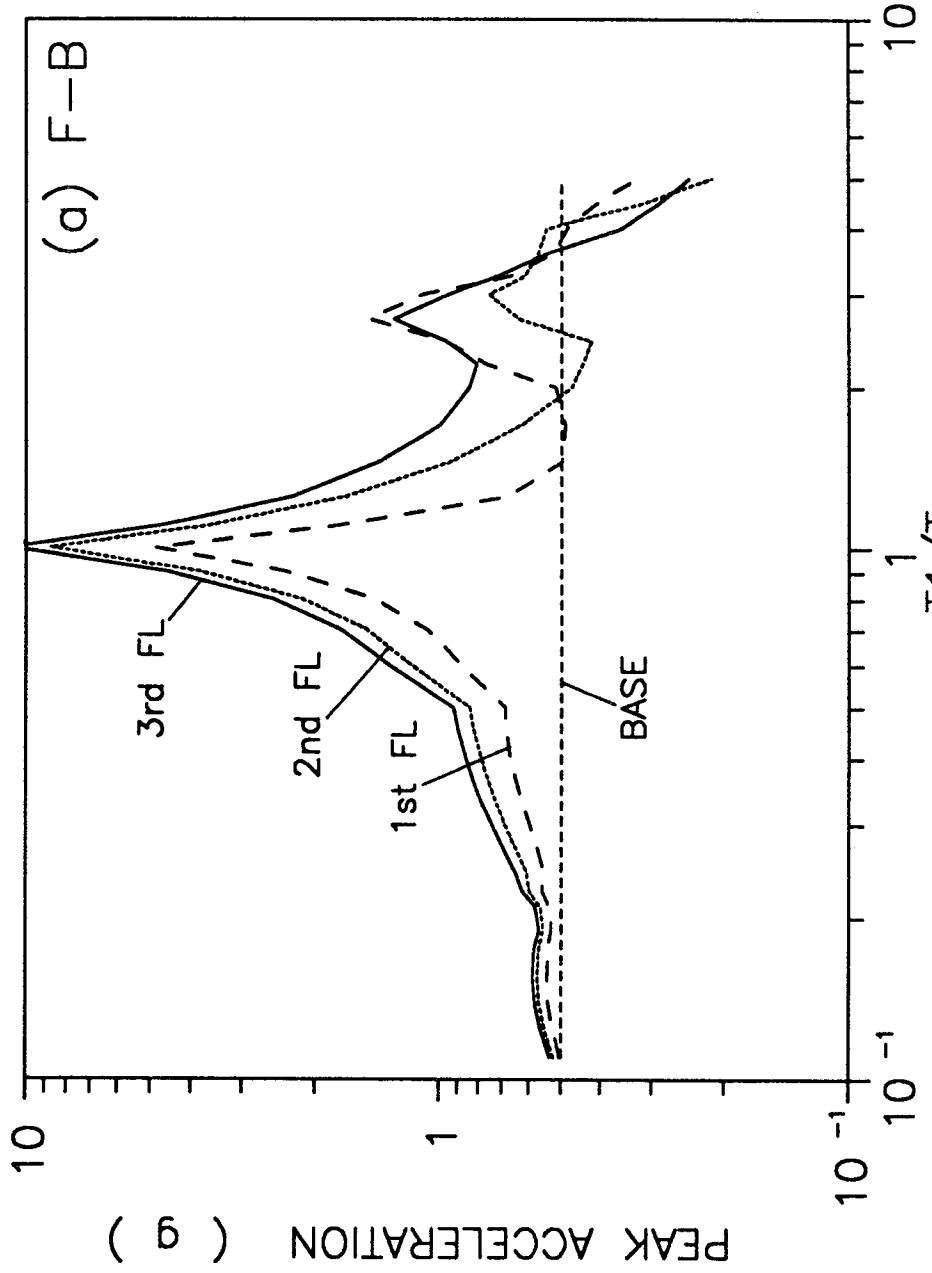

Figure 4-7 Variations of Peak Absolute Acceleration at Various Floors

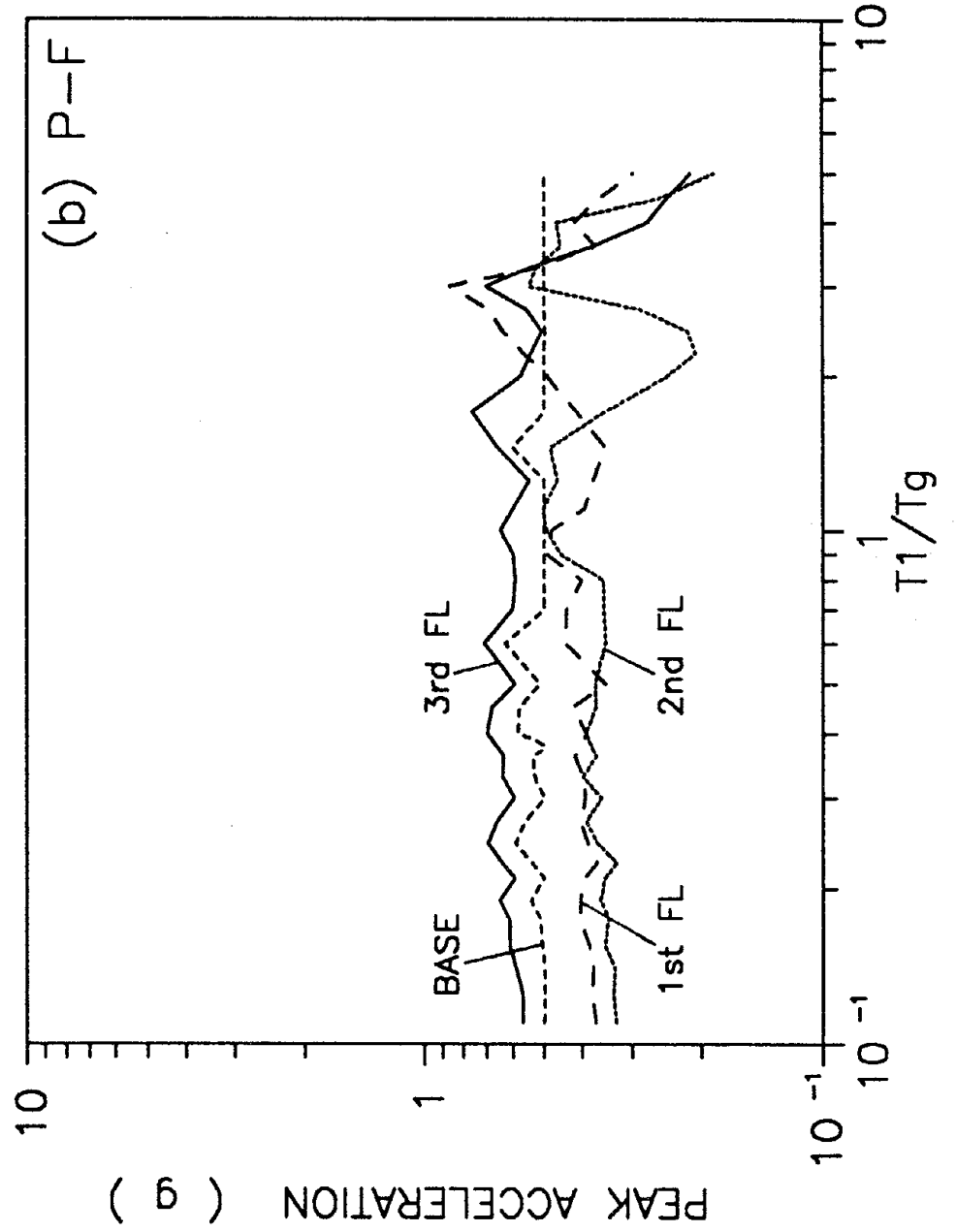
(b) P-F
PEAK ACCELERATION (g)
10
1
10^{-1}
10^{-1}
1
10
$T1/Tg$
BASE
3rd FL
2nd FL
1st FL

Figure 4-7

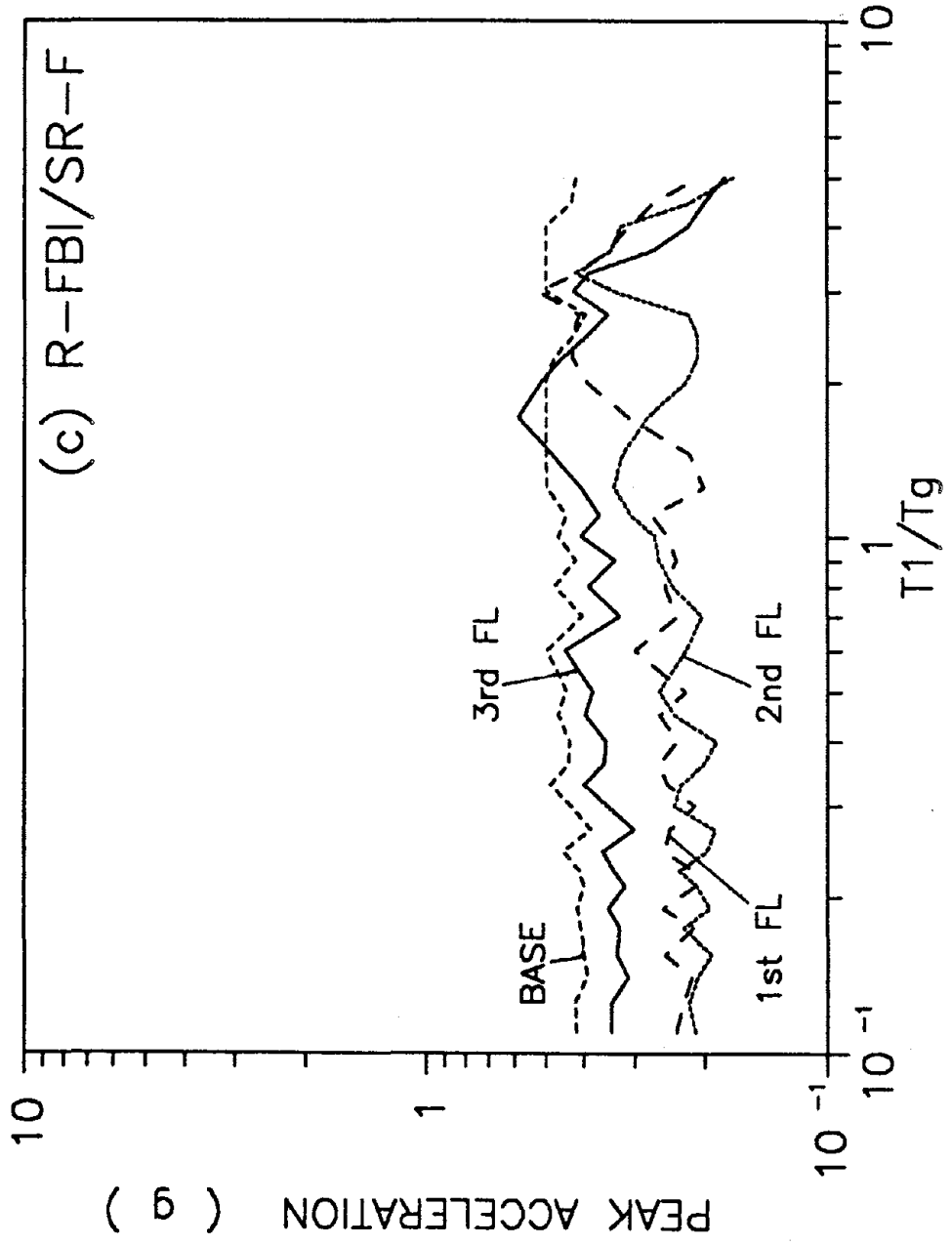
(c) R-FBI/SR-F
PEAK ACCELERATION (g)
10
1
10^{-1}
10^{-1}
1
10
T1/Tg
BASE
3rd FL
2nd FL
1st FL

Figure 4-7

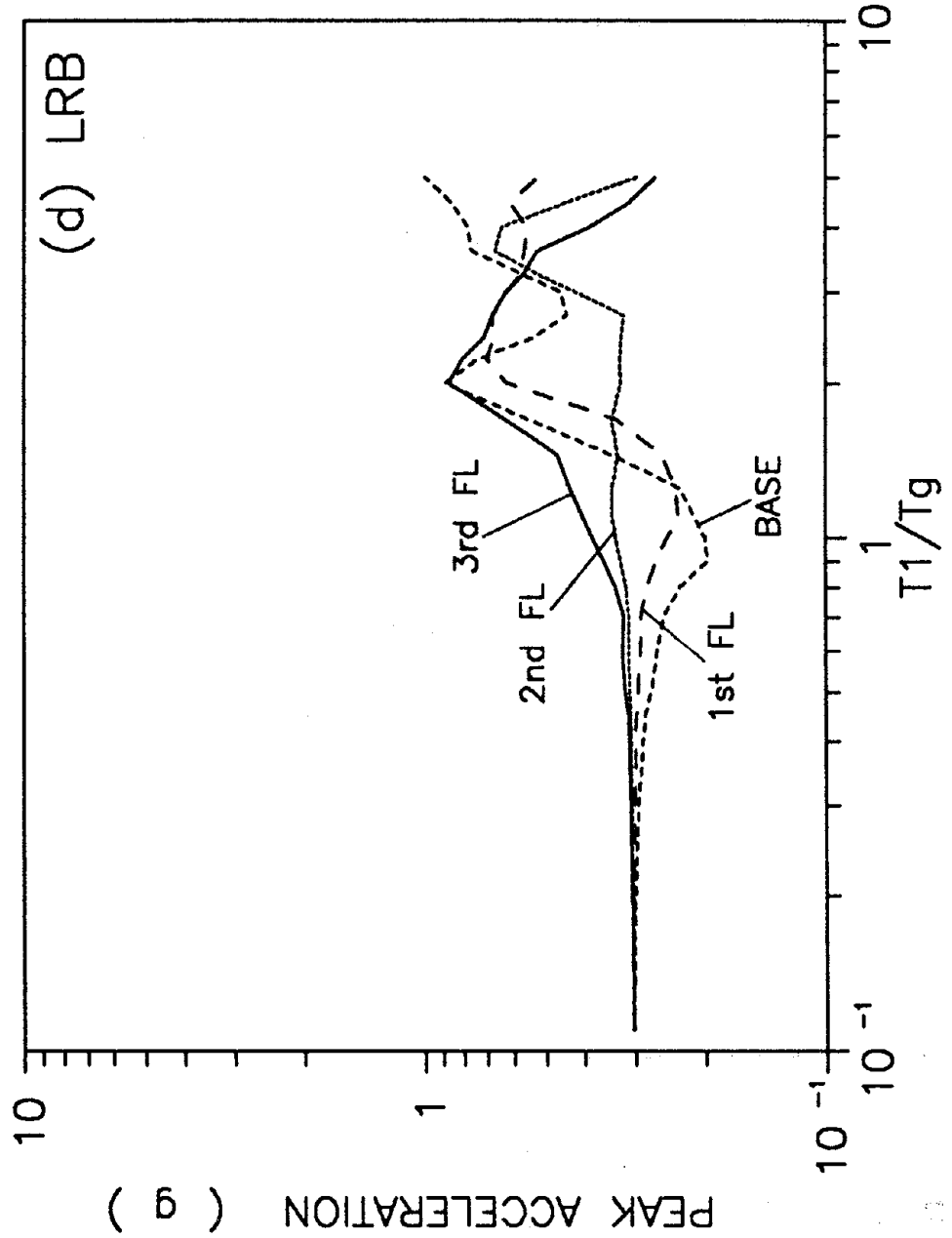
(d) LRB
PEAK ACCELERATION (g)
10
1
10^{-1}
10^{-1}
1
10
T1/Tg
3rd FL
2nd FL
1st FL
BASE

Figure 4–7

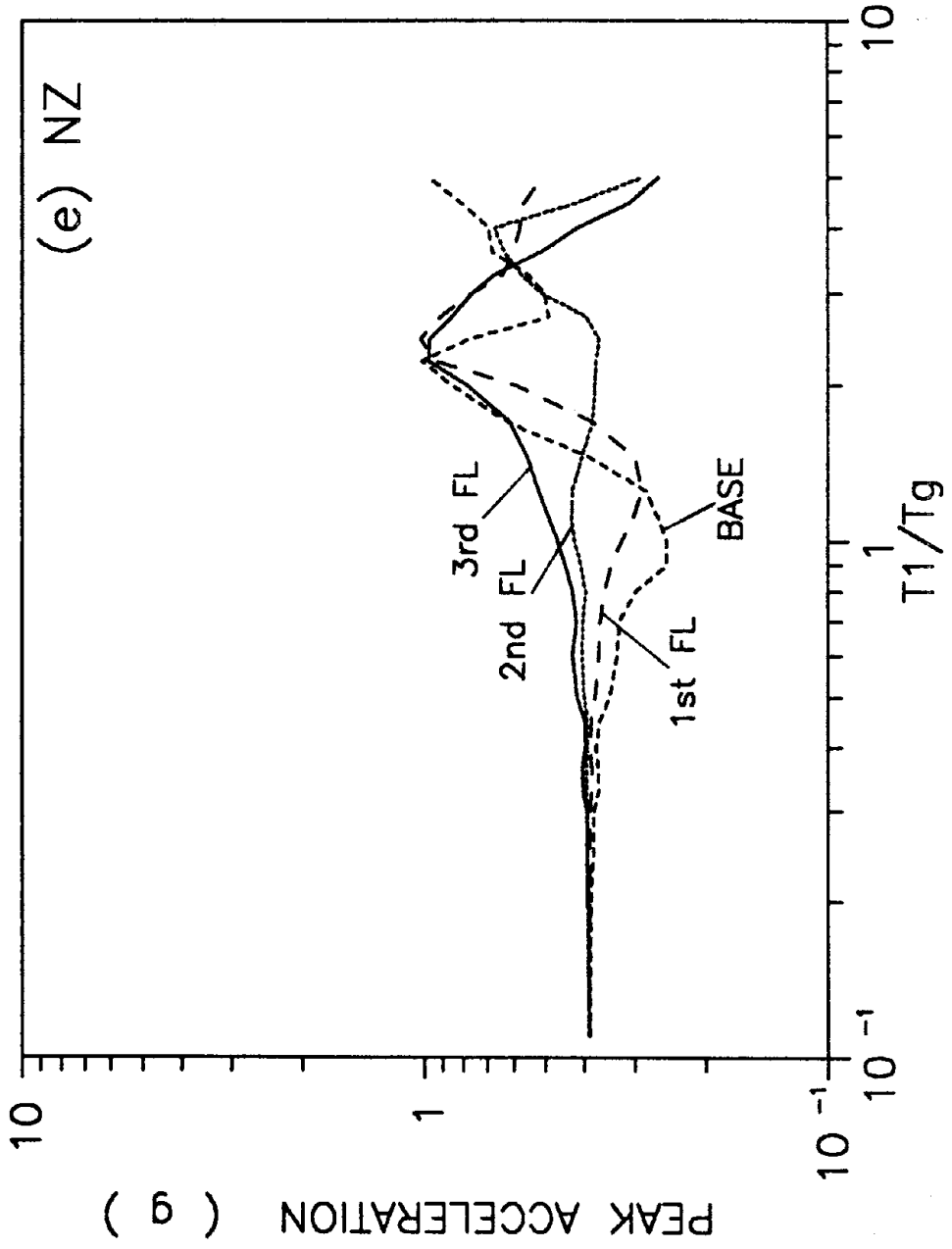
(e) NZ
PEAK ACCELERATION (g)
10
1
10^{-1}
10^{-1}
1
10
T1/Tg
3rd FL
2nd FL
1st FL
BASE

Figure 4–7

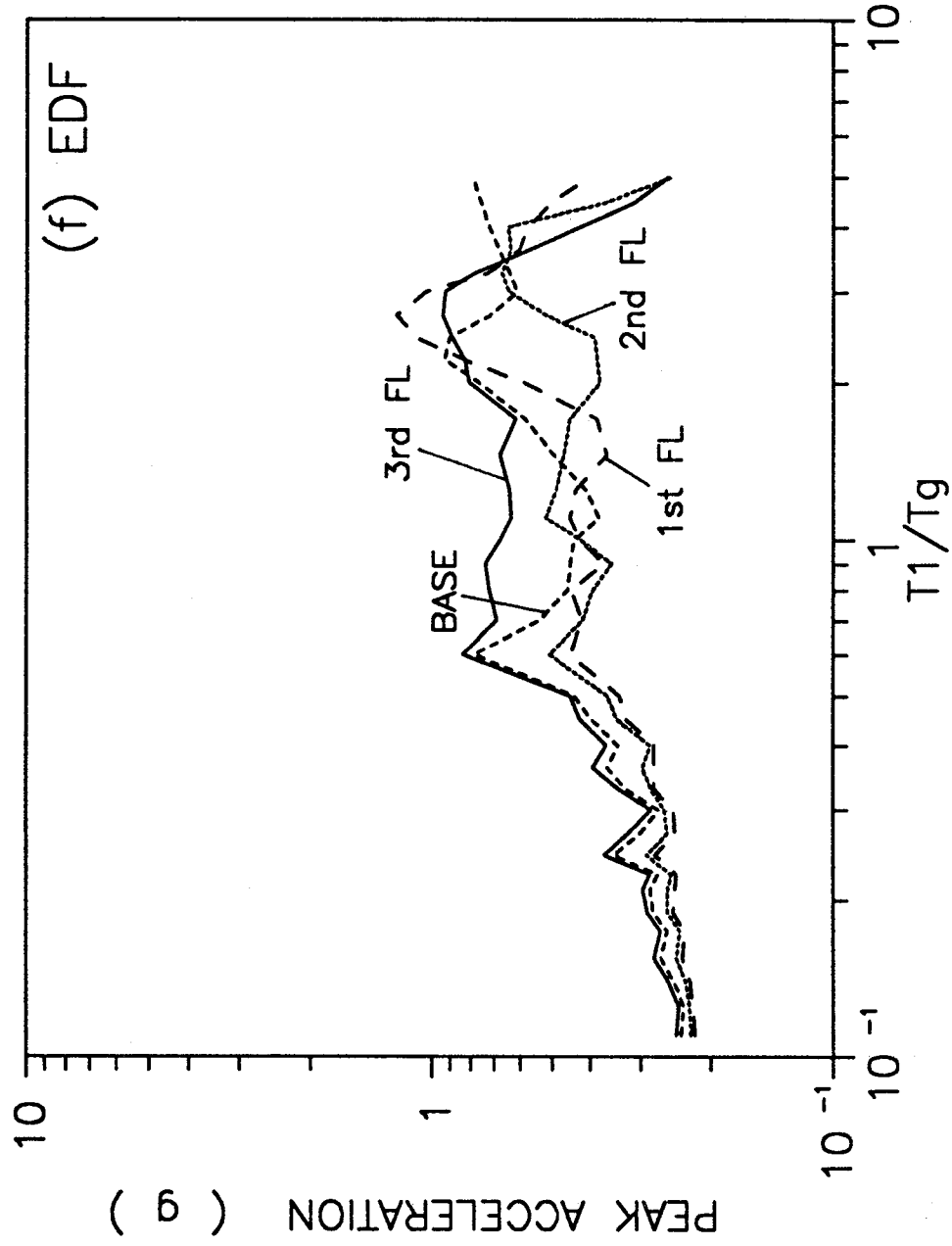
(f) EDF
PEAK ACCELERATION (g)
10
1
10^{-1}
10^{-1}
1
10
T1/Tg
BASE
3rd FL
2nd FL
1st FL

Figure 4–7

period ratios less than 2, the third floor has the highest peak acceleration responses because of the amplifying effects of the structure; however, the peak acceleration of the base floor is larger than those of the first and the second floors due to the actions of the slip-stick transition shocks. Figure 4-7b also shows that the peak acceleration responses of the structure with a P-F isolator remain almost constant, while the corresponding responses of the fixed-base structure strongly depends on the value of period ratio.

In Figure 4-7c, the peak acceleration responses at various floors for the R-FBI/SR-F systems are shown. It is observed that peak acceleration at the base (about $0.4g$) is generally higher than those of the upper floors. The acceleration spectra of the first and the second floors are comparable (about $0.2g$) and are lower than that of the third floor. The other general features of the acceleration response spectra shown in this figure are somewhat similar to those of the P-F base isolator. Figure 4-7c also shows that the peak accelerations of structure with the R-FBI/SR-F base isolators are generally much lower than those isolated by the P-F system and the fixed-base structure.

The peak acceleration responses at various floors of a structure with a LRB base isolation system are plotted versus period ratio in Figure 4-7d. It is observed that the acceleration response spectra curves of various floors almost coincide for period ratios less than 0.8, and remain a constant at about $0.3g$. This implies that the structure isolated by the LRB base isolator responds in its rigid body mode for $T_1/T_g \leq 0.8$. For period ratios of the order of one or larger, the interactions among various floors of the structure and between the structure and the isolator are significant, and peak accelerations of various floors increase accordingly.

Figure 4-7e shows the peak acceleration responses at various floors for the NZ base isolator. Comparing Figures 4-7e and 4-7d, it is clearly observed that the behaviors of the spectra curves for the NZ system are similar to those of the LRB base isolator; however, the magnitudes of the peak acceleration for the NZ system are somewhat higher than those of the LRB. Figure 4-7e also shows that the isolated structure is vibrating in its rigid body mode with a peak absolute acceleration of about $0.4g$ for $T_1/T_g < 0.7$.

The peak accelerations at various floor for the EDF base isolator are shown in Figure 4-7f. It is observed that the peak acceleration responses of the base floor are

higher than those of the first and the second floor for period ratios less than unity. The figure also shows that the peak accelerations gradually increases as the stiffness of the structure decreases. For flexible structures the interactions between various floors and the base isolator become quite significant and the acceleration response spectra curves increase to about 0.7 to 1 g.

Based on the results presented, it is concluded that the base isolation systems substantially reduce the peak transmitted acceleration and the column stresses. In particular, the resonance peak of the fixed-base structure is totally eliminated for the base isolated structures. Among the isolators studied, the R-FBI/SR-F systems lead to the lowest structural deflection, and the NZ system produces the lowest base displacement while the P-F system generates the highest base displacement. The peak accelerations transmitted by the LRB, the NZ, and the R-FBI/SR-F base isolator are comparable. The P-F and the EDF systems lead to higher peak accelerations. Furthermore, the base isolated structure, unlike the fixed-base one, do not amplify the ground excitation to a significant extent.

4.3 Effects of Structural Damping

In this section, the effects of variation of the damping ratio of the structure, ζ_1, on the peak responses for various base isolation systems are studied. The corresponding results for the fixed-base structure is also shown for reference. A structure with a fundamental natural period of 0.3 *sec* is used in this study. The peak absolute acceleration responses at the top of the structure, the maximum relative base displacements, and the maximum deflections of the structure are evaluated for a range of values of ζ_1. The results are shown in Figures 4-8 through 4-10.

The peak acceleration responses for different systems are plotted versus ζ_1 in Figure 4-8. It is observed that damping has no noticeable effect on the peak responses for the LRB and the NZ systems. However, the peak accelerations for the friction-type isolators decrease with an increase in ζ_1. This is because the accelerations pulses generated by the shock loadings due to the slip-stick and slip reversal transitions of the frictional systems are significantly reduced by the structural damping as they propagate through the floors. Figure 4-8 also shows that the peak acceleration transmitted to the top floor by the R-FBI/SR-F systems is the lowest among all the isolators considered for $\zeta_1 > 0.02$. For $\zeta_1 \leq 0.02$, however, the laminated rubber

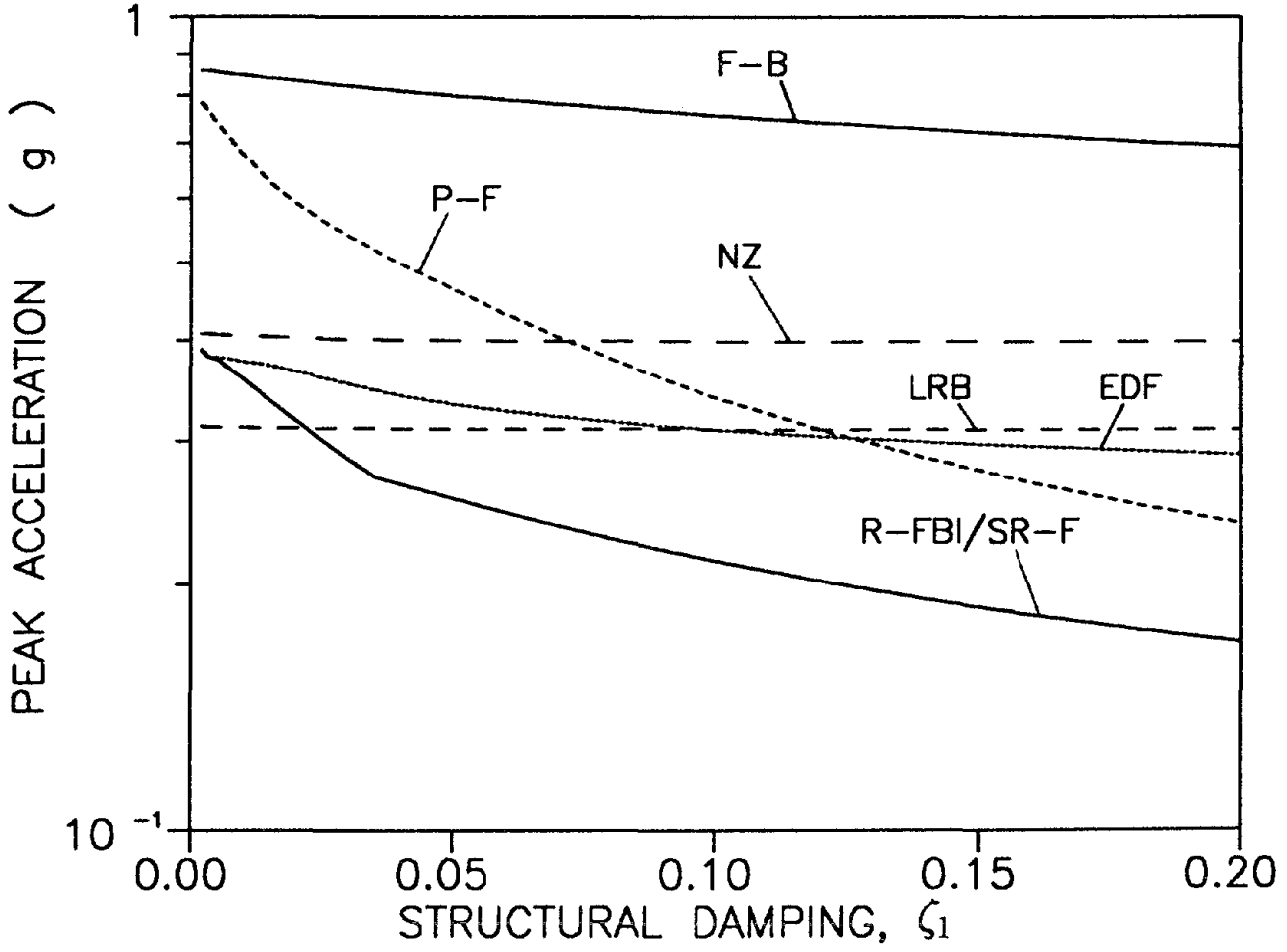

Figure 4–8 Variations of Peak Absolute Acceleration at the Top of Structure with Structural Damping

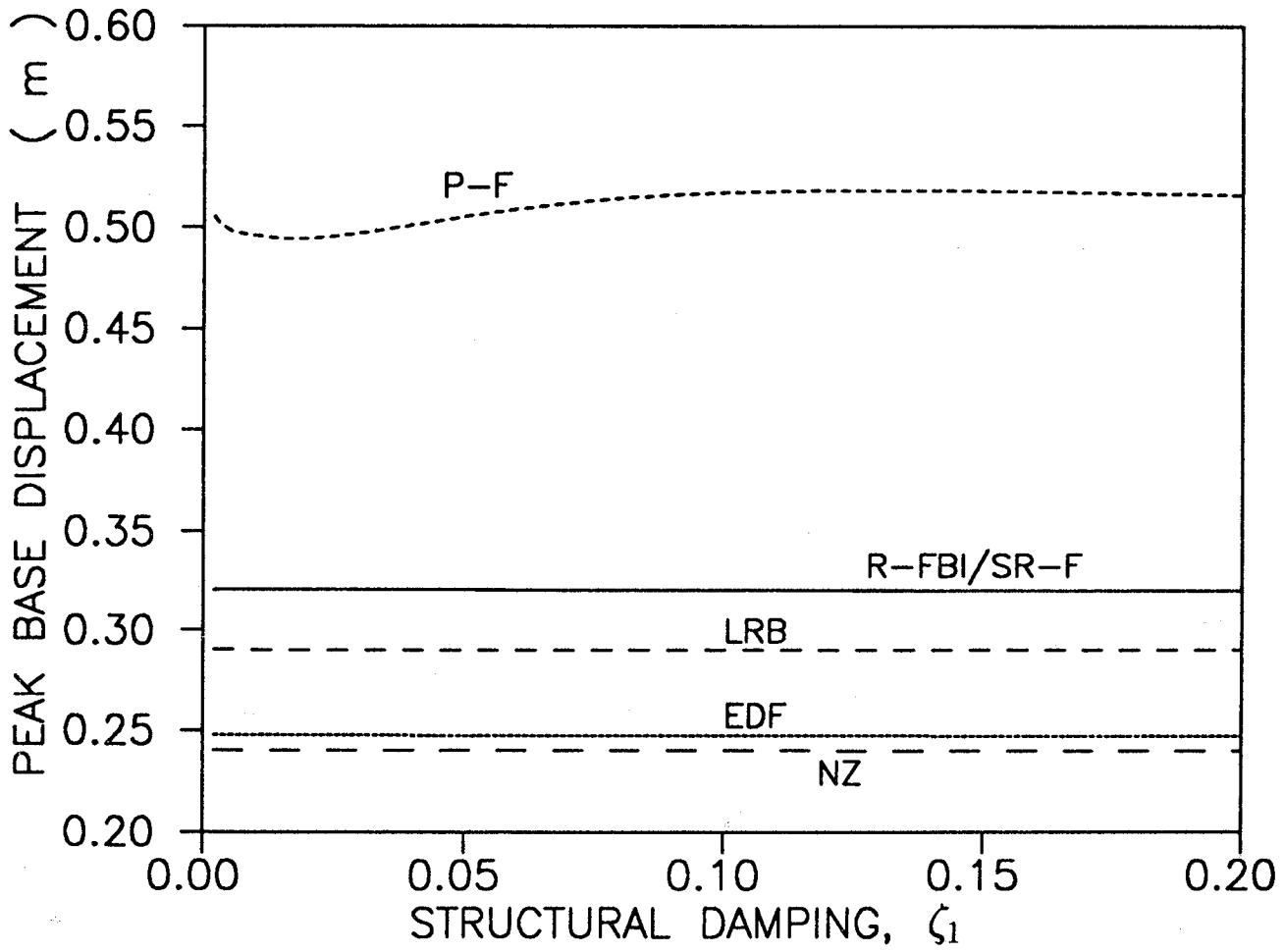

Figure 4–9 Variations of Peak Base Displacement with Structural Damping

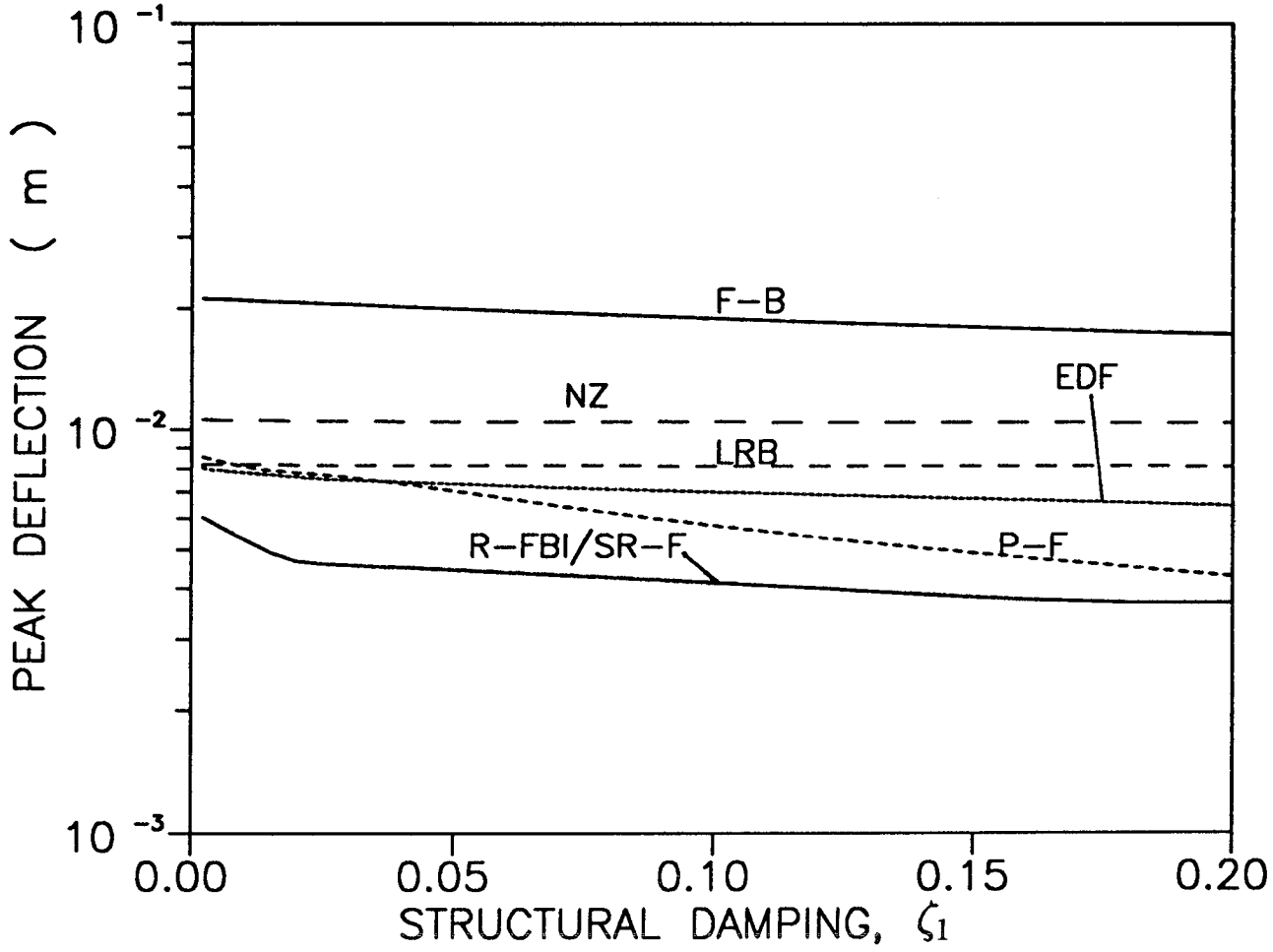

Figure 4-10 Variations of Peak Deflection with Structural Damping

bearing transmits the least amount of acceleration to the top of the structure. The results for the fixed-base structure shows that an increase in ζ_1 somewhat reduces the peak acceleration of the top floor.

Figure 4-9 shows the effects of variations of the damping coefficients on the maximum base displacement responses for various systems. It is observed that the peak base displacement responses are not sensitive to the variations in the damping coefficients of the structure. This is because the base isolated structure behaves essentially as a rigid block and the structural damping has no effect on the peak base displacement. For the P-F isolator, the peak base displacement shows slight variation with ζ_1 for small values of damping coefficient.

Variations of the maximum deflection with damping coefficient for various base isolation systems are shown in Figure 4-10. The corresponding results for the fixed-base structure are also plotted in this figure for comparison. It is observed that variations of ζ_1 do not affect the peak deflection responses significantly except for the P-F system. Slight reductions of the peak deflections of the fixed-base structure and the structure isolated by the EDF and the R-FBI/SR-F systems with structural damping is also noticed in Figure 4-10. This figure also shows that the R-FBI/SR-F systems lead to the lowest peak deflection for the entire range of damping coefficient considered.

From the results presented in this section, it may be concluded that as damping ratio of the structure increases, the peak acceleration of the structure with a frictional base isolation system decreases. However, the variation in the damping ratio has no noticeable effects on the peak deflection or peak base displacement responses.

4.4 Effects of Mass Ratio

In the following, the sensitivity of the peak responses to variations in mass ratio (α_b) for different base isolation systems are studied. The mass ratio is varied from 0.1 to 0.5, and the peak responses of a three-floor structure with a fundamental natural period of 0.3 *sec* are evaluated. The results are plotted in Figures 4-11 through 4-14.

Figure 4-11 shows the peak absolute acceleration responses at the top of the structure versus mass ratio for different base isolation systems. It is observed that

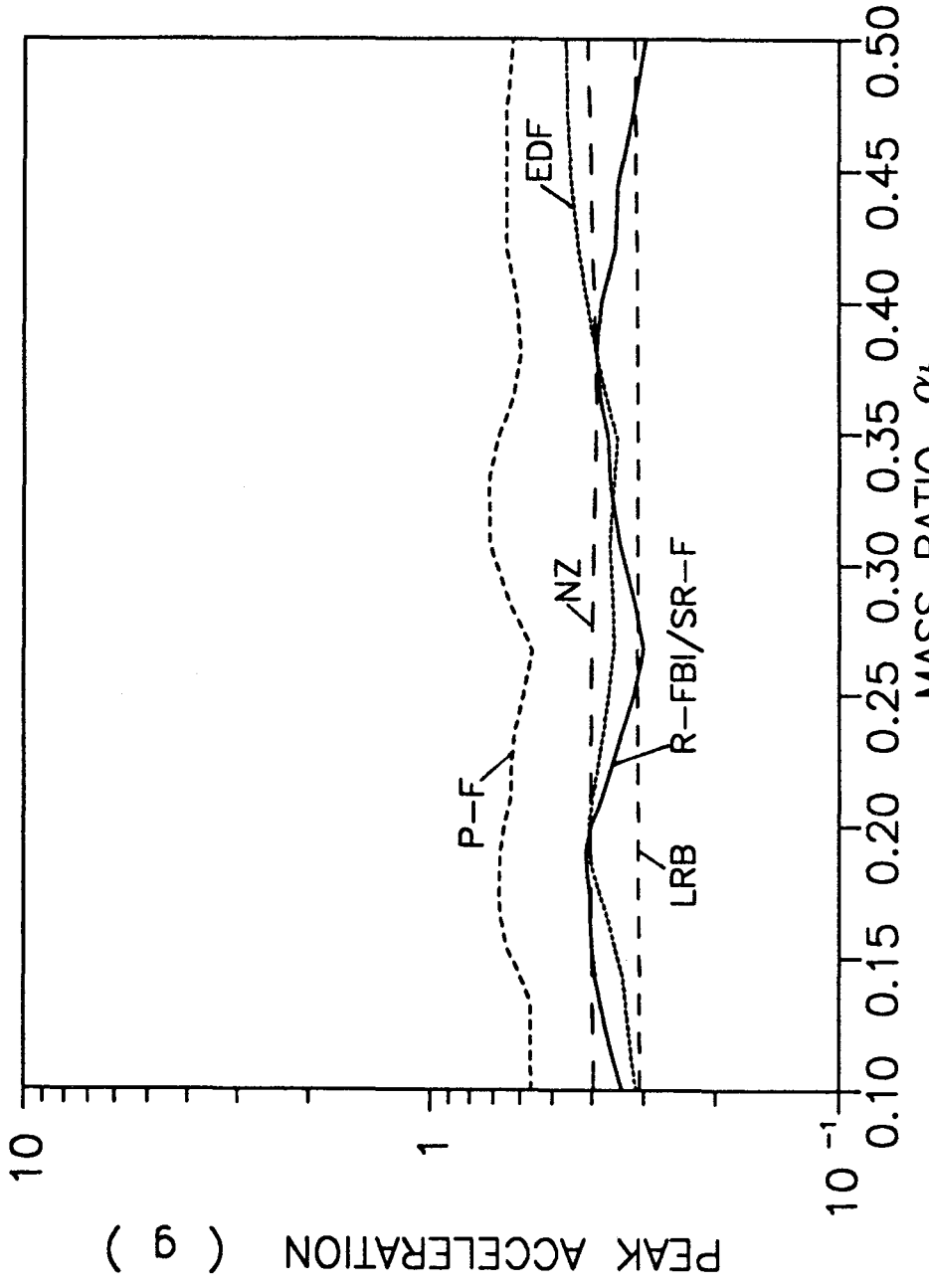

Figure 4–11 Variations of Peak Absolute Acceleration at the Top of Structure with Mass Ratio

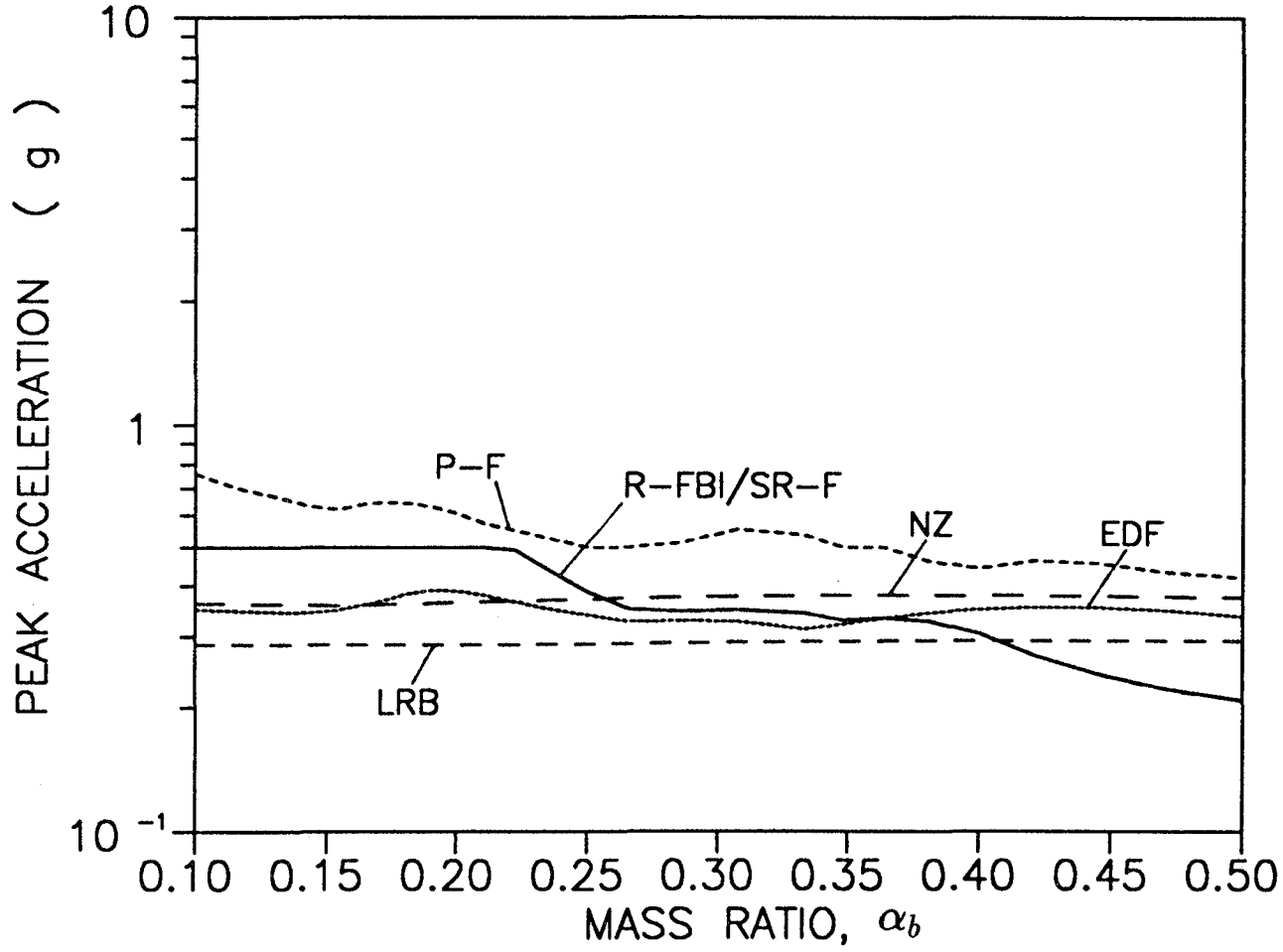

Figure 4–12 Variations of Peak Absolute Acceleration at the Base of Structure with Mass Ratio

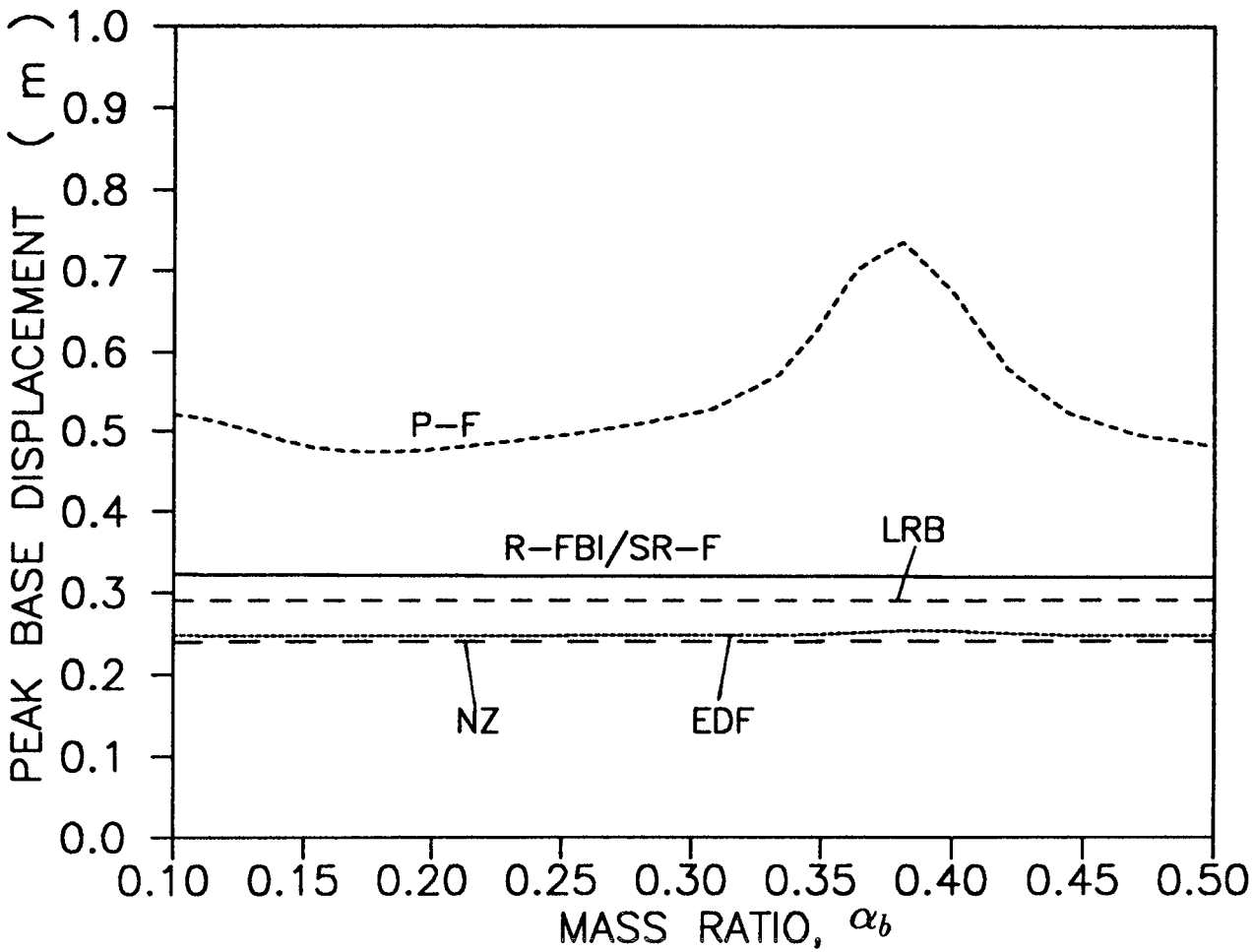

Figure 4–13 Variations of Peak Base Displacement with Mass Ratio

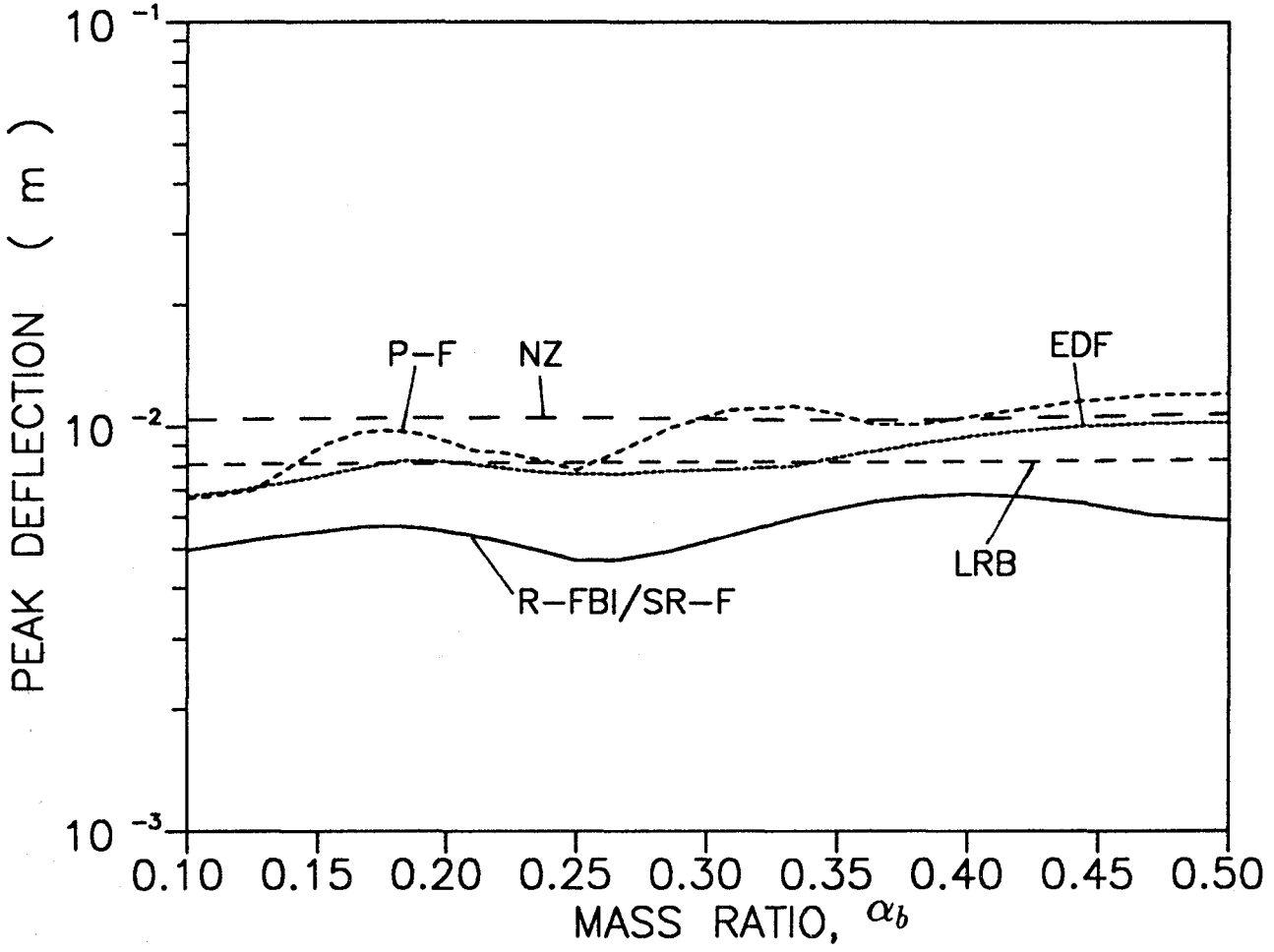

Figure 4-14 Variations of Peak Deflection with Mass Ratio

the peak acceleration responses remain constant or vary slightly with mass ratio.

The peak absolute acceleration responses at the base, $(\ddot{x}_g + \ddot{s})|_{max}$, for various isolation systems are shown in Figure 4-12. This figure shows that for the P-F and the R-FBI/SR-F systems, the peak accelerations transmitted to the base decrease as the mass ratio increases; while they remain almost constant for the LRB and the NZ systems. The reason is that the peak acceleration for the frictional base isolation systems are transmitted to the base during the slip-stick and slip-reversal transition by shock loadings. The amplitudes of these friction pulse forces are proportional inversely to the mass ratio as is noted in Appendix A. Comparing Figures 4-11 and 4-12, it is observed that the peak accelerations at the top floor for the P-F and the R-FBI/SR-F systems are lower than those of the base for certain ranges of mass ratio.

Figure 4-13 shows the maximum base displacement responses for various base isolation systems. It is noticed that for the entire range of mass ratio, the peak base displacements remain almost constants of about 0.25 m for the EDF and the NZ systems and about 0.3 to 0.32 m for the LRB and the R-FBI/SR-F systems. For the P-F isolator, however, the peak base displacement increases as the mass ratio increases, and reaches a peak of about 0.72 m for the mass ratio of about 0.38. Away from this peak, the maximum base displacement for the P-F isolator is about 0.5 m.

The peak deflection responses of the structure with various base isolation systems are shown in Figure 4-14. It is observed that the peak deflection responses of different isolators (with the exception of P-F system) remain almost constant or vary slightly for the entire range of the mass ratio considered. This figure also shows that the R-FBI/SR-F systems generate the least amount of deflection (about 0.5 cm) for the entire range of mass ratio considered.

Based on these results, it may be concluded that the variations of mass ratio have no noticeable effects on the performances of the base isolators considered. The exception is the peak base displacement for the P-F base isolator which varies somewhat with the mass ratio.

4.5 Effects of Friction Coefficient

In this section, the sensitivity of responses of friction-type base isolators to the variations in friction coefficient are investigated. The study is of interest because a certain degree of deviation in friction coefficient from its nominal design value is unavoidable due to construction imperfection and aging process. The friction coefficients of these isolators are varied in a range of preselected values, and the peak responses of the structure are evaluated. The resulting peak absolute acceleration responses at the top of the structure are shown in Figure 4-15.

Figure 4-15a shows the results of the sensitivity analysis for the P-F and the R-FBI systems. It is observed that the amplitudes of the acceleration response spectra for the R-FBI and the P-F systems are almost constant for period ratios less than unity. Figure 4-15a also shows that the peak acceleration responses increase rapidly as the friction coefficient increases. That is, the peak acceleration responses of the P-F and the R-FBI systems are quite sensitive to substantial changes in magnitude of friction coefficient. For example, the peak acceleration levels for the R-FBI system with a friction coefficient of 0.03, 0.05 and 0.07 are about $0.25g$, $0.35g$ and $0.45g$ for period ratios less than unity. Similarly, the peak acceleration for the P-F isolator jumps from $0.6g$ to $0.9g$ when the friction coefficient is changed from 0.1 to 0.2.

Figure 4-15b shows the acceleration spectra curves at the top of the three-story structure which is isolated by the EDF system. It is observed that the peak acceleration transmitted to the structure generally increase with period ratio. Figure 4-15b also shows the peak acceleration transmitted by the EDF base isolator is also quite sensitive to the variations in magnitude of friction coefficient. For example, when the value of friction coefficient increases from 0.15 to 0.25, the peak acceleration increases from $0.2g$ to $0.3g$ for relatively rigid structures and from $0.6g$ to $0.9g$ for flexible structures with period ratio of about 0.7 to 0.8.

The peak acceleration responses for the SR-F system with different friction coefficients of the upper friction plate, μ, are shown in Figure 4-15c. The friction coefficient of the body plate is kept fixed ($\mu_1 = 0.05$) in this study. As mentioned earlier, for $\mu = 0.2$, no sliding in the upper plate of the SR-F system occurs, and its response coincides with that of the corresponding R-FBI system. Figure 4-15c shows that as the friction coefficient of the upper plate reduces from 0.2 to 0.08, the peak acceleration responses remain almost the same. This is because small amount

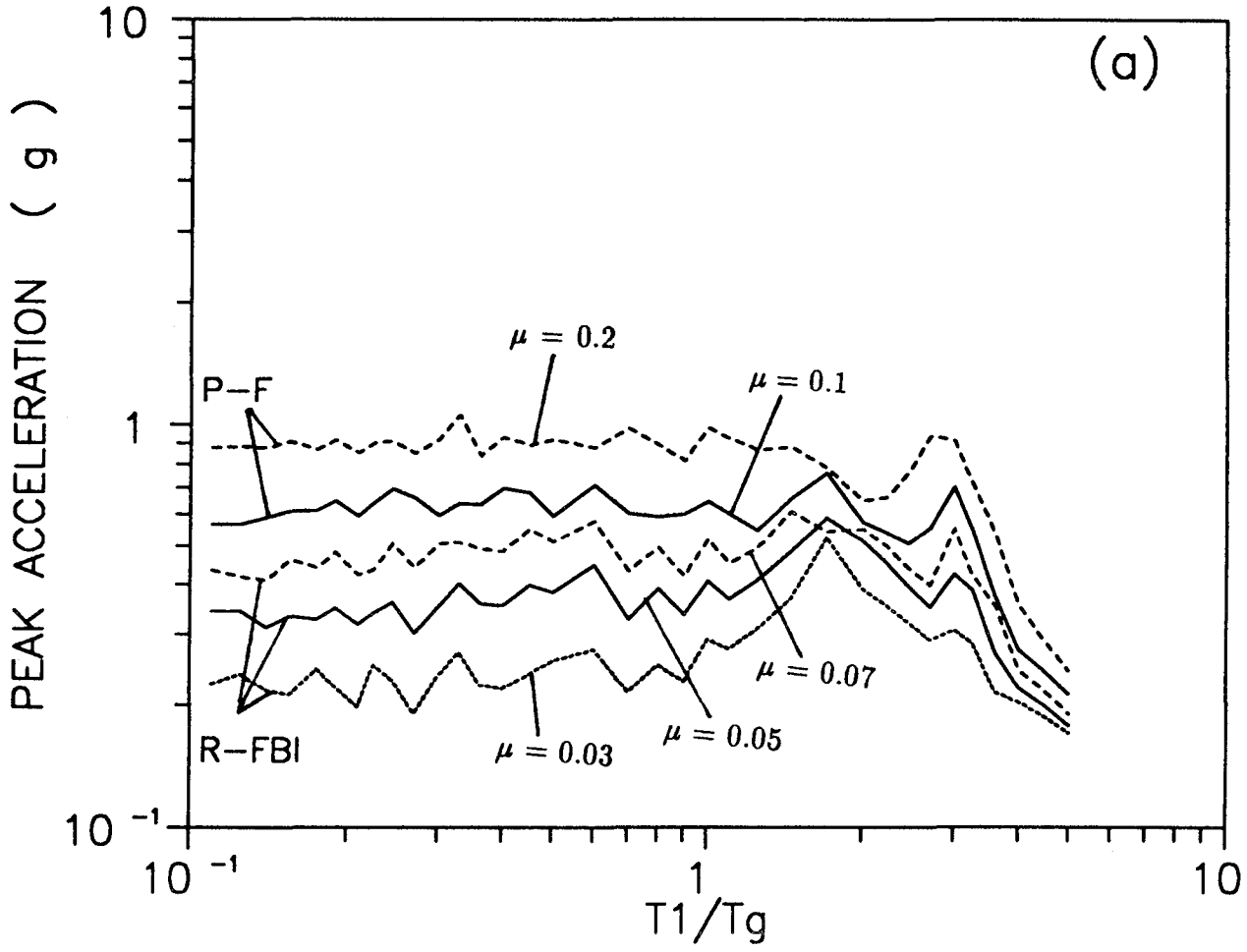

Figure 4–15 Variations of Peak Absolute Acceleration at the Top of Structure with Period Ratio for Various Friction Coefficients

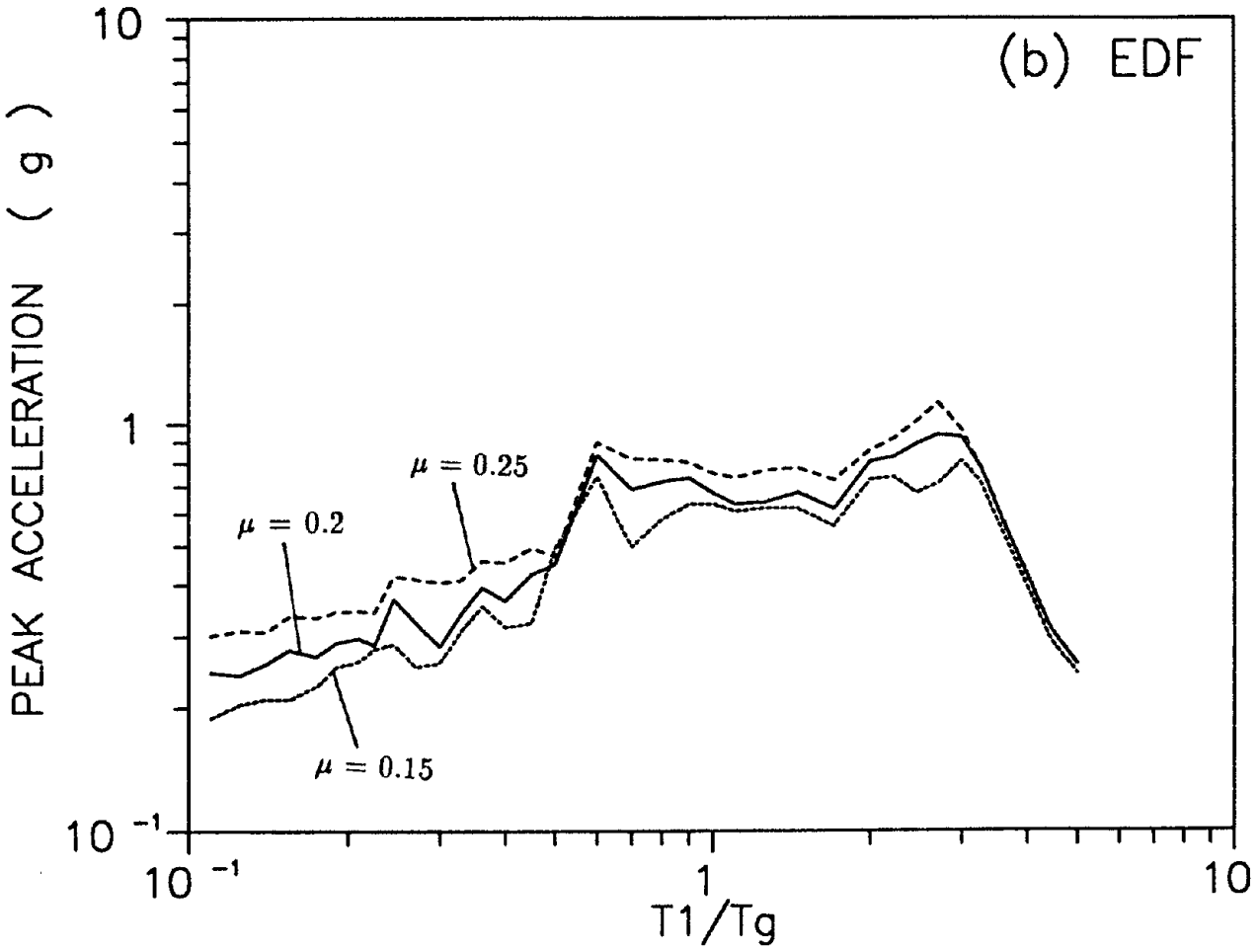

Figure 4–15

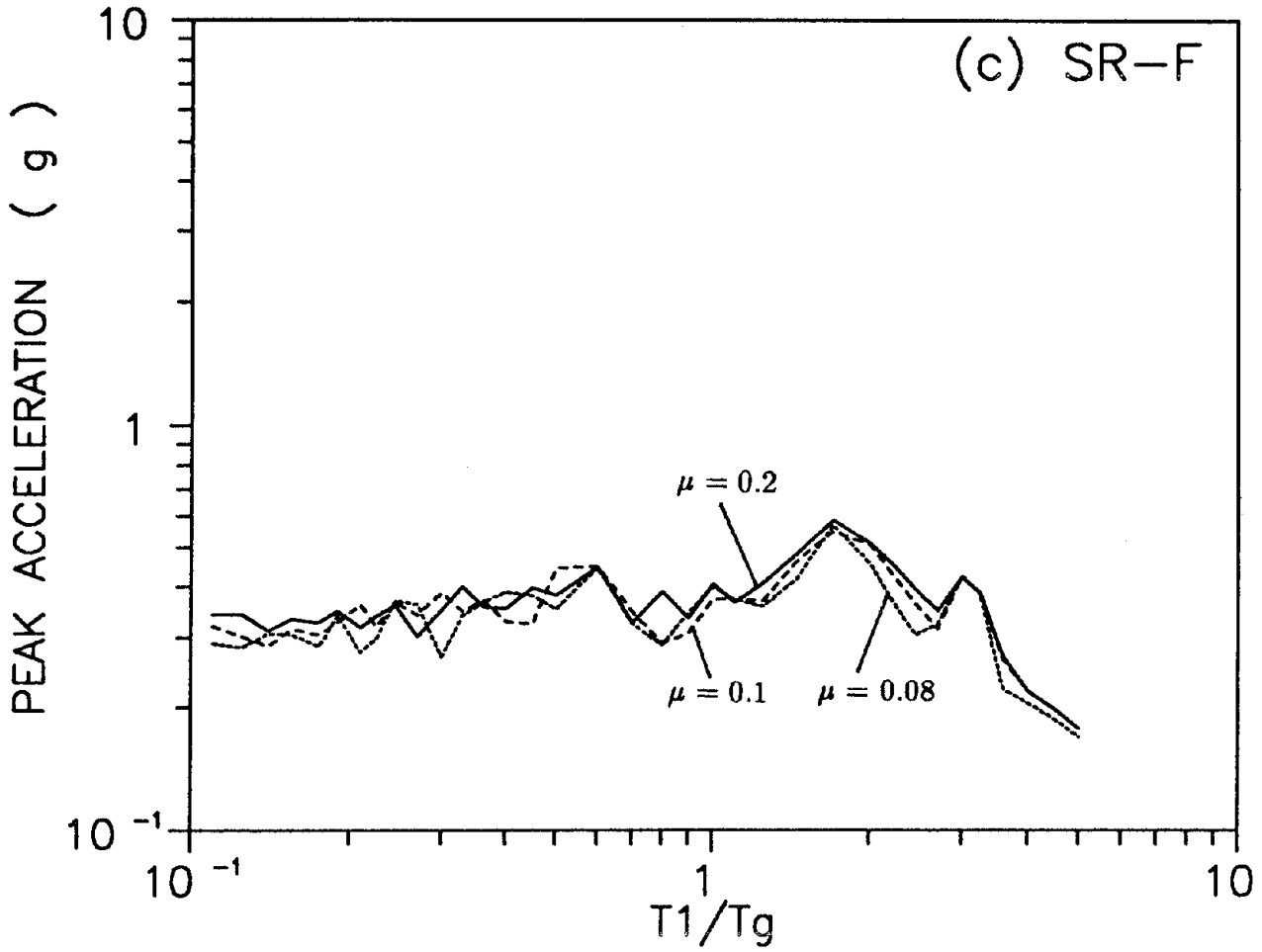

Figure 4-15

of sliding occurs in the upper friction plate for the ground excitation considered here. These results indicate that the peak acceleration transmitted by the SR-F base isolation system is insensitive to the variations in the friction coefficient of the upper plate.

The effects of variations of friction coefficient on the maximum relative base displacements for various friction-type base isolators are shown in Figures 4-16a through c. These figures show that, in general, the relative base displacement reduces as the friction coefficient increases. Figure 4-16a shows the variations of $s|_{max}$ with period ratio for the P-F and the R-FBI systems. From this figure, it is noticed that the peak displacement response spectra for the P-F system contain sharp peaks at period ratio of about 0.9. These peaks reach to about 1.2 m and 0.6 m for friction coefficients of 0.1 and 0.2, respectively. For $T_1/T_g < 0.8$, away from these peaks, the corresponding maximum base displacements are about 0.5 m and 0.2 m. That is, by doubling the friction coefficient, the peak base displacement is dropped by a factor of 2.5. Figure 4-16a also shows while friction coefficient significantly affect the magnitudes of the displacement response spectra curves for the P-F system, their shapes remain almost the same. It is also observed that peak displacement responses for the P-F isolator decrease rapidly for period ratios larger than one. In particular, no sliding is observed for $\mu = 0.2$ with $T_1/T_g > 3$.

The peak base displacements for the R-FBI system with different friction coefficients are also shown in Figure 4-16a. It is observed that the displacement response spectra curves for the R-FBI system remain almost constant for the entire range of natural period considered. Furthermore, their amplitude changes only slightly (from 0.3 m to 0.35 m) when μ is varied from 0.07 to 0.03. By comparing the responses of the R-FBI system with those of the P-F system, it is clear that the restoring forces of the rubber installed in the R-FBI system reduces the horizontal relative base displacements to a significant extent and eliminates the sharp peaks observed in the displacement response spectra curves of the P-F system.

Figure 4-16b shows the peak base displacement responses for the EDF system for several values of friction coefficient. As mentioned earlier, the displacement response spectra for the EDF system contain sharp peaks similar to those of the P-F system at period ratio of about 0.9. These peaks are clearly observed in Figure 4-16b for μ equal to 0.15 and 0.2. For $\mu = 0.25$, the resonance peak disappears. This figure

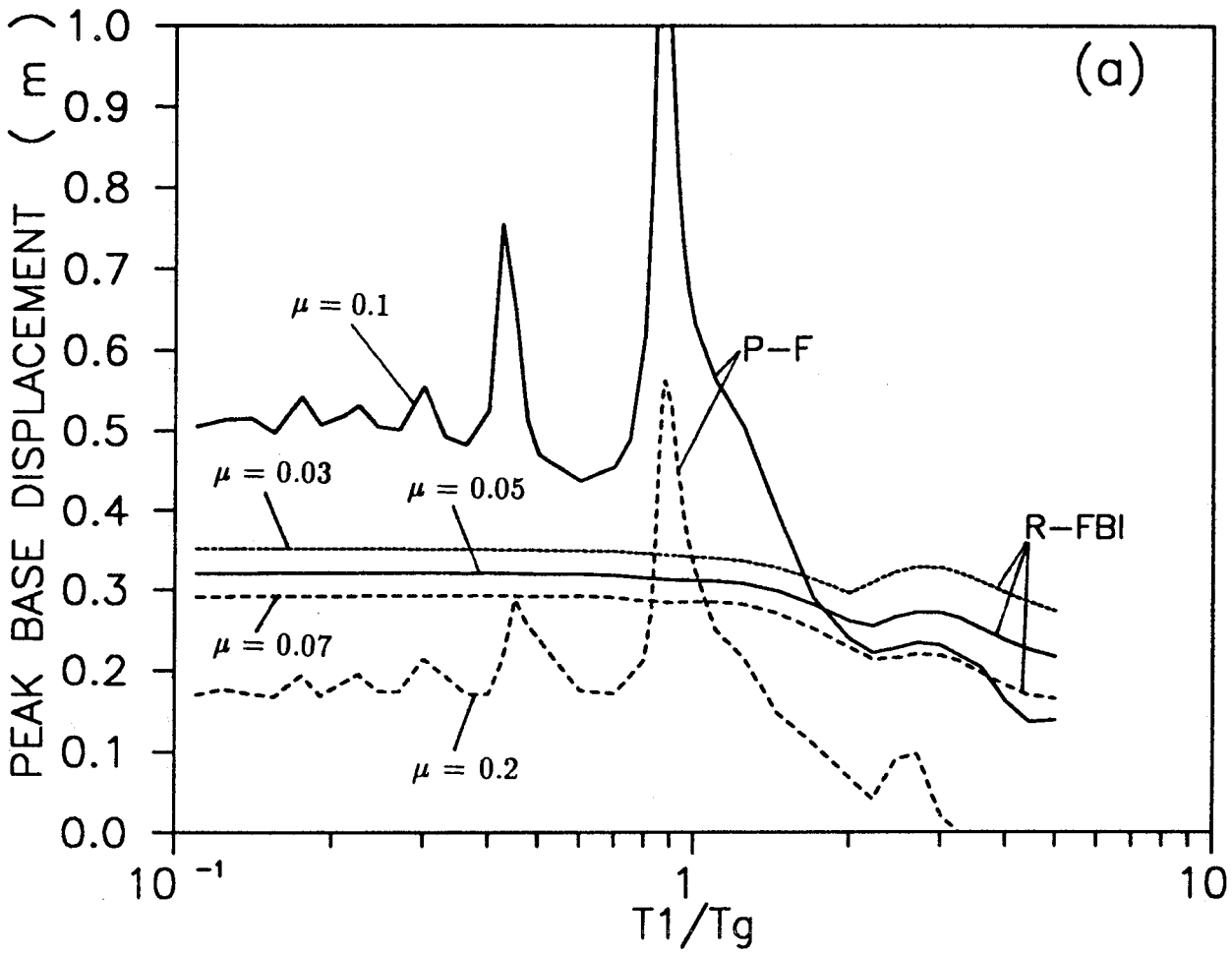

Figure 4–16 Variations of Peak Base Displacement with Period Ratio for Various Friction Coefficients

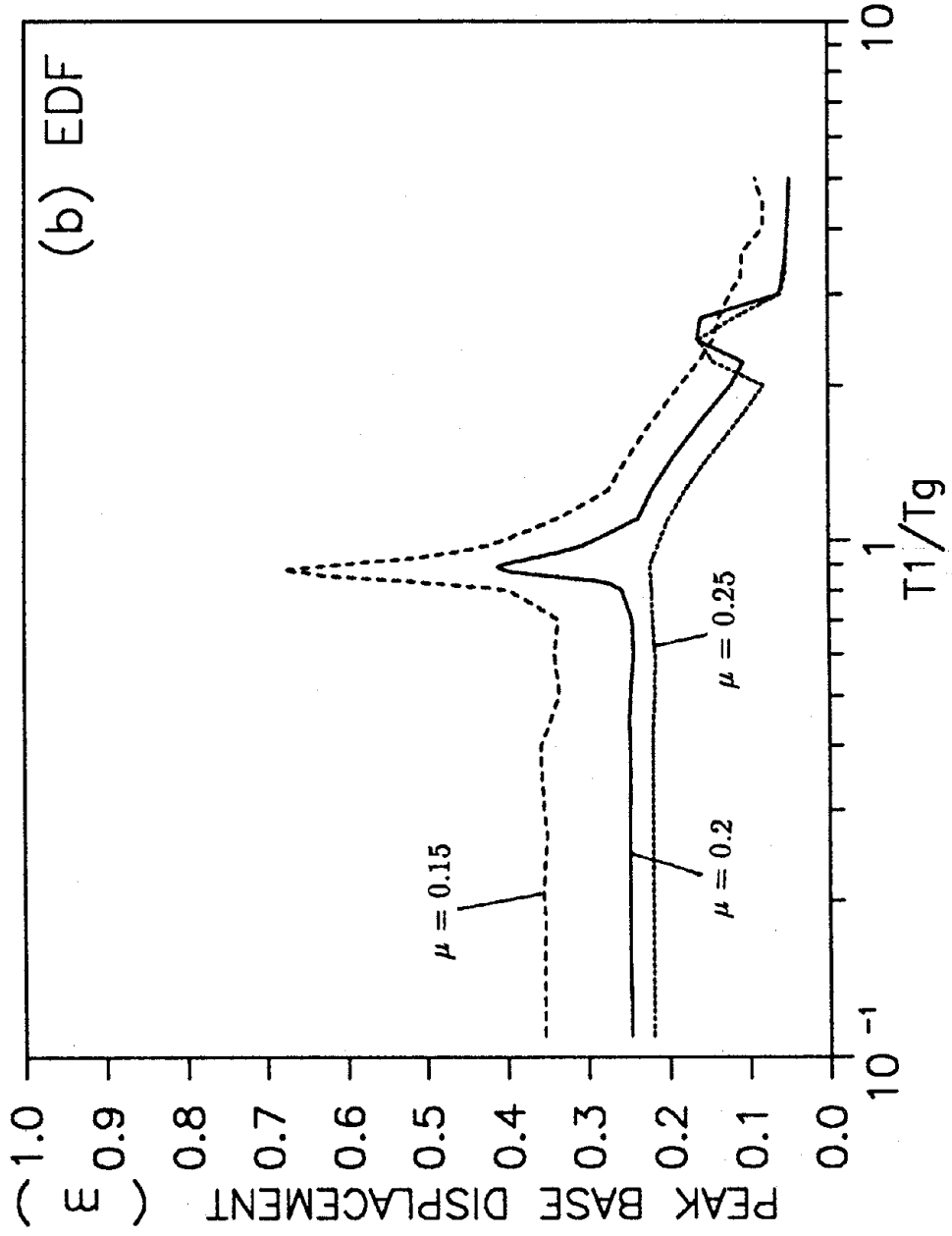
(b) EDF
PEAK BASE DISPLACEMENT (m)
1.0
0.9
0.8
0.7
0.6
0.5
0.4
0.3
0.2
0.1
0.0
10^{-1}
1
10
T1/Tg
$\mu = 0.15$
$\mu = 0.2$
$\mu = 0.25$

Figure 4–16

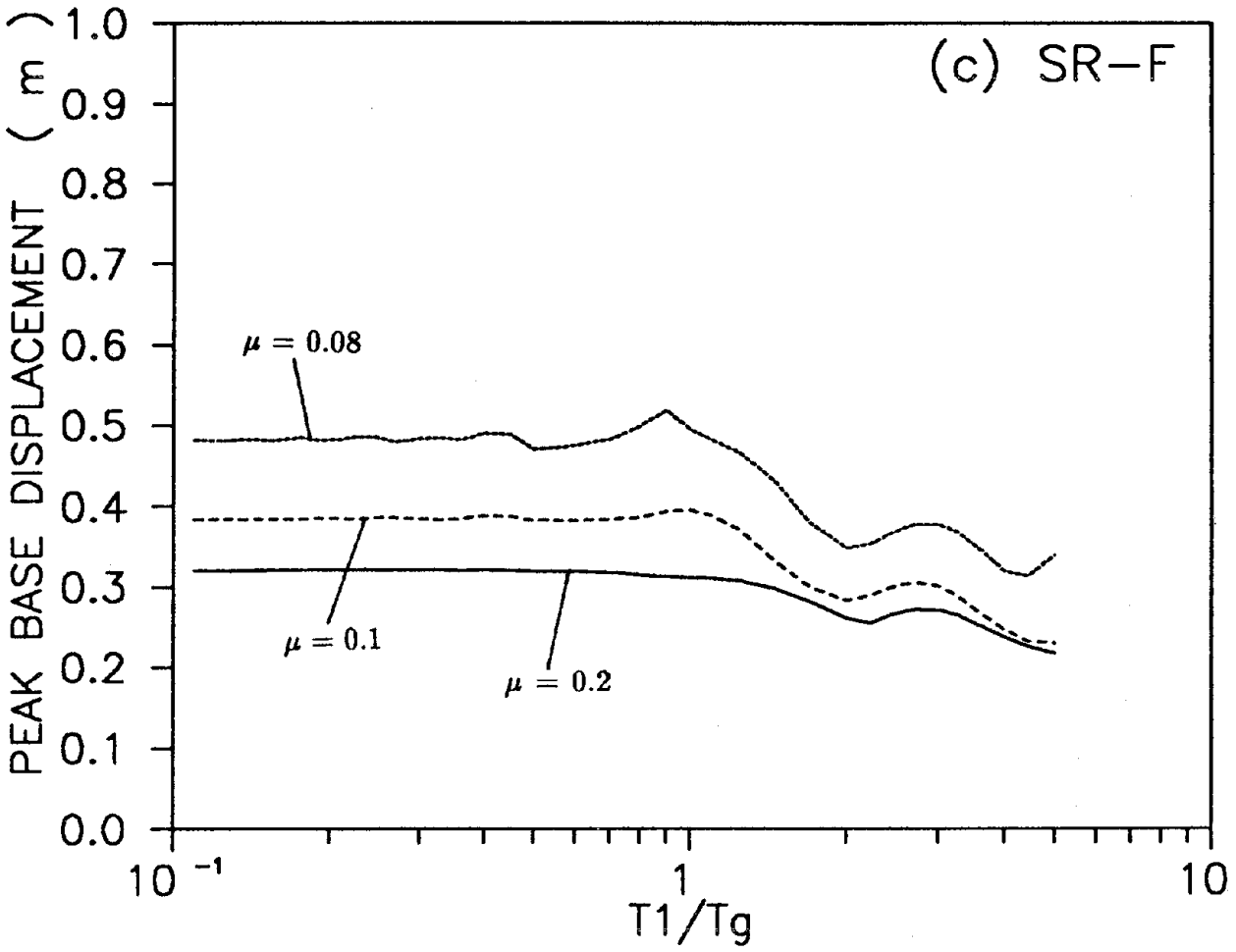
(c) SR-F
PEAK BASE DISPLACEMENT (m)
1.0
0.9
0.8
0.7
0.6
0.5
0.4
0.3
0.2
0.1
0.0
μ = 0.08
μ = 0.1
μ = 0.2
10 -1
1
10
T1/Tg

Figure 4-16

also shows that, for period ratio less than 0.8, displacement response spectra curves remain almost constant about 0.35 m and 0.25 m for μ's of 0.15 and 0.2, respectively.

Figure 4-16c shows the peak base displacement responses for the SR-F system with $\mu_1 = 0.05$ and various friction coefficients of the upper plate. It is observed that the maximum base displacement increases as the magnitude of μ decreases. For period ratio less than one, the peak displacements remain constants of about 0.32 m, 0.38 m and 0.48 m for friction coefficients of 0.2, 0.1, and 0.08, respectively.

In Figure 4-17, the effects of variations of friction coefficient on the maximum deflection of the structure for different base isolators are illustrated. Figure 4-17a shows the maximum deflections for the P-F and the R-FBI systems. It is observed that the peak deflection somewhat increases with an increase in friction coefficient. For example, for a structure with a fundamental natural period of 0.3 sec ($T_1/T_g = 0.375$), when the friction coefficient of the P-F isolator increases from 0.1 to 0.2, the maximum deflection increases from about 0.9 cm to 1.3 cm. For the same structure with a R-FBI system, the peak deflections are about 0.4 cm to 0.7 cm when friction coefficient varies between 0.03 to 0.07.

The deflection response spectra curves for the EDF system are shown in Figure 4-17b where a slight increase of the peak deflection with friction coefficient is observed. For a structure with a fundamental natural period of 0.3 sec, the peak deflection increases from about 0.6 cm to 0.9 cm as friction coefficient increases from 0.15 to 0.25.

The peak deflection response spectra for the SR-F system with $\mu_1 = 0.05$ and different values of μ are shown in Figure 4-17c. It is observed that the peak deflection responses remain almost the same as the friction coefficient of the upper friction plate is varied. That is, the peak deflection of the structure with a SR-F base isolation system is insensitive to variations in μ.

Figures 4-15 through 4-17 show that the peak responses of the structure with frictional base isolation systems vary significantly when the friction coefficient changes substantially. However, small variations in the friction coefficient lead only to slight changes in the response spectra curves.

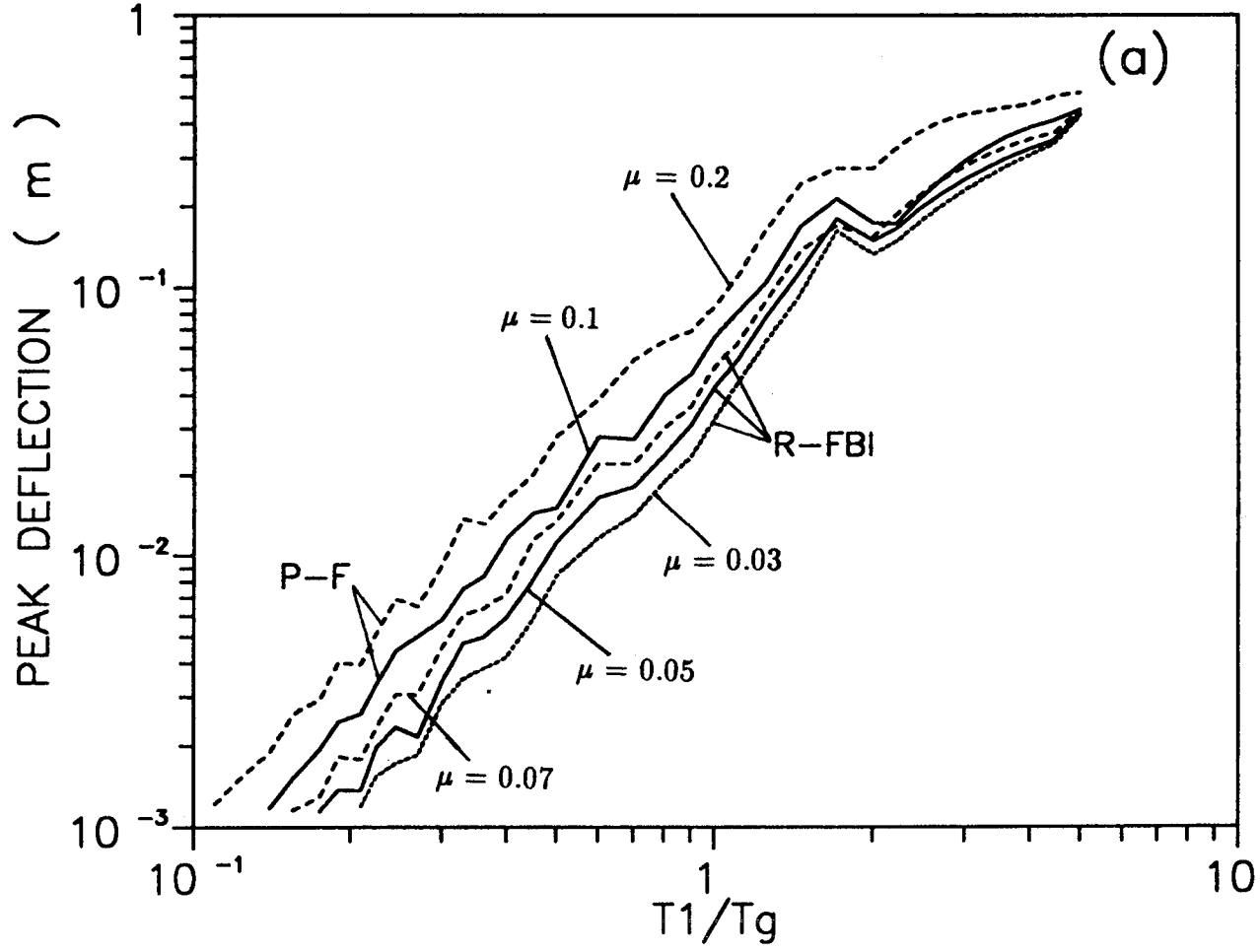

Figure 4–17 Variations of Peak Deflection with Period Ratio for Various Friction Coefficients

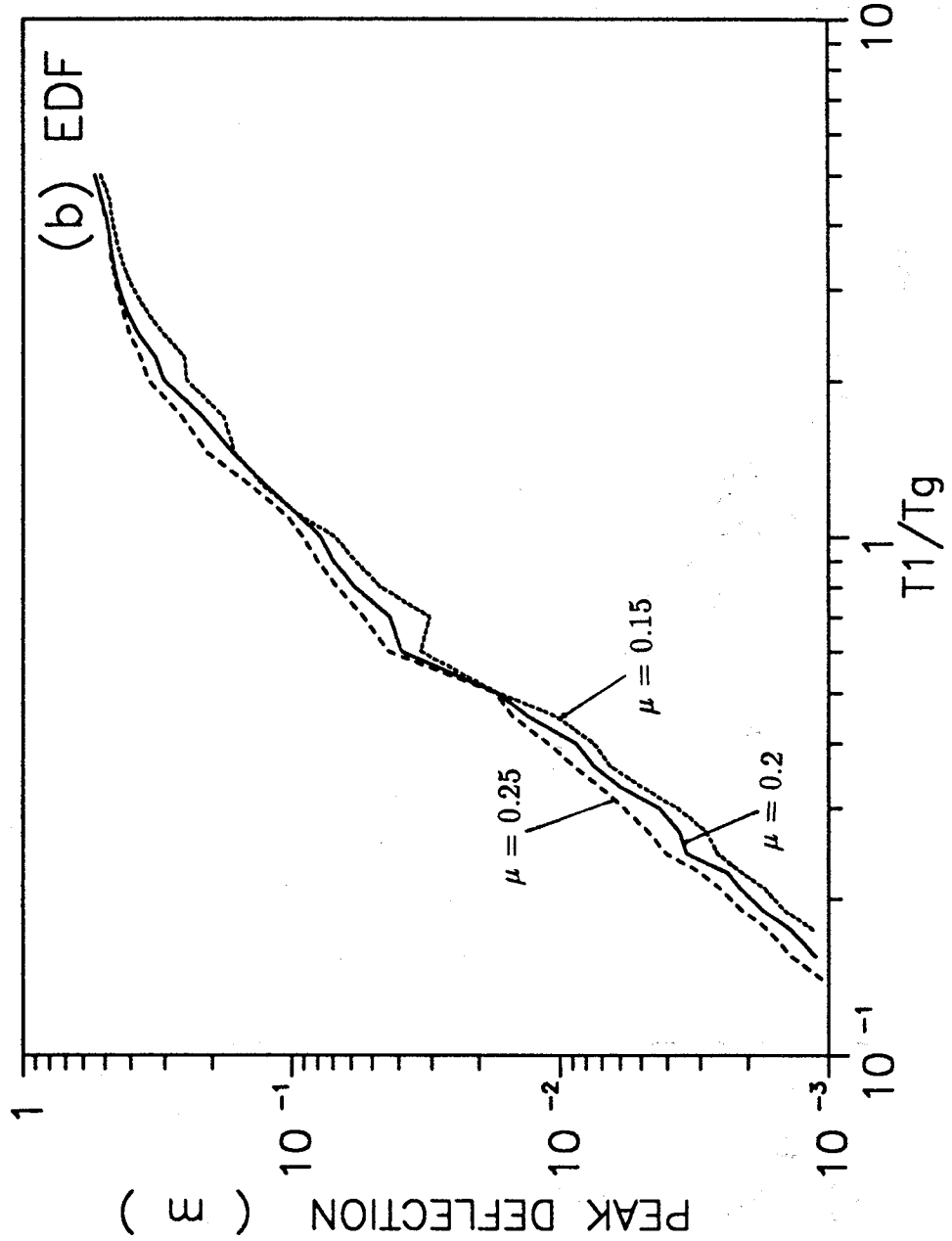
(b) EDF
PEAK DEFLECTION (m)
1
10 -1
10 -2
10 -3
10 -1
1
10
T1/Tg
μ = 0.15
μ = 0.2
μ = 0.25

Figure 4–17

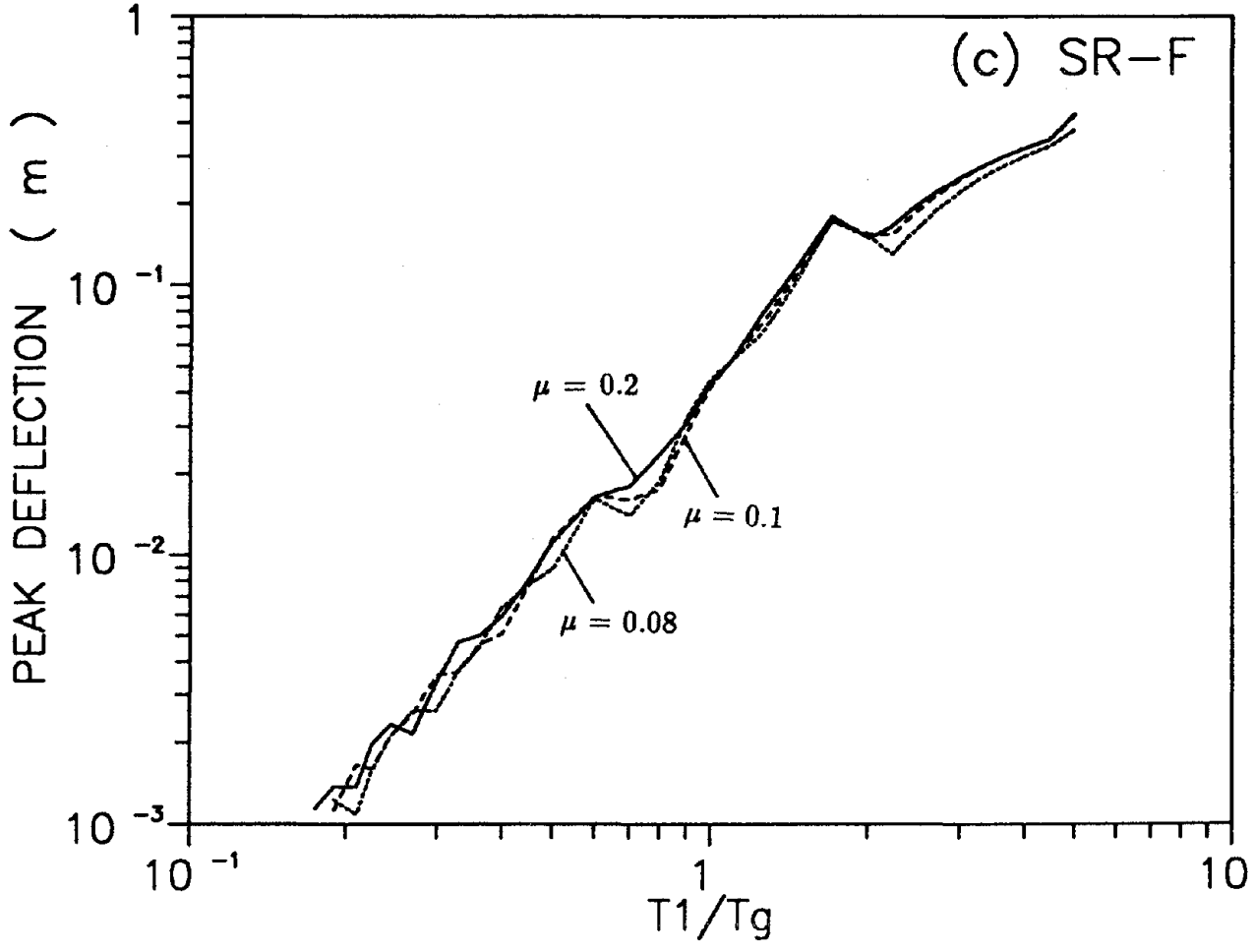

Figure 4−17

4.6 Velocity-Dependent Friction Coefficient

It is well known that the friction coefficients between surfaces are not constants and vary with a number of kinematic and dynamic parameters [31]. The most important factors affecting the friction coefficient are the relative velocity between surfaces and the normal force. The recent data of [32] for teflon-steel interfaces suggests that μ increases with the relative velocity and decreases with the interface pressure. There has been questions concerning the significances of velocity-dependent friction coefficients on the performances of various frictional base isolation systems. In this section, the sensitivity of the peak responses of the R-FBI system to the velocity-dependent friction coefficient is studied. A structure with a fundamental natural period of 0.3 *sec* is used. A sinusoidal ground excitation with an amplitude of $0.5g$ and a period of 0.8 *sec* is considered. The velocity-dependence of friction coefficient is assumed to be given as

$$\mu = \mu_o + \beta_o \frac{|\dot{s}|}{\nu} \tag{4.1}$$

where μ_o is the static friction coefficient, $\dot{s}$ is the relative sliding velocity, ν is the number of friction plates of the R-FBI system, and β_o is a constant. Several values of β_o up to 0.7 sec/m are used in the analysis. These imply significant variations of μ with $\dot{s}$.

Figures 4-18 through 4-20 show the peak absolute acceleration, the peak base displacement, and the peak deflection response spectra for the R-FBI systems with $\mu_o = 0.05$ and various values of β_o. The peak velocity responses, $\dot{s}|_{max}$, are also plotted in Figure 4-18 for reference. It is observed that the peak sliding velocities are of the order of 1 m/sec. That is, μ varies from 0.05 to 0.1 or 0.12 corresponding to $\beta_o = 0.5$ or 0.7 sec/m, respectively, for a R-FBI isolator with ten friction plates.

Figure 4-18 shows that the peak accelerations remain the same for various values of β_o considered here. This is because the peak acceleration responses for the R-FBI systems are mainly generated by the slip-stick and slip reversal shock loadings. These motion transitions occur at $\dot{s} = 0$ for which μ is equal to μ_o. Therefore, the velocity dependence of friction coefficient has no significant effect on the acceleration response spectra.

Figure 4-19 shows the peak base displacement responses for various values of β_o. It is noticed that the base displacement response spectrum decreases slightly

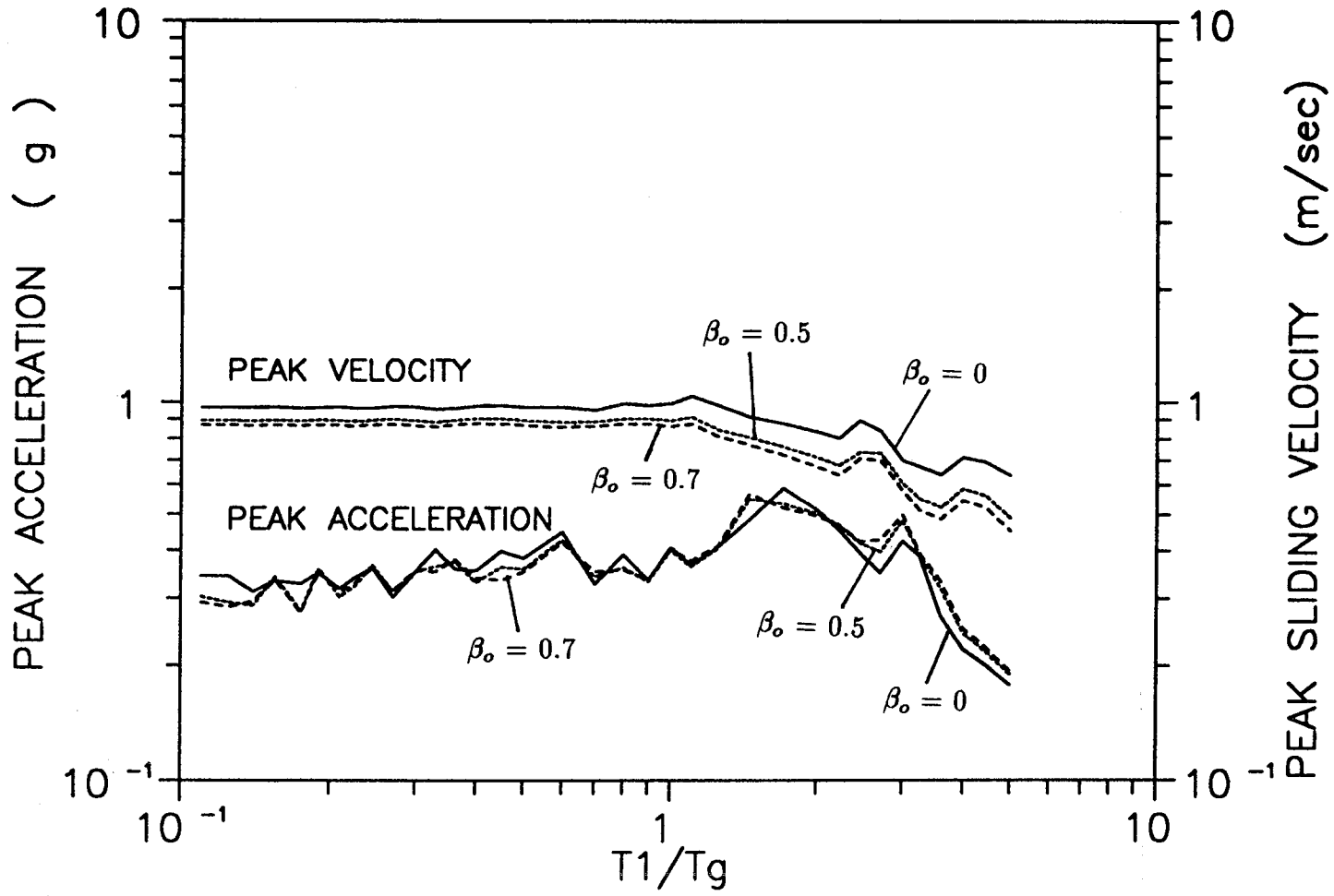

Figure 4–18 Variations of Peak Absolute Acceleration at the Top of Structure and Peak Sliding Velocity with Period Ratio for the R–FBI System for Several Velocity–Dependent Friction Models

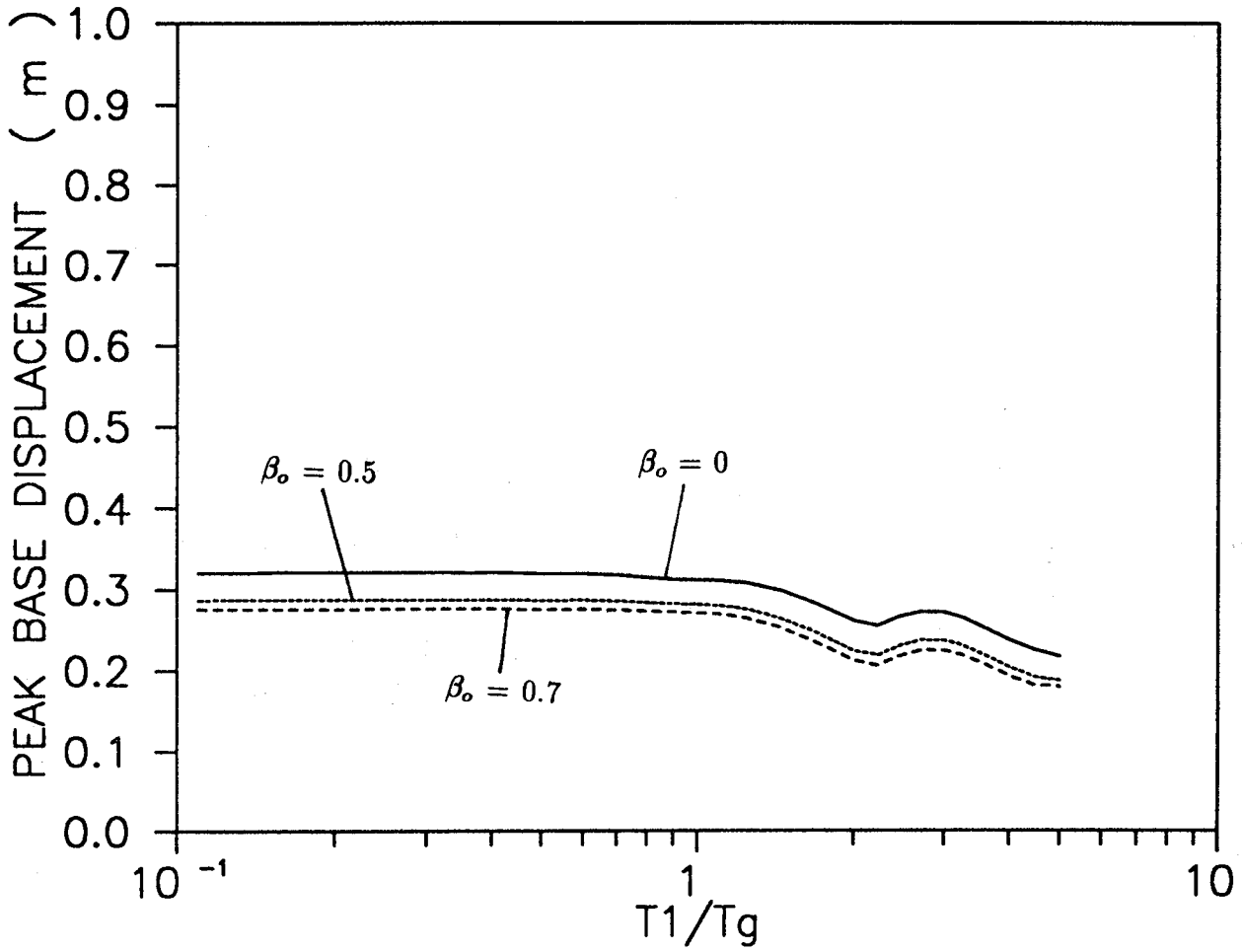

Figure 4–19 Variations of Peak Base Displacement with Period Ratio for the R–FBI System for Several Velocity–Dependent Friction Models

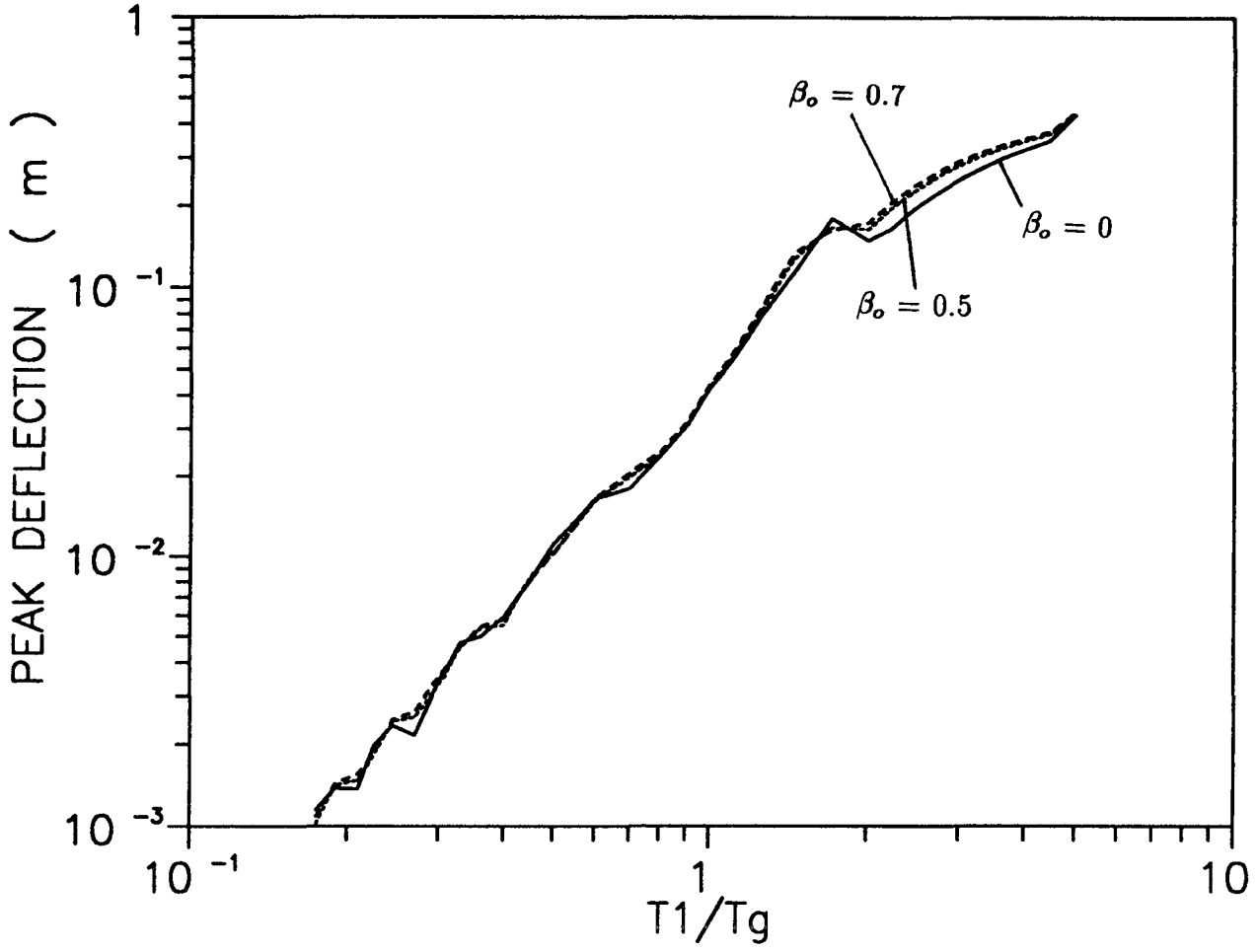

Figure 4–20 Variations of Peak Deflection with Period Ratio for the R–FBI System for Several Velocity–Dependent Friction Models

as β_o increases due to the larger sliding resistance. As noted before, the peak displacements remain the same for structures with different T_1.

The peak deflection responses are shown in Figure 4-20. It is noticed that the velocity-dependent friction coefficient feature has negligible effects to the peak deflection response for the R-FBI system. As the magnitude of β_o varies from 0.0 to 0.7, no noticeable variation is observed for period ratios less than unity.

The values of β_o used in here are much larger than those suggested by the data of [32]. Nevertheless, Figures 4-18 through 4-20 show that consideration of the velocity dependence of the friction coefficient has negligible effects on the performance of the R-FBI system. Hence, the Coulumb friction law with a constant μ may be used to simulate the behavior of the R-FBI system. In their experiments, Constantinou et al. [32] noticed non-stick continuous sliding and motion direction reversal. However, additional experiments are needed to clarify this observation.

4.7 Effects of Damping of Isolation System

The effects of the damping coefficient of the base isolators on the peak responses for various systems are investigated in this section. A structure with a fundamental natural period of 0.3 *sec* is used, and the results are shown in Figures 4-21 through 4-23.

The peak absolute acceleration responses at the top of the structure for various systems are plotted versus ζ_o in Figure 4-21. It is observed that the damping coefficient of the base isolation systems considered here has little effect on the peak acceleration responses. A careful examination of Figure 4-21 shows that as the value of ζ_o increases, the peak acceleration responses slightly decrease at first and then somewhat increase with further increase in ζ_o. This behavior may be explained as follows: As ζ_o increases the energy dissipation of the isolators increases which causes the transmitted peak acceleration to reduce. However, for large values of ζ_o, the isolators become rather stiff and the peak accelerations increase accordingly. For $\zeta_o > 0.45$, sliding in the upper friction plate of the SR-F system occurs. In this range of ζ_o, the peak acceleration response for the SR-F system is slightly lower than that of the R-FBI system. Figure 4-21 also shows that variations of the peak acceleration in the entire range of ζ_o considered is less than $0.05g$ for all the systems considered.

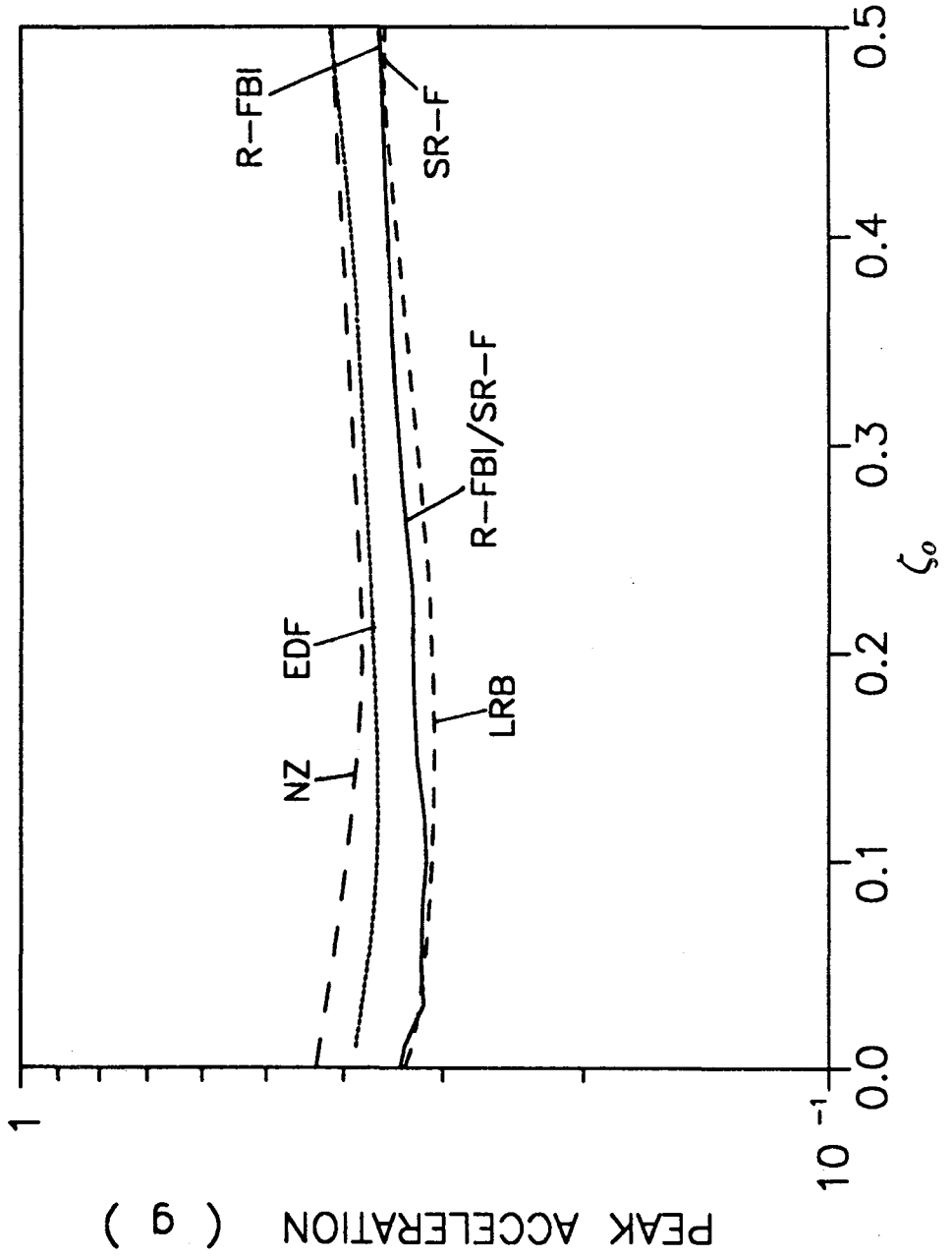

Figure 4-21 Variations of Peak Absolute Acceleration at the Top of Structure with Damping of Isolation System

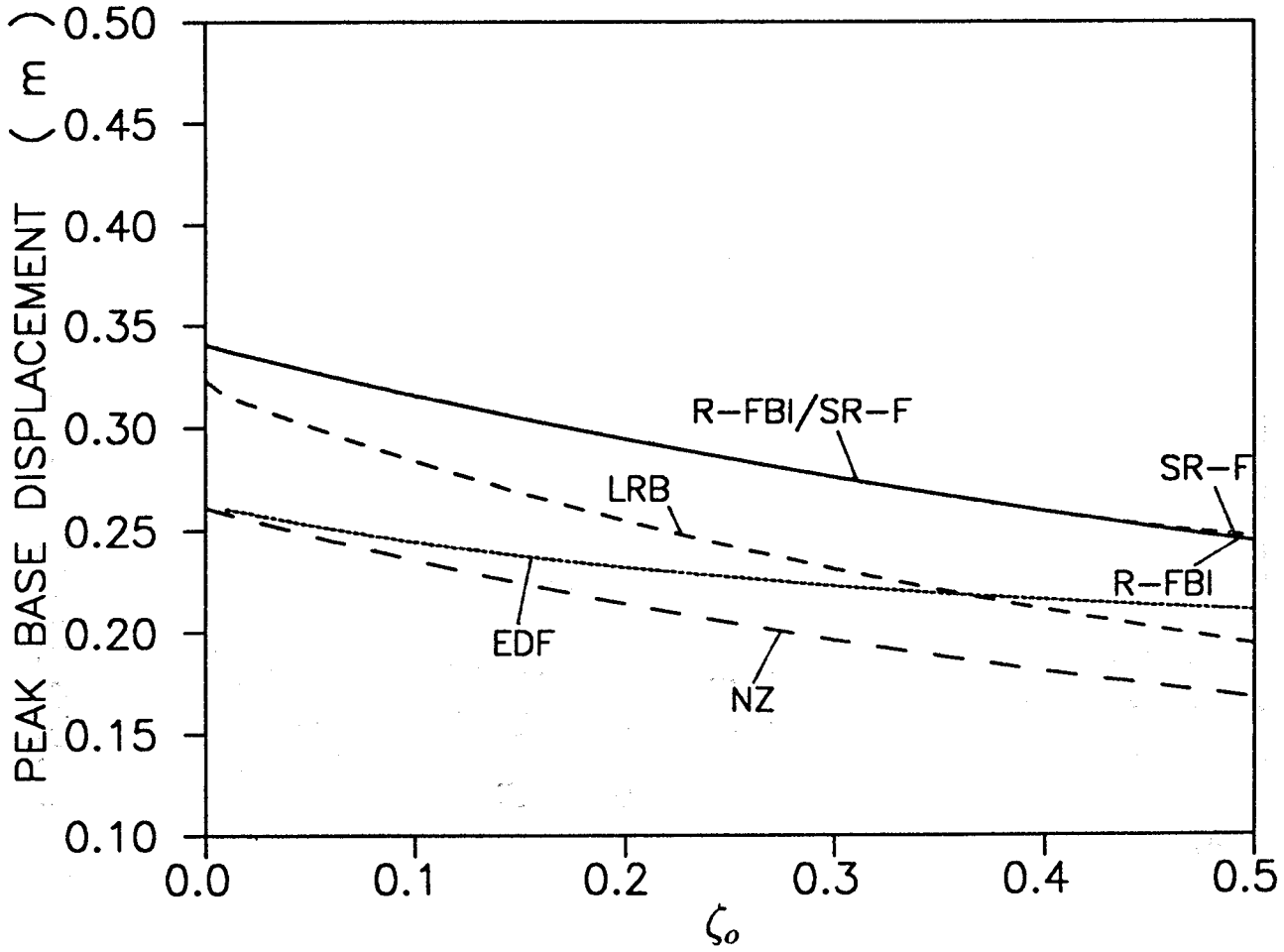

Figure 4-22 Variations of Peak Base Displacement with Damping of Isolation System

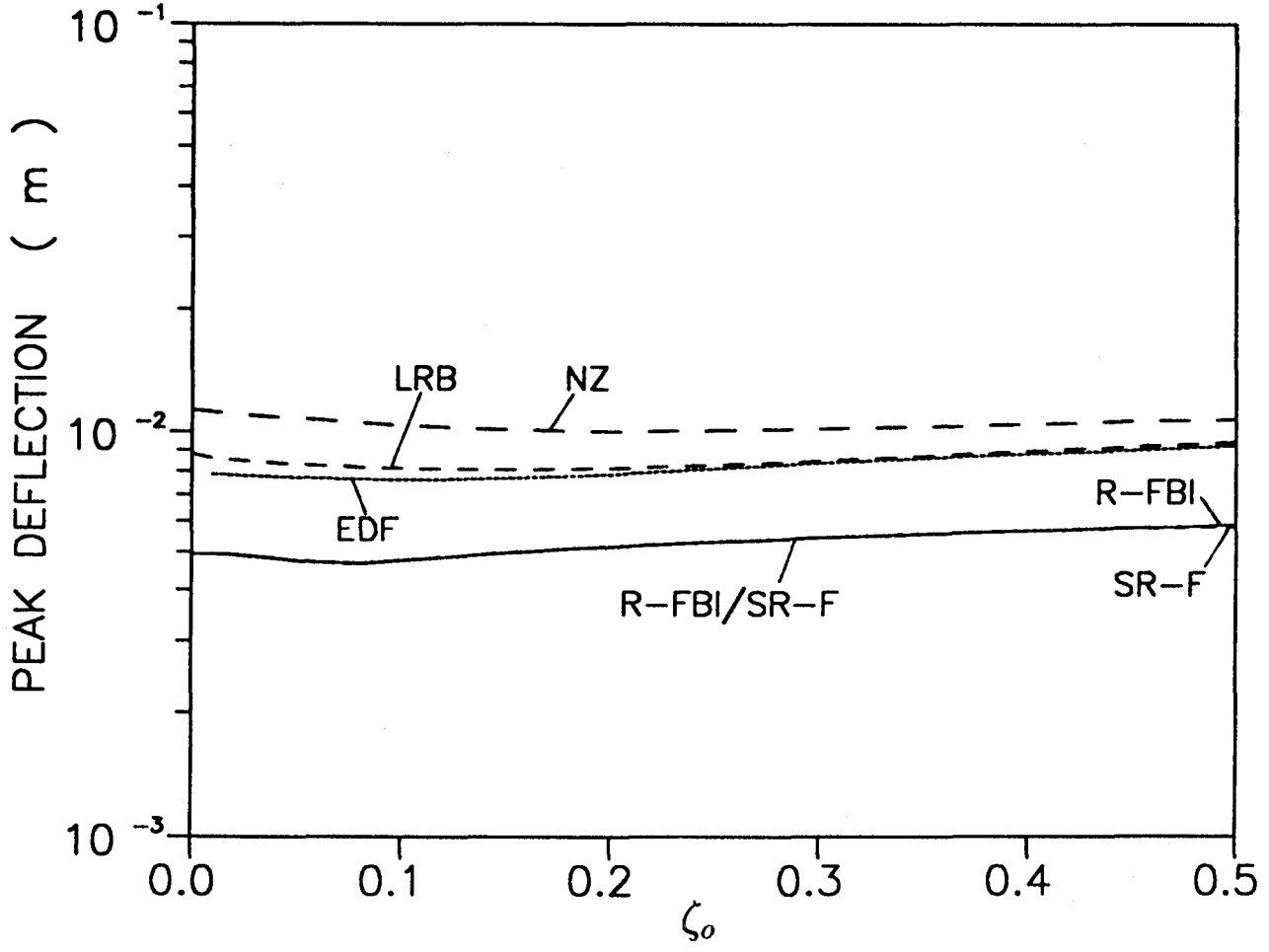

Figure 4-23 Variations of Peak Deflection with Damping of Isolation System

Figure 4-22 shows the effects of ζ_o on the maximum base displacement responses for various base isolation systems. It is observed that as the value of ζ_o increases, the peak base displacements decrease monotonically. The results show that the peak displacement of the LRB system is most sensitive to variation in ζ_o. As the value of ζ_o increases from zero to thirty percents, the maximum displacement of the LRB decreases by about 9 *cm*. For ζ_o larger than about 0.45, the peak displacement of the SR-F system is slightly larger than that of the R-FBI system due to the occurrence of sliding in the upper friction plate.

The effects of variations of ζ_o on the the maximum deflection responses for various isolation systems are shown in Figure 4-23. It appears that, like the peak accelerations, the peak deflections are insensitive to variations in ζ_o. Furthermore, in the range of small ζ_o, as damping increases, the peak deflections decrease slightly to a minimum and then increase somewhat as ζ_o further increases. However the total amount of variations is small, and less than 0.2 *cm* for all the isolators considered here.

Based on the results of this section, it may be concluded that the damping of isolator only slightly affects the relative base displacements and has no effect on the peak transmitted accelerations or the peak deflections of the structure.

4.8 Effects of Natural Period of the Isolation System

This section considers the effects of variations in the natural period of the isolator on the peak responses for various base isolation systems. For a structure with a fundamental natural period of 0.3 *sec*, the peak responses for different systems for T_o varying between 0.6 to 6 *sec* are evaluated and the results shown in Figures 4-24 through 4-26.

Figure 4-24 shows the peak acceleration responses at the top of the structure for various base isolation systems. It is observed that the R-FBI, the LRB, and the NZ systems show resonance peaks with magnitudes of about $4g$ at $T_o \simeq 0.8$ *sec*. For $T_o > 3$ *sec*, the peak accelerations of the SR-F system coincides with that of the R-FBI system and remains at a constant level of about $0.4g$. Figure 4-24 also shows that the peak acceleration response of the EDF system becomes identical to that of the LRB system for $T_o > 2.7$ *sec*. It is also noticed that the peak acceleration of the LRB decreases rapidly as T_o increases, while that of the NZ approaches a constant

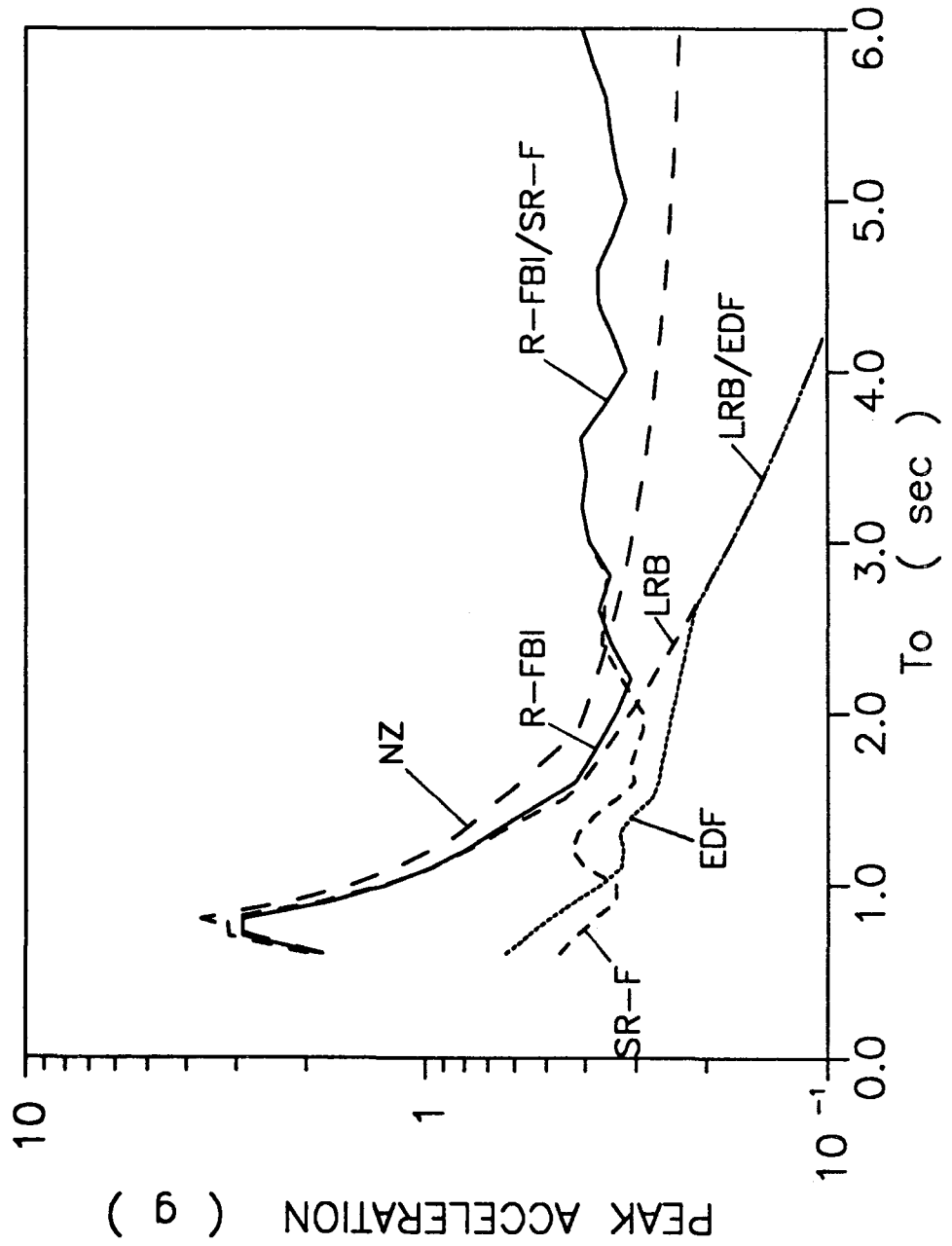

Figure 4–24 Variations of Peak Absolute Acceleration at the Top of Structure with Natural Period of Isolation System

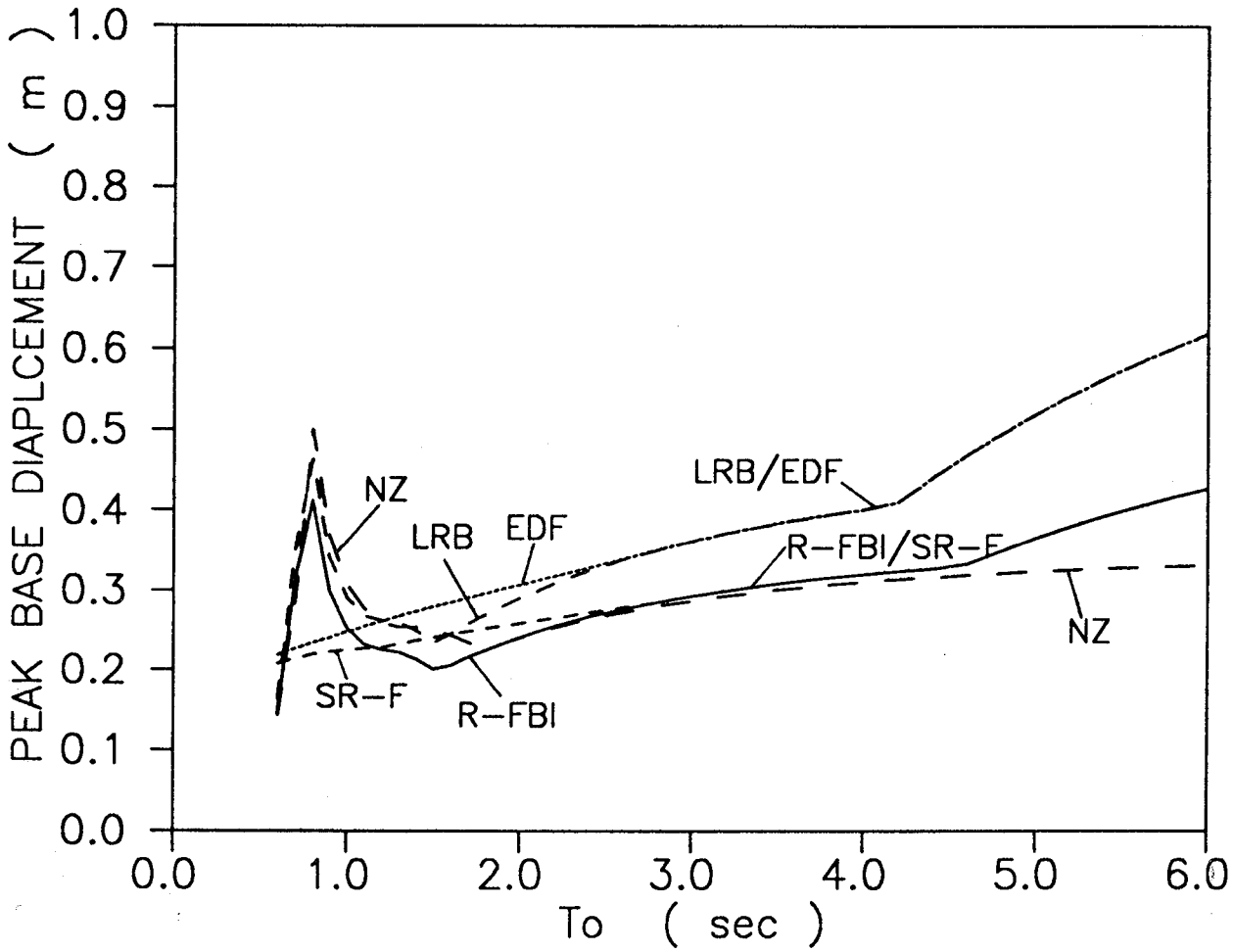

Figure 4-25 Variations of Peak Base Displacement with Natural Period of Isolation System

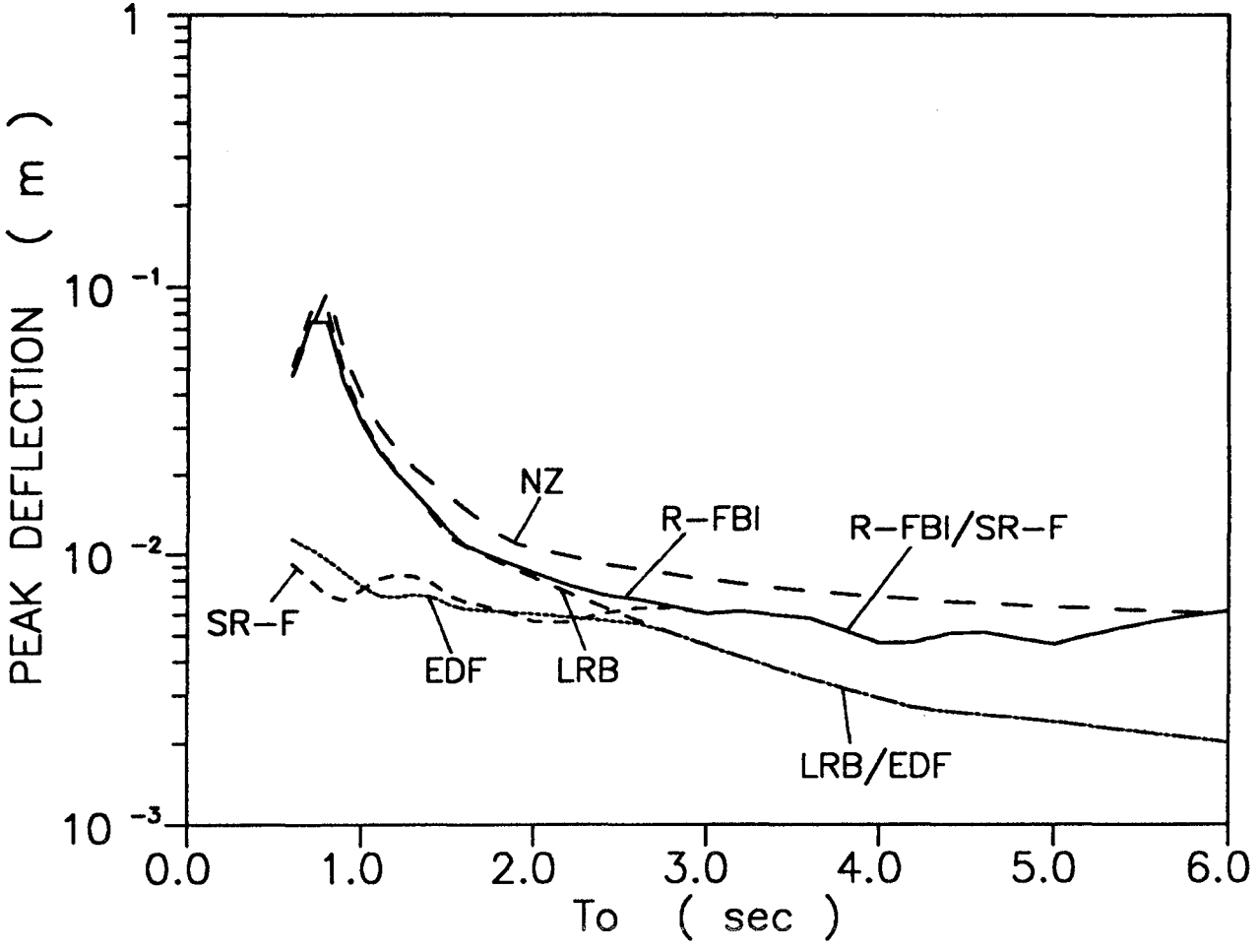

Figure 4-26 Variations of Peak Deflection with Natural Period of Isolation System

level of about $0.2g$.

The peak base displacement responses for various base isolation systems are shown in Figure 4-25. For T_o of about 0.8 *sec*, the R-FBI, the LRB, and the NZ system show resonance peaks with magnitudes of 0.4 to 0.5 m. For T_o larger than 2 *sec*, the peak base displacement responses increase with the natural period of the isolation system for all systems considered.

Figure 4-26 shows the peak deflection responses for various systems versus the natural period, T_o. It is noticed that the behaviors of the peak deflection spectra are similar to those of the peak acceleration spectra shown in Figure 4-26. The R-FBI, the LRB, and the NZ systems show resonance peaks with amplitudes of about 8 to 10 *cm* at $T_o \simeq 0.8$ *sec*. For $T_o > 2$ *sec*, the peak deflections for the R-FBI and the NZ systems remains constants of the order of 0.5 *cm* to 1 *cm*. The peak deflection response of the LRB system decreases gradually as T_o increases. For T_o greater than 2.7 to 3 *sec*, the peak deflections for the SR-F and the R-FBI systems and those for the EDF and the LRB systems coincide.

Figures 4-24 through 4-26 show the response spectra of the LRB, the NZ and the R-FBI systems have sharp peaks whenever the natural frequencies of these isolators coincide with the frequency of ground excitation. The responses of the SR-F and the EDF systems, however, are devoid of such resonance peaks. This is due to the presence of the upper friction plates which provide additional means of energy dissipation for these latter systems.

4.9 Effects of Amplitude of Ground Excitation

In this section, the effects of an increase in the intensity of ground excitation are studied. A sinusoidal ground acceleration as given by Eq.(3.3) with an amplitude of g and $T_g = 0.8$ *sec* is used to simulate a strong earthquake. The peak structural responses are evaluated and the results are plotted in Figures 4-27 through 4-29 versus period ratio, T_1/T_g. The results are compared with those obtained for an amplitude of $0.5g$, and the sensitivity of performances of various base isolators to the variation in the amplitude of the ground excitation is discussed.

The acceleration response spectra at the top of the structure for various base isolation systems and the fixed-base structure are shown in Figure 4-27. It is observed

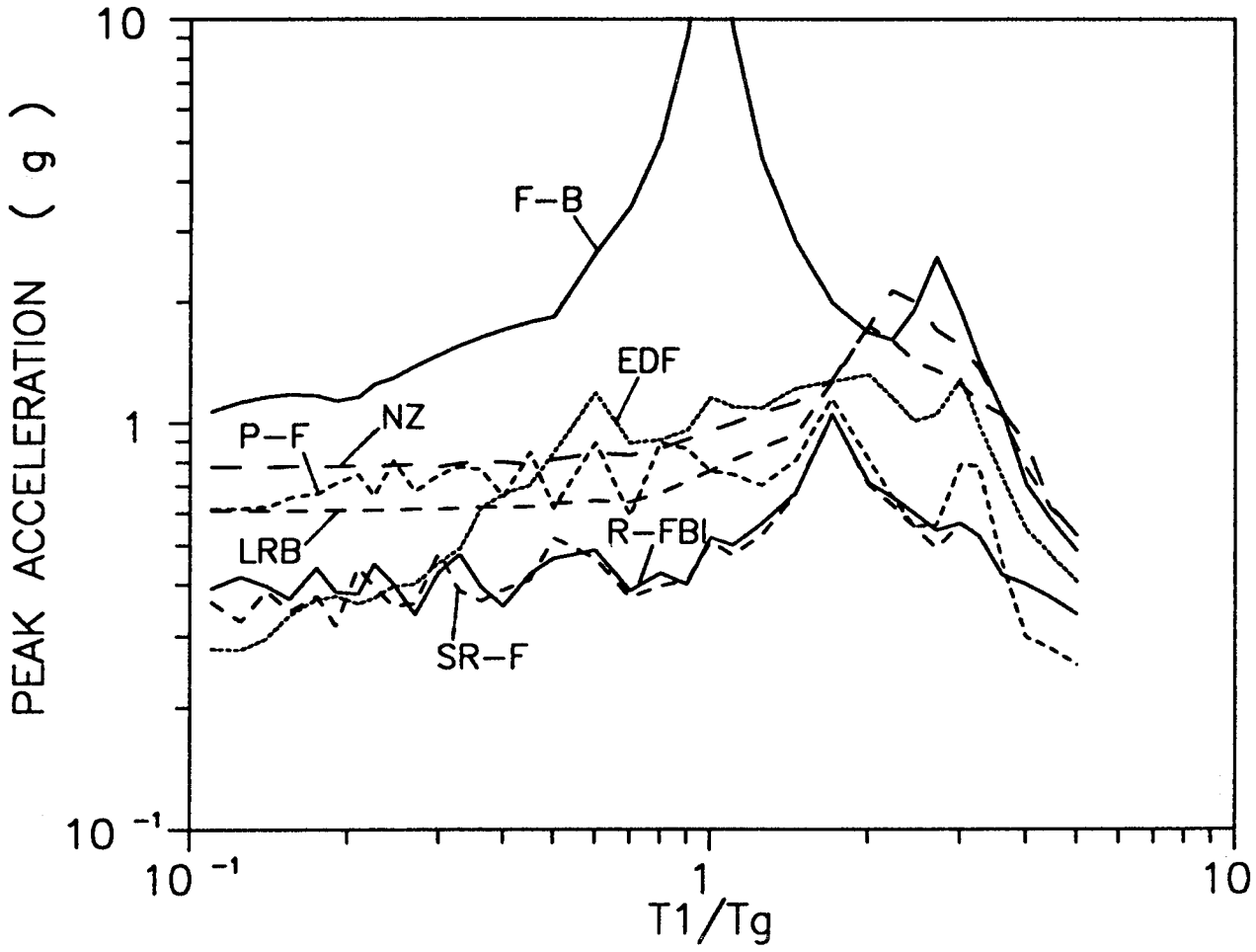

Figure 4-27 Variations of Peak Absolute Acceleration at the Top of Structure with Period Ratio for a Ground Excitation with an Amplitude of g

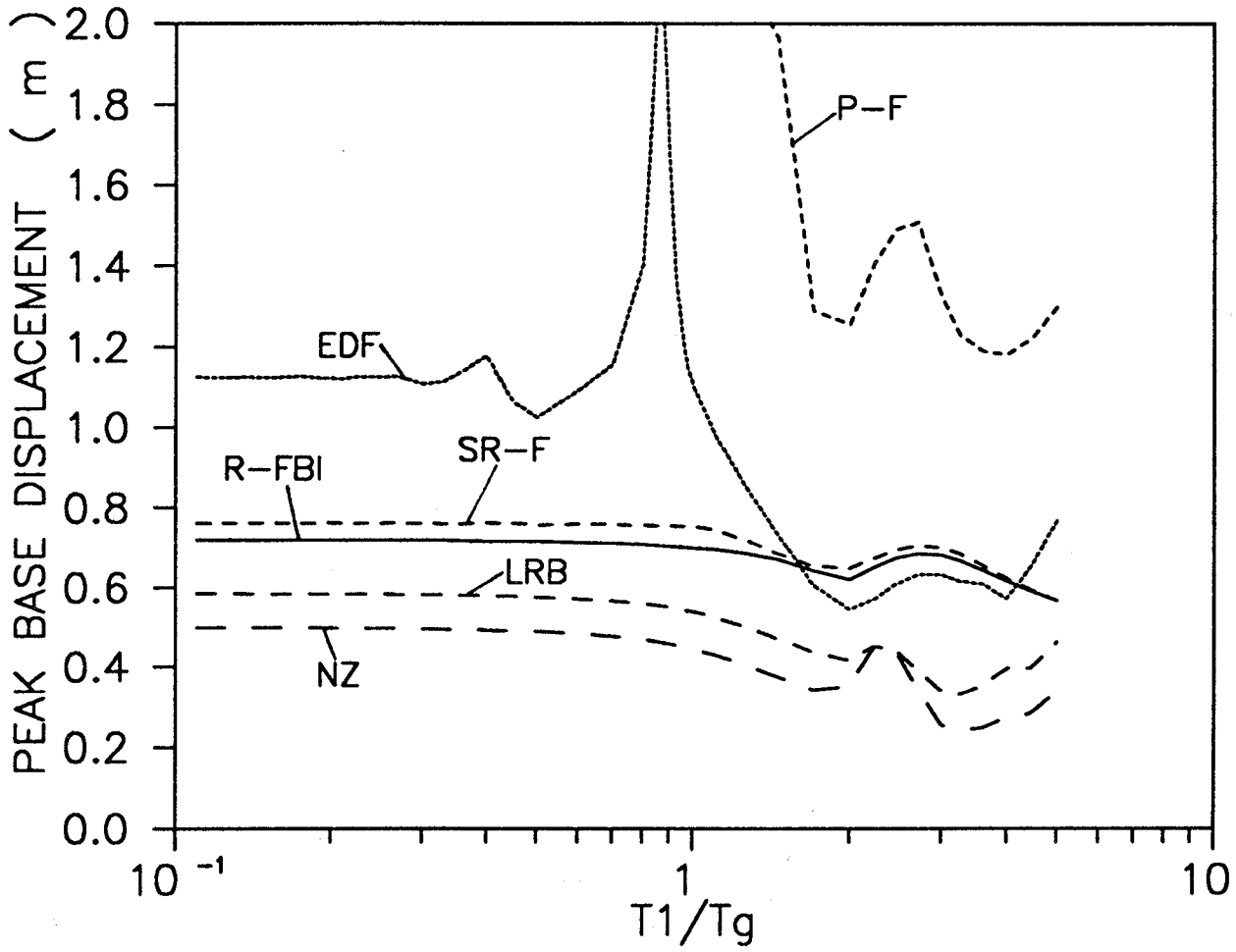

Figure 4–28 Variations of Peak Base Displacement with Period Ratio for a Ground Excitation with an Amplitude of g

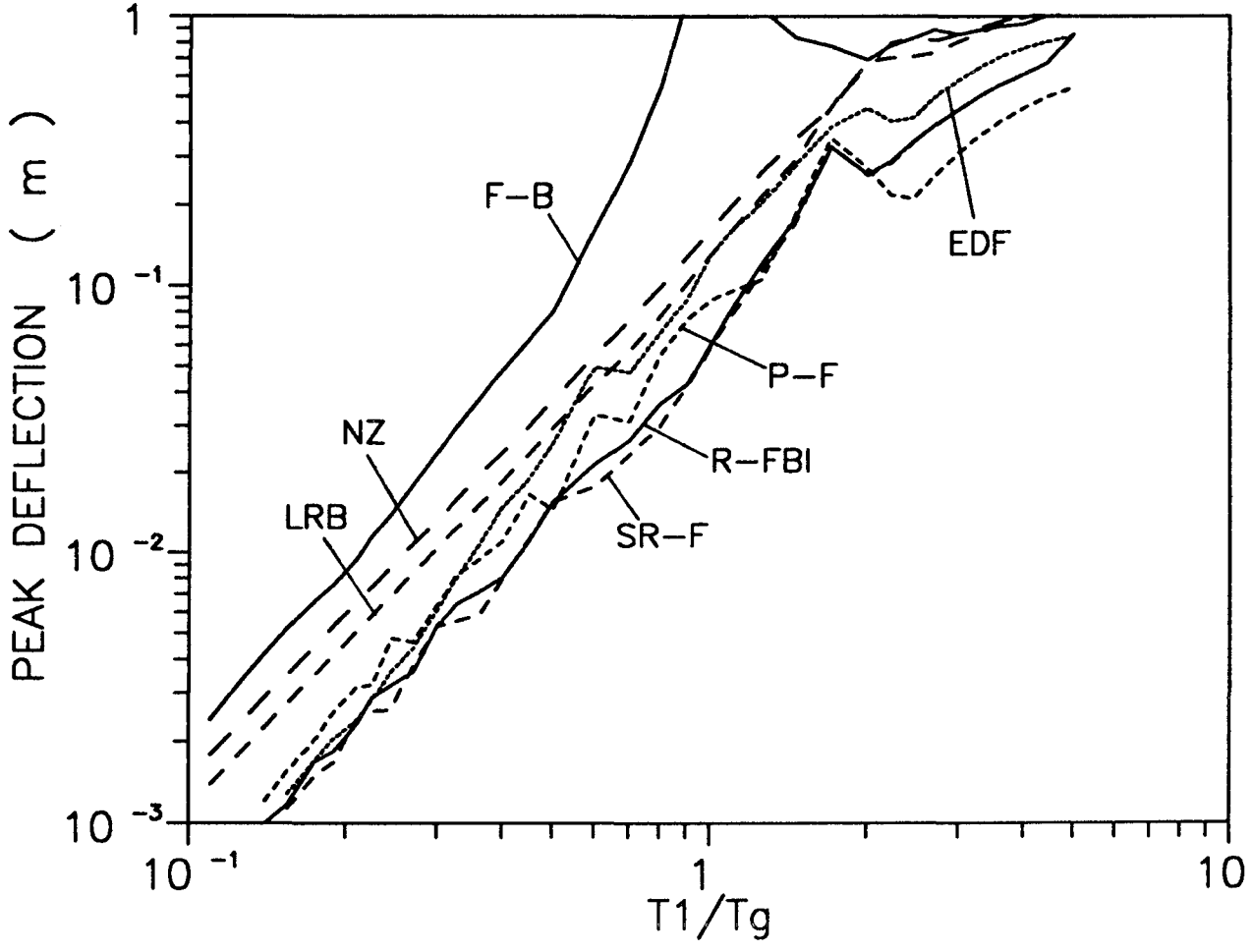

Figure 4-29 Variations of Peak Deflection with Period Ratio for a Ground Excitation with an Amplitude of g

that the resonance peak of the fixed-base structure has an extremely high peak value (more than $20g$). For the structure with various base isolation systems, the resonance peak is eliminated and the peak accelerations at $T_1/T_g \simeq 1$ are reduced by more than twenty times. For the ground excitation considered here, sliding in the upper friction plate of the SR-F system occurs, nevertheless, the peak acceleration responses remain almost the same as those of the R-FBI system. Figure 4-27 shows, with the exception of the EDF system, the acceleration response spectra curves of the isolated structure remain almost constant for $T_1/T_g < 1$. In this range, the R-FBI/SR-F systems lead to a peak acceleration of about $0.4g$ which is the lowest among the isolators considered. The peak accelerations for the LRB, the NZ and the P-F are about 0.6 to $0.8g$. Comparing the acceleration response spectra curves shown in Figure 4-27 with their counterparts shown in Figure 4-4, it is observed that the peak accelerations for the LRB, the NZ system, and the fixed-base structure are roughly doubled when the amplitude of ground excitation is doubled. However, the peak accelerations for the R-FBI/SR-F are increased only by about 10% and those of P-F and the EDF systems are increased by about 15%.

Figure 4-28 shows the peak base displacement responses for various base isolation systems. It is noticed that the maximum relative base displacements for the EDF and the P-F systems contain sharp peaks with magnitudes of more than 2 m and 3 m for a period ratio of about 0.9 which are much larger than those of the other base isolation systems; furthermore, for the NZ, the LRB, the R-FBI, and the SR-F systems, the peak displacement response spectra are approximately constant for $T_1/T_g < 1$ with magnitudes of about 0.5 m to 0.75 m. Comparing Figure 4-28 with the corresponding results shown in Figure 4-5, it is observed that the peak displacement responses for the LRB, the NZ, and the R-FBI systems are roughly doubled as the amplitude of the ground excitation is increased from $0.5g$ to g.

The maximum deflection responses for various systems are shown in Figure 4-29. The deflection response spectrum curve for the fixed-base structure shows a large peak with magnitude more than 3 m at $T_1/T_g \simeq 1$. The peak deflection responses for the base isolated structure are much lower than that of the fixed-base one and do not have resonance peaks. For a structure with a fundamental natural period of 0.3 *sec*, the peak deflection responses for the base isolated structure range from a minimum of about 0.6 *cm* for the R-FBI and the SR-F systems to a maximum

of about 2 *cm* for the NZ system. The corresponding fixed-base structure shows a maximum deflection of about 4 *cm*. Comparison of Figures 4-6 and 4-29 shows that the peak deflection responses for the LRB, the NZ base isolation systems and the fixed-base structure are doubled when the amplitude of the ground excitation is doubled, while for the frictional system the increase is about 25%.

The presented results show that the peak acceleration and deflection responses of the frictional base isolation systems increase only slightly with a substantial increase in the intensity of the ground excitation. The peak responses of the LRB and the NZ system increase in direct proportion to the amplitude of ground acceleration. The base displacements for the P-F and the EDF systems may become unacceptably large under certain conditions. Figures 4-27 through 4-29 show that for a high intensity ground excitation, the R-FBI and the SR-F base isolation systems lead to the lowest peak acceleration and peak deflection. The corresponding peak base displacement is also quite reasonable.

4.10 Effects of Frequency Content of Ground Excitation

In this section, sensitivities of peak responses to the variations in the frequency content of the ground excitation for various base isolation systems are studied. A structure with a fundamental natural period of 0.3 *sec* is considered, and a sinusoidal ground excitation with an amplitude of $0.5g$ is used. The peak responses are evaluated and the results are plotted versus T_g in Figures 4-30 through 4-32.

Figure 4-30 shows the peak acceleration responses for various systems and for the fixed-base structure. It is observed that the acceleration response spectrum of the fixed-base structure has a resonance peak of about $10g$ at $T_g = 0.3$ *sec*; furthermore, a secondary peak is observed at $T_g \simeq 0.11$ *sec* which is due to the resonance between the second mode of the structure and the ground excitation. The peak acceleration response for the P-F isolator (with $\mu = 0.1$) is almost constant with a magnitude of about $0.6g$ throughout the entire range of T_g considered. For $T_g < 1$ *sec*, the peak accelerations for the SR-F and the R-FBI systems coincide and are about $0.4g$. However, for $T_g > 1$, the response of the R-FBI increases with T_g while the peak acceleration of the SR-F system decreases slightly.

Figure 4-30 shows that the fundamental natural period of 0.3 *sec* for the fixed-base structure is shifted to about 2 *sec* for the LRB and the NZ systems and to about

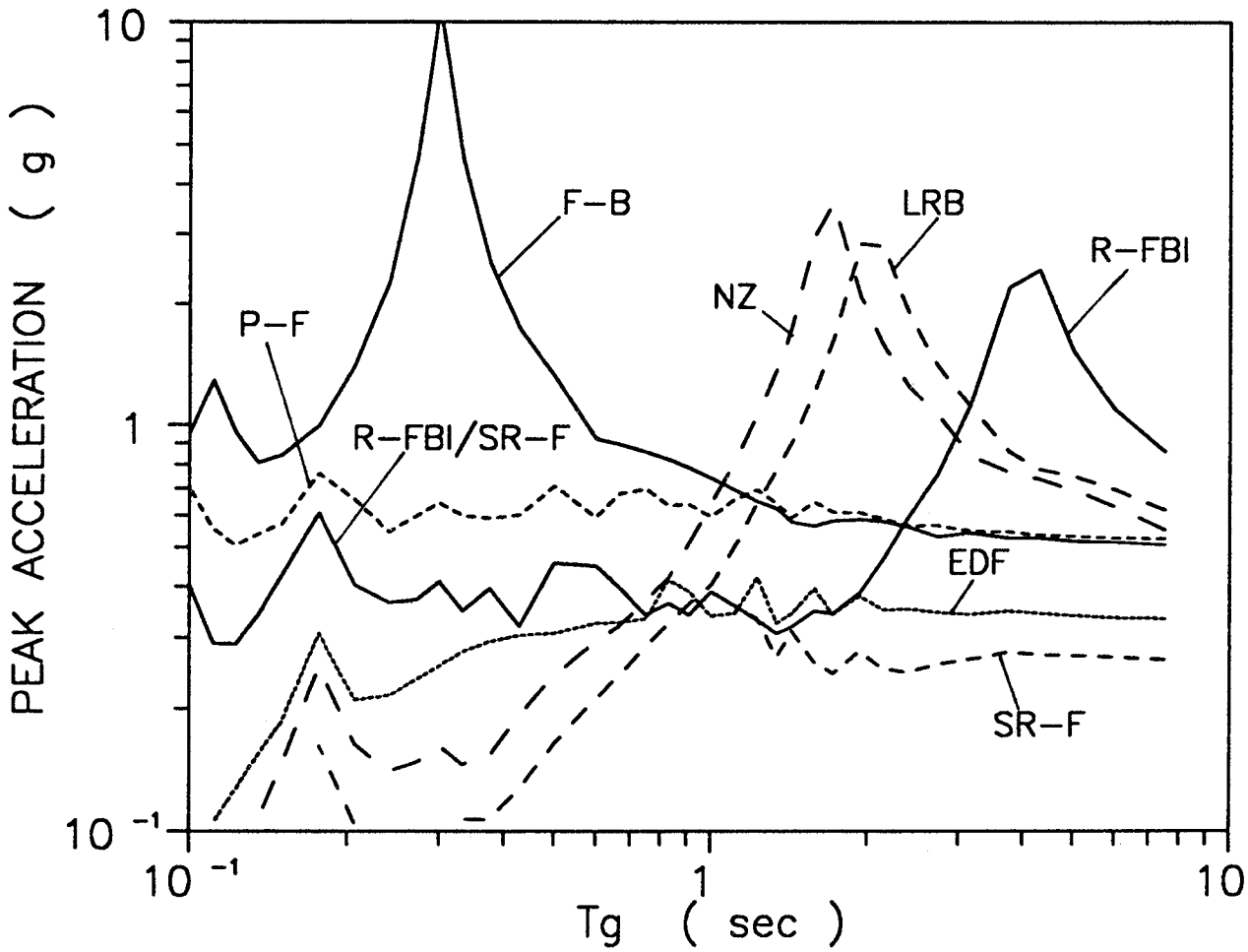

Figure 4–30 Variations of Peak Absolute Acceleration at the Top of Structure with Period of Ground Excitation

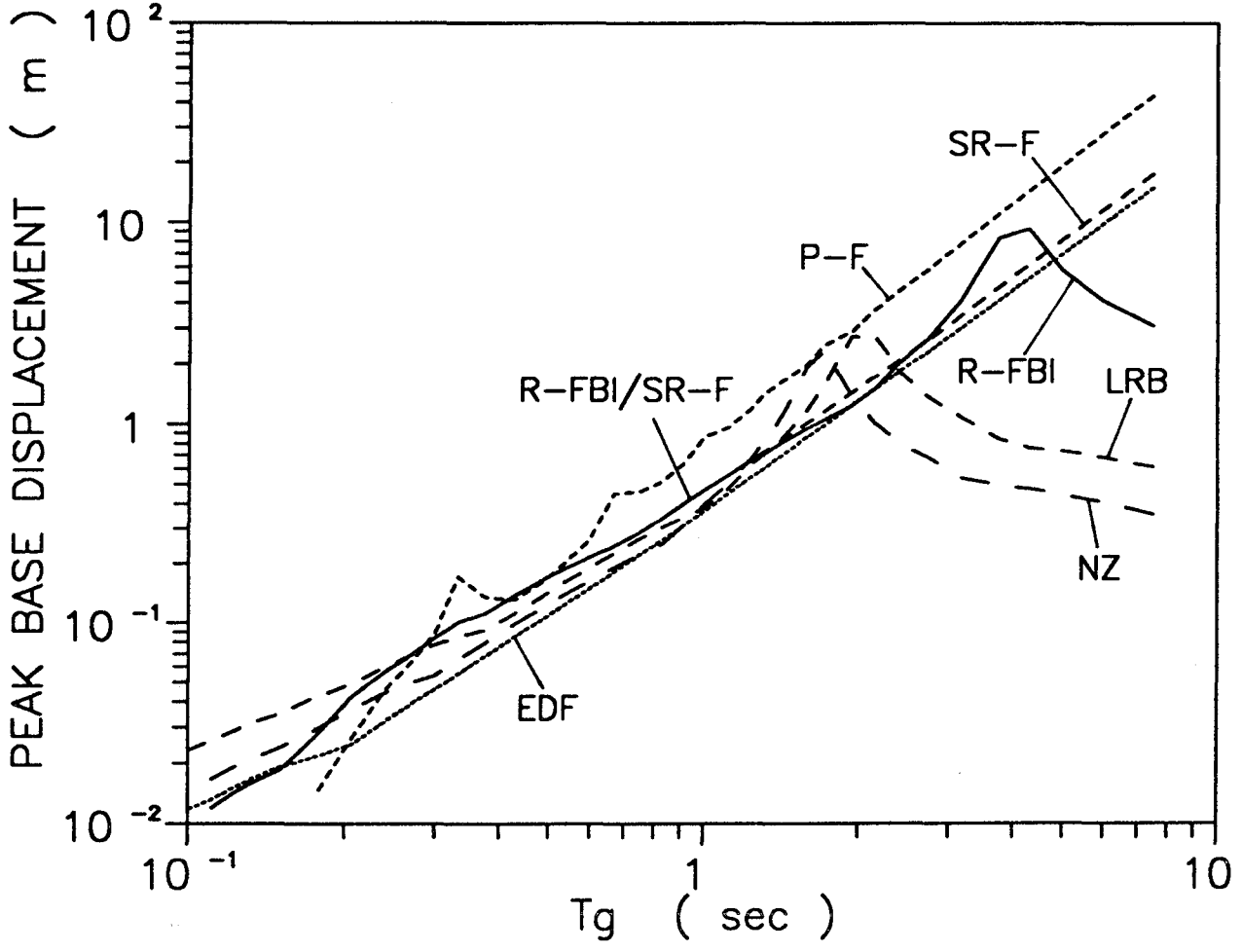

Figure 4-31 Variations of Peak Base Displacement with Period of Ground Excitation

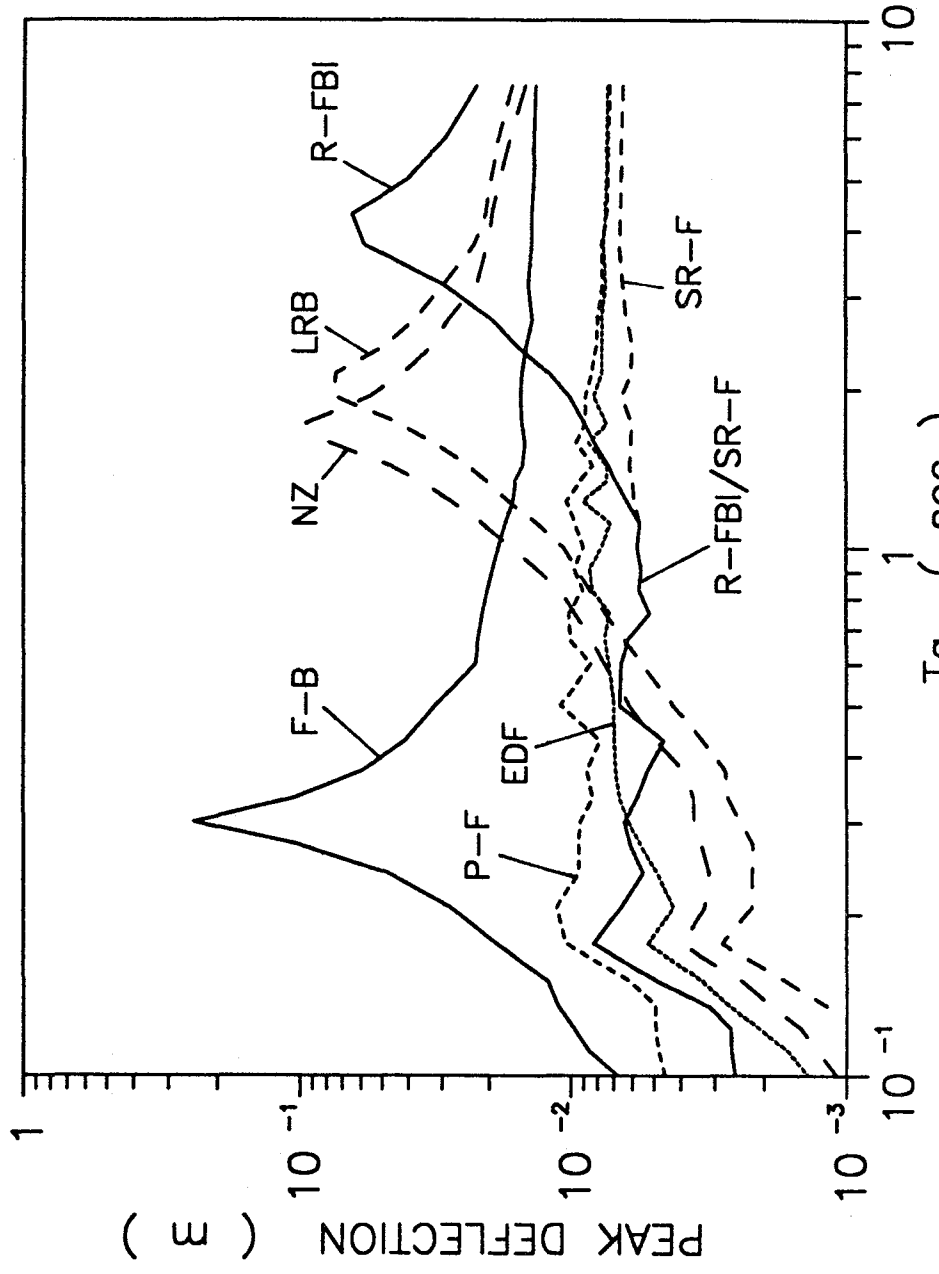

Figure 4-32 Variations of Peak Deflection with Period of Ground Excitation

4 *sec* for the R-FBI system. The presence of the upper friction plates in the EDF and the SR-F base isolation system eliminates the resonance peak altogether. It is also noticed that secondary resonance peaks for the LRB, the NZ, and the R-FBI systems occur at $T_g \simeq 0.17$ *sec*. For $T_g < 0.7$ *sec*, the LRB and the NZ systems lead to the lowest peak acceleration responses; while, the SR-F and the EDF systems generate the lowest peak accelerations for $T_g > 1$ *sec*.

Figure 4-31 shows that the maximum base displacement responses generally increases with T_g. It is observed that for $T_g > 0.5$ *sec*, the P-F system leads to the largest peak base displacement response among the base isolation systems considered. The peak base displacement responses for the LRB and the NZ systems increase with T_g up to about 2 *sec*, at which resonance peaks with magnitudes of about three meters appear. The R-FBI system shows a resonance peak at $T_g \simeq 4$ *sec* with a magnitude of about 10 *m*. Figure 4-31 also shows the displacements of the P-F, the EDF, and the SR-F isolators which contain pure-friction elements increase monotonically as T_g increases.

The variations of the maximum deflections versus T_g for various base isolation systems are displayed in Figure 4-32. It is observed that the deflection spectrum of the fixed-base structure shows a resonance peak of about 23 *cm* at $T_g = 0.3$ *sec*. The LRB and the NZ systems lead to resonance peak deflections of about 7 to 9 *cm* at $T_g \simeq 2$ *sec*, while that of the R-FBI system shows a resonance peak of about 7 *cm* at $T_g \simeq 4$ *sec*. The peak deflections for the P-F, the EDF, and the SR-F systems remain constants of about 0.6 *cm* to 0.9 *cm* for the entire range of $T_g > 0.2$ *sec*. For $T_g < 0.6$ *sec*, the LRB and NZ systems lead to the least peak deflection responses, while, the P-F, the EDF, and the SR-F systems generate the lowest peak deflections for $T_g > 2$ *sec*.

These results show that the peak responses of the R-FBI, the LRB, and the NZ systems are rather sensitive to the frequency contents of ground excitation. In particular, when the periods of the ground excitation are close to the natural period of these isolation systems, significant increase in the peak responses may occur. In contrast, the P-F, the EDF, and the SR-F systems appear to be insensitive to the variations in the frequency contents of the ground acceleration.

SECTION 5

CONCLUSIONS

A multi-story structure with several leading base isolation systems subject to a sinusoidal ground excitation is considered. The peak acceleration, the maximum base displacement, and the peak deflection responses are evaluated and the performance of the different base isolation systems are analyzed. Several sensitivity studies by varying the parameters of the structure, the isolation systems, and the ground excitation are also performed. Based on the present results, the following conclusions may be drawn:

1. The base isolation systems are highly effective in reducing the ground acceleration transmitted to the superstructure and the column stresses generated in the structure. Comparison of responses of the base isolated structure with those of the fixed-base one show that an isolation system could reduce peak acceleration and peak deflection responses by a factor of ten or more with a manageable relative base displacement.

2. For a ground acceleration of $0.5g$, the LRB lead to the lowest peak acceleration transmitted to the structure. For high intensity ground excitations (about $1g$), the R-FBI/SR-F systems transmit the lowest peak acceleration.

3. For moderate to high intensity ground excitations, the R-FBI/SR-F systems lead to the lowest peak deflections and column stresses among the base isolators considered.

4. The NZ system generally leads to the lowest relative base displacements.

5. Whenever the frequency of ground excitation is close to the natural frequencies of the LRB, the NZ, the R-FBI systems, resonance peaks are noticed in their response spectra curves. No such peaks appear in the peak responses of the SR-F and the EDF systems. Thus, these latter base isolation systems appear to be insensitive to severe frequency content of the ground excitation.

6. The frictional systems are relatively insensitive to increase in the intensity of ground motion. When the intensity of the ground excitation is doubled, the peak responses of the frictional base isolation systems increase by about 10% to

25%. While, the peak responses of the linear isolator and the fixed-base structure increases in direct proportion to the intensity of the ground acceleration.

7. The peak responses for frictional systems vary when the friction coefficient changes; however, small variations in the friction coefficient lead only to slight changes in the response spectra curves.

8. The velocity-dependence of friction coefficient has no noticeable effect on the peak responses for the R-FBI system.

9. The variations of mass ratio have no significant effect on the peak responses of the base isolated structure.

10. The peak acceleration of the structure with a frictional base isolation system decreases slightly as damping ratio of the structure increases; however, damping has no noticeable effect on the peak deflection and peak base displacement responses.

11. The peak responses of the structure are insensitive to the variations in the damping of the isolator.

12. Small variations in the natural period of various base isolation systems do not affect their peak responses appreciably.

REFERENCES

1. Kelly, J.M., *Aseismic Base Isolation, Shock Vib. Dig.,* 14, *pp. 17-25 (1982).*

2. Kelly, J.M., *Aseismic Base Isolation: Review and Bibliography, Soil Dyn. Earthquake Engng.,* 5, *pp. 202-216 (1986).*

3. Chen, D. and Clough, R.W., *Earthquake Response of Structures with Friction Sliding Motion, Earthquake Engineering Research Center, University of California, Berkeley, CA (1981).*

4. Mostaghel, N. and Tanbakuchi, J., *Response of Sliding Structures to Earthquake Support Motion, Earthquake Engng. Struct. Dyn.,* 11, *pp. 729-748 (1983).*

5. Kelly, J.M. and Beucke, K.E., *A Friction Damped Base Isolation System with Fail-Safe Characteristics, Earthquake Engng. Struct. Dyn.,* 11, *pp. 33-56 (1983).*

6. Ahmadi, G. and Mostaghel, N., *On Dynamics of a Structure with a Frictional Foundation. J. De Mecanique Theorique et Appliquee,* 3, *pp. 271-285 (1984).*

7. Younis, C.J. and Tadjbakhsh, I.G., *Response of Sliding Rigid Structure to Base Excitation, ASCE, J. Engng. Mech.,* 110, *pp. 417-432 (1984).*

8. Ahmadi, G., *Stochastic Earthquake Response of Structures on Sliding Foundation. Int. J. Engng. Sci.,* 121, *pp. 93-102 (1983).*

9. Constantinou, M.C. and Tadjbakhsh, I.G., *Response of a Sliding Structures to Filtered Random Excitation, J. Structural Mech.,* 12, *pp. 401-418 (1984).*

10. Su, L., Orabi, I.I. and Ahmadi, G., *Nonstationary Earthquake Response of a Sliding Rigid Structure, to appear.*

11. Li, L., *Base Isolation Measure For Aseismic Building in China, Proc. 8WCEE, San Francisco, July 21–28, Vol.VI, pp. 791-798 (1984).*

12. Li, L., *Advances in Base Isolation in China, Presented at the 3rd International Conference on Soil Dynamics and Earthquake Engineering, June 22-24, Princeton University, Princeton, NJ (1987).*

13. Kelly, J.M., and Hodder, S.B., *Experimental Study of Lead and Elastomeric Dampers for Base Isolation Systems in Laminated Neopreme Bearings, Bul-*

letin of New Zealand National Society for Earthquake Engineering, 15, *pp. 53-67 (1982).*

14. Mostaghel, N., *Resilient-Friction Base Isolator, Report No. UTEC 84-097, The University of Utah (1984).*

15. Mostaghel, N., Hejazi, M. and Khodaverdian, M., *Response of Structures Supported on Resilient-Friction Base Isolator, Proceed. Third U.S. National Conference on Earthquake Engineering, Charleston, South Carolina, August 1986, pp. 1993-2003.*

16. Mostaghel, N. and Khodaverdian, M., *Dynamics of Resilient-Friction Base Isolator (R-FBI), Earthquake Engng. Struct. Dyn.* 15, *pp. 379-390 (1987).*

17. Mostaghel, N. and Khodaverdian, M., *Seismic Response of Structures Supported on R-FBI System, Report No. UTEC 87-035, The University of Utah September 1987.*

18. Buckle, I.G., *New Zealand Seismic Base Isolation Concepts and Their Application to Nuclear Engineering, Nuclear Engng. and Design,* 84, *pp. 313-326 (1985).*

19. Skinner, R.J., Kelly, J.M. and Heine, A.J., *Hysteretic Dampers for Earthquake-Resistant Structures, Earthquake Engng. Struct. Dyn.,* 3, *pp. 287-296 (1975).*

20. Constantinou, M.C., and Tadjbakhsh, I.G., *Hysteretic Dampers in Base Isolation: Random Approach, ASCE, J. Structural Engng.,* 111, *pp. 705-721 (1985).*

21. Robinson, W.H. and Tucker, A.G., *A Lead-Rubber Shear Damper, Bull. New Zealand Nat. Soci. Earthquake Engng.,* 10, *pp.151-153 (1977).*

22. Gueraud, R., Noel-Leroux, J.-P., Livolant, M., and Michalopoulos, A.P., *Seismic Isolation Using Sliding-Elastomer Bearing Pads, Nuclear Engng. and Design,* 84, *pp. 363–377, (1985).*

23. Su, L., Ahmadi, G. and Tadjbakhsh, I.G., *A Comparative Study of Base Isolation Systems, Report No. MIE-150, Clarkson University, August 1987.*

24. Su, L., Ahmadi, G. and Tadjbakhsh, I.G., *A Comparative Study of Performances of Various Base Isolation Systems Part I: Shear Beam Structures, Report No. MIE-153, Clarkson University, October 1987.*

25. Huffmann, G.R., *Full Base Isolation for Earthquake Protection by Helical Springs and Viscodampers, Nuclear Engng. and Design, 84, pp. 331-338 (1985).*

26. Derham , C.J., *Nonlinear Natural Rubber Bearings for Seismic Isolation, ATC-17, Seminar on Base Isolation and Passive Energy Dissipation, California, March, (1986)*

27. Tajirian, F.F., Kelly, J.M., *Seismic and Shock Isolation System for Modular Power Plants, The 1987 Pressure Vessels and Piping Conference, California, (1987)*

28. Ikonomou, A.S., *Alexisismon Seismic Isolation Levels for Translational and Rotational Seismic Input, Proc. 8WCEE, San Francisco, July 21-28, Vol.V, pp. 975-982 (1984).*

29. Wen, W.K., *Equivalent Linearization for Hysteretic Systems under Random Excitation, J. Appl. Mech., 47, pp. 150-154 (1980).*

30. *International Mathematics and Statistics Library, IMSL Inc., (1987)*

31. Kragelskii, I.V., *Friction and Wear, Butterworths, (1965)*

32. Constantinou, M.C., Caccese, John, and Harris, Harry G., *Frictional characteristics of Teflon-Steel Interfaces Under Dynamic Conditions, Earthquake Engng. Struct. Dyn., 15, pp. 751-759 (1987).*

Appendix A

The purpose of this Appendix is to provide a derivation for the criterion given by (2.8) for the reversal of the sliding direction. Here, the R-FBI system is considered, however, the results are equally applicable to the P-F system as well. The equations governing the motion of the R-FBI system and the motion of the base isolated structure are given by Eqs.(2.11) and (2.2), respectively. Consider the case when the sliding direction is changed without any sticking period. Eqs.(2.2) and (2.11) remain valid and govern the subsequent motion of the structure and the isolator with $\widehat{sgn}(\dot{s})$ taking a sign opposite to its previous value. Thus, at the instant of reversal of sliding direction, the friction force term in Eq.(2.11) changes discontinuously by an amount of $2\mu g$. This will produce jumps in the magnitude of the relative accelerations $\ddot{s}$, and $\ddot{x}_i$. Demanding that Eqs.(2.2) and (2.11) must hold, the jumps $[\![\ddot{s}]\!]$ and $[\![\ddot{x}_i]\!]$ may be evaluated. Since x_i, $\dot{x}_i$, and $\ddot{x}_g$ are continuous, Eq.(2.2) requires that

$$[\![\ddot{x}_i]\!] = -[\![\ddot{s}]\!] \ . \tag{A.1}$$

Eq.(2.11) then implies

$$[\![\ddot{s}]\!] = \frac{2\mu g}{1 - \sum_{i=1}^{n} \alpha_i} \ , \tag{A.2}$$

where it is assumed that s and $\dot{s}$ are continuous functions. Using Eq.(2.3), it follows that

$$[\![\ddot{s}]\!] = 2\mu g \, \frac{M}{m_b} \ , \tag{A.3}$$

and

$$[\![\ddot{x}_i]\!] = -[\![\ddot{s}]\!] \ . \tag{A.4}$$

Therefore, for a continuous $\ddot{x}_g$, (2.8) is the necessary and sufficient condition for the nonstick reversal of sliding direction. The highly unlikely case for which $\dot{s}$ and $\ddot{s}$ become simultaneously zero corresponds to a smooth transition to a stick condition.

An alternative way for determining subsequent state of motion whenever $\dot{s}$ becomes zero during a sliding phase is to assumed that the stick condition prevails momentarily. Assuming that the relative sliding acceleration at this moment is $\ddot{s}_o$, a discontinuous jump of $\ddot{s}_o$ on the relative accelerations $\ddot{x}_i$ is then introduced. This is because the absolute accelerations at the upper floors must remain unchanged during the slip-stick transition with the relative acceleration of the ith floor given by $\ddot{x}_i + \ddot{s}_o$. The criterion given by (2.12) may then be used to determine the subsequent state of motion. Accordingly, for the stick condition to continue, the inequality

$$|\ddot{x}_g + \omega_o^2 s + \textstyle\sum_{i=1}^{n} \alpha_i (\ddot{x}_i + \ddot{s}_o)| < \mu g \ , \tag{A.5}$$

must be satisfied. Rearranging Eq.(2.11) with $\ddot{s}$ being replaced by $\ddot{s}_o$, one finds

$$\ddot{x}_g + \omega_o^2 s + \sum_{i=1}^{n} \alpha_i \ddot{x}_i = -\ddot{s}_o - \mu g \ \widehat{sgn}(\dot{s}) \ , \tag{A.6}$$

where $\widehat{sgn}(\dot{s})$ takes the sign of the previous sliding phase (which is opposite to the sign of $\ddot{s}_o$). Substituting Eq.(A.6) into Eq.(A.5) and using (2.3), one finds

$$|\tfrac{m_b}{M}|\ddot{s}_o| - \mu g| < \mu g. \tag{A.7}$$

Criterion (A.7) for stick condition may be restated as

$$|\ddot{s}_o| < 2\mu g \ \frac{M}{m_b} \ . \tag{A.8}$$

Therefore, it is concluded that the inequality $|\ddot{s}_o| \geq 2\mu g M/m_b$ is the criterion for the sliding structure to reverse sliding direction without stick. For the rigid structure limit, this criterion reduces to $|\ddot{s}_o| \geq 2\mu g$ as expected.

Appendix B

In this appendix, the parameters of the structural modal used in this study are described. Furthermore, the corresponding modal matrix and modal equations are also presented. As mentioned before, the structural model considered is a three-floor building with identical mass for each floor, m, and identical column stiffness, k. The equation of motion of the building is given by Eq.(2.2) with the mass, damping and stiffness matrices given as,

$$[m] = m\begin{bmatrix} 1 & 0 & 0 \\ 0 & 1 & 0 \\ 0 & 0 & 1 \end{bmatrix}, \quad [c] = c\begin{bmatrix} 2 & -1 & 0 \\ -1 & 2 & -1 \\ 0 & -1 & 1 \end{bmatrix}, \quad [k] = k\begin{bmatrix} 2 & -1 & 0 \\ -1 & 2 & -1 \\ 0 & -1 & 1 \end{bmatrix} \tag{B.1}$$

where c is the damping coefficient.

The corresponding natural frequencies, ω_i, and the modal matrix, $[\phi]$, are given by,

$$\omega_1 = \sqrt{0.19806\frac{k}{m}}\ , \quad \omega_2 = \sqrt{1.55496\frac{k}{m}}\ , \quad \omega_3 = \sqrt{3.24698\frac{k}{m}}\ , \tag{B.2}$$

and

$$[\phi] = \begin{bmatrix} 0.59100 & 0.73697 & 0.32798 \\ -0.73697 & 0.32798 & 0.59100 \\ 0.32798 & -0.59100 & 0.73697 \end{bmatrix} \tag{B.3}$$

Using the transformation $\{x\} = [\phi]\{q\}$, the equations of motion in terms of modal coordinates q_i may be restated as

$$\ddot{q}_3 + 3.24698\frac{c}{m}\dot{q}_3 + 3.24698\frac{k}{m}q_3 = -0.18201(\ddot{s} + \ddot{x}_g)\ , \tag{B.4}$$

$$\ddot{q}_2 + 1.55496\frac{c}{m}\dot{q}_2 + 1.55496\frac{k}{m}q_2 = -0.47395(\ddot{s} + \ddot{x}_g)\ , \tag{B.5}$$

$$\ddot{q}_1 + 0.19806\frac{c}{m}\dot{q}_1 + 0.19806\frac{k}{m}q_1 = -1.65595(\ddot{s} + \ddot{x}_g)\ , \tag{B.6}$$

where the subscripts 1, 2, and 3 indicate the modes of vibration.

Appendix C

The purpose of this appendix is to describe the explicit form of the equations of motion for the R-FBI system used in the numerical evaluation. Due to the inertial coupling terms, the compact form of the equations of motion given by Eqs.(2.2) and (2.11) are not suitable for the Runge-Kutta numerical integration scheme. Multiplying Eq.(2.2) by $[m]^{-1}$, the result may be restated as

$$\{\ddot{x}\} = -[m]^{-1}[c]\{\dot{x}\} - [m]^{-1}[k]\{x\} - (\ddot{s} + \ddot{x}_g)\{1\} \ . \tag{C.1}$$

Solving for $\ddot{x}_i$ and using the result in Eq.(2.11), it follows that

$$\ddot{s} = -\ddot{x}_g - \frac{2\zeta_o\omega_o\dot{s} + \omega_o^2 s + \mu g \ \widehat{sgn}(\dot{s})}{\alpha_b} + \frac{c_1\dot{x}_1 + k_1 x_1}{m_b} \ , \tag{C.2}$$

Using Eq.(C.2) to eliminate $\ddot{s}$ in Eq.(2.2) one finds,

$$\begin{aligned} [m]\{\ddot{x}\} \ = \ & -[c]\{\dot{x}\} - [k]\{x\} + (\frac{2\zeta_o\omega_o\dot{s} + \omega_o^2 s + \mu g \ \widehat{sgn}(\dot{s})}{\alpha_b} \\ & - \frac{c_1\dot{x}_1 + k_1 x_1}{m_b})[m]\{1\} \ . \end{aligned} \tag{C.3}$$

Eqs.(C.2) and (C.3) are the explicit form of the equations of motion for the R-FBI system which is used in the Runge-Kutta numerical integration. For other isolation systems, similar equations are formulated prior to numerical integrations.

NATIONAL CENTER FOR EARTHQUAKE ENGINEERING RESEARCH
LIST OF PUBLISHED TECHNICAL REPORTS

The National Center for Earthquake Engineering Research (NCEER) publishes technical reports on a variety of subjects related to earthquake engineering written by authors funded through NCEER. These reports are available from both NCEER's Publications Department and the National Technical Information Service (NTIS). Requests for reports should be directed to the Publications Department, National Center for Earthquake Engineering Research, State University of New York at Buffalo, Red Jacket Quadrangle, Buffalo, New York 14261. Reports can also be requested through NTIS, 5285 Port Royal Road, Springfield, Virginia 22161. NTIS accession numbers are shown in parenthesis, if available.

NCEER-87-0001 "First-Year Program in Research, Education and Technology Transfer," 3/5/87, (PB88-134275/AS).

NCEER-87-0002 "Experimental Evaluation of Instantaneous Optimal Algorithms for Structural Control," by R.C. Lin, T.T. Soong and A.M. Reinhorn, 4/20/87, (PB88-134341/AS).

NCEER-87-0003 "Experimentation Using the Earthquake Simulation Facilities at University at Buffalo," by A.M. Reinhorn and R.L. Ketter, to be published.

NCEER-87-0004 "The System Characteristics and Performance of a Shaking Table," by J.S. Hwang, K.C. Chang and G.C. Lee, 6/1/87, (PB88-134259/AS).

NCEER-87-0005 "A Finite Element Formulation for Nonlinear Viscoplastic Material Using a Q Model," by O. Gyebi and G. Dasgupta, 11/2/87, (PB88-213764/AS).

NCEER-87-0006 "Symbolic Manipulation Program (SMP) - Algebraic Codes for Two and Three Dimensional Finite Element Formulations," by X. Lee and G. Dasgupta, 11/9/87, (PB88-219522/AS).

NCEER-87-0007 "Instantaneous Optimal Control Laws for Tall Buildings Under Seismic Excitations," by J.N. Yang, A. Akbarpour and P. Ghaemmaghami, 6/10/87, (PB88-134333/AS).

NCEER-87-0008 "IDARC: Inelastic Damage Analysis of Reinforced Concrete-Frame Shear-Wall Structures," by Y.J. Park, A.M. Reinhorn and S.K. Kunnath, 7/20/87, (PB88-134325/AS).

NCEER-87-0009 "Liquefaction Potential for New York State: A Preliminary Report on Sites in Manhattan and Buffalo," by M. Budhu, V. Vijayakumar, R.F. Giese and L. Baumgras, 8/31/87, (PB88-163704/AS).

NCEER-87-0010 "Vertical and Torsional Vibration of Foundations in Inhomogeneous Media," by A.S. Veletsos and K.W. Dotson, 6/1/87, (PB88-134291/AS).

NCEER-87-0011 "Seismic Probabilistic Risk Assessment and Seismic Margin Studies for Nuclear Power Plants," by Howard H.M. Hwang, 6/15/87, (PB88-134267/AS).

NCEER-87-0012 "Parametric Studies of Frequency Response of Secondary Systems Under Ground-Acceleration Excitations," by Y. Yong and Y.K. Lin, 6/10/87, (PB88-134309/AS).

NCEER-87-0013 "Frequency Response of Secondary Systems Under Seismic Excitations," by J.A. HoLung, J. Cai and Y.K. Lin, 7/31/87, (PB88-134317/AS).

NCEER-87-0014 "Modelling Earthquake Ground Motions in Seismically Active Regions Using Parametric Time Series Methods," G.W. Ellis and A.S. Cakmak, 8/25/87, (PB88-134283/AS).

NCEER-87-0015 "Detection and Assessment of Seismic Structural Damage," by E. DiPasquale and A.S. Cakmak, 8/25/87, (PB88-163712/AS).

NCEER-87-0016 "Pipeline Experiment at Parkfield, California," by J. Isenberg and E. Richardson, 9/15/87, (PB88-163720/AS).

NCEER-87-0017 "Digital Simulations of Seismic Ground Motion," by M. Shinozuka, G. Deodatis and T. Harada, 8/31/87, (PB88-155197/AS).

NCEER-87-0018 "Practical Considerations for Structural Control: System Uncertainty, System Time Delay and Truncation of Small Forces," J. Yang and A. Akbarpour, 8/10/87, (PB88-163738/AS).

NCEER-87-0019 "Modal Analysis of Nonclassically Damped Structural Systems Using Canonical Transformation," by J.N. Yang, S. Sarkani and F.X. Long, 9/27/87, (PB88-187851/AS).

NCEER-87-0020 "A Nonstationary Solution in Random Vibration Theory," by J.R. Red-Horse and P.D. Spanos, 11/3/87, (PB88-163746/AS).

NCEER-87-0021 "Horizontal Impedances for Radially Inhomogeneous Viscoelastic Soil Layers," by A.S. Veletsos and K.W. Dotson, 10/15/87, (PB88-150859/AS).

NCEER-87-0022 "Seismic Damage Assessment of Reinforced Concrete Members," by Y.S. Chung, C. Meyer and M. Shinozuka, 10/9/87, (PB88-150867/AS).

NCEER-87-0023 "Active Structural Control in Civil Engineering," by T.T. Soong, 11/11/87, (PB88-187778/AS).

NCEER-87-0024 "Vertical and Torsional Impedances for Radially Inhomogeneous Viscoelastic Soil Layers," by K.W. Dotson and A.S. Veletsos, 12/87, (PB88-187786/AS).

NCEER-87-0025 "Proceedings from the Symposium on Seismic Hazards, Ground Motions, Soil-Liquefaction and Engineering Practice in Eastern North America, October 20-22, 1987, edited by K.H. Jacob, 12/87, (PB88-188115/AS).

NCEER-87-0026 "Report on the Whittier-Narrows, California, Earthquake of October 1, 1987," by J. Pantelic and A. Reinhorn, 11/87, (PB88-187752/AS).

NCEER-87-0027 "Design of a Modular Program for Transient Nonlinear Analysis of Large 3-D Building Structures," by S. Srivastav and J.F. Abel, 12/30/87, (PB88-187950/AS).

NCEER-87-0028 "Second-Year Program in Research, Education and Technology Transfer," 3/8/88, (PB88-219480/AS).

NCEER-88-0001 "Workshop on Seismic Computer Analysis and Design With Interactive Graphics," by J.F. Abel and C.H. Conley, 1/18/88, (PB88-187760/AS).

NCEER-88-0002 "Optimal Control of Nonlinear Structures," J.N. Yang, F.X. Long and D. Wong, 1/22/88, (PB88-213772/AS).

NCEER-88-0003 "Substructuring Techniques in the Time Domain for Primary-Secondary Structural Systems," by G. D. Manolis and G. Juhn, 2/10/88, (PB88-213780/AS).

NCEER-88-0004 "Iterative Seismic Analysis of Primary-Secondary Systems," by A. Singhal, L.D. Lutes and P. Spanos, 2/23/88, (PB88-213798/AS).

NCEER-88-0005 "Stochastic Finite Element Expansion for Random Media," P. D. Spanos and R. Ghanem, 3/14/88, (PB88-213806/AS).

NCEER-88-0006 "Combining Structural Optimization and Structural Control," F. Y. Cheng and C. P. Pantelides, 1/10/88, (PB88-213814/AS).

NCEER-88-0007 "Seismic Performance Assessment of Code-Designed Structures," H.H-M. Hwang, J. Jaw and H. Shau, 3/20/88, (PB88-219423/AS).

NCEER-88-0008 "Reliability Analysis of Code-Designed Structures Under Natural Hazards," H.H-M. Hwang, H. Ushiba and M. Shinozuka, 2/29/88.

NCEER-88-0009 "Seismic Fragility Analysis of Shear Wall Structures," J-W Jaw and H.H-M. Hwang, 4/30/88.

NCEER-88-0010 "Base Isolation of a Multi-Story Building Under a Harmonic Ground Motion - A Comparison of Performances of Various Systems," F-G Fan, G. Ahmadi and I.G. Tadjbakhsh, 5/18/88.